Neurotoxicity and aggregation of β-synuclein and its P123H and V70M mutants associated with dementia with Lewy bodies

Dissertation

in partial fulfillment for the award of the degree

"Doctor rerum naturalium" (Dr. rer. nat.)

of the Georg-August-University of Göttingen

within the doctoral program *"Molecular Physiology of the Brain"*

of the *"Georg-August-University School of Science (GAUSS)"*

submitted by

Maryna Psol

born in Zaporizhzhia (Ukraine)

Göttingen, April 2018

Declaration

Hereby I declare that this thesis entitled:

"Neurotoxicity and aggregation of β-synuclein and its P123H and V70M mutants associated with dementia with Lewy bodies"

has been written independently and with no other sources and aids than quoted.

Maryna Psol

Göttingen, April 2018

Thesis committee:

Dr. Sebastian Kügler, Department of Neurology, University Medical Center Göttingen

Prof. Dr. Tiago Outeiro, NeuroDegeneration and Restorative Research, University Medical Center Göttingen

Prof. Dr. Markus Zweckstetter, Protein structure determination using MRI, Max-Planck Institute for Biophysical Chemistry

Examination committee:

Dr. Camin Dean, Trans-synaptic Signaling group, European Neuroscience Institute Göttingen

Prof. Dr. Thomas Dresbach, Department of Anatomy and Embryology, University Medical Center Göttingen

Prof. Dr. Silvio Rizzoli, Department of Neuro-and Sensory Physiology, University Medical Center Göttingen

Date of disputation: 26th of June 2018

Table of contents:

List of figures

List of tables

1. Introduction

1.1. Neurodegenerative disorders

Neurodegenerative disorders (NDDs) encompass a wide range of pathologies which are characterized by progressive loss of neurons in central and peripheral nervous systems. Alongside with cardiovascular diseases and cancer, NDDs belong to the most common causes of death and disability in the industrialized world, and their role constantly increases with the aging of the world population. Alzheimer's (AD) and Parkinson's (PD) diseases are the most prevalent NDDs affecting, respectively, more than 35 and 6.3 million people worldwide (Bourdenx *et al.*, 2015). Besides, NDDs include dementia with Lewy bodies (DLB), fronto-temporal dementia (FTD), amyotrophic lateral sclerosis (ALS) etc., as well as rare rapidly progressive prion disorders such as Creutzfeldt-Jakob disease (CJD). Most of the NDD cases are sporadic or idiopathic, meaning that the etiology of the disease is not known, and only in a small subset of the familial NDD cases genetic causes were found (de Pedro-Cuesta *et al.*, 2015). NDDs do not only have debilitating effects on patients' health and quality of life but also create an immense socio-economic burden. NDDs differ in clinical presentations, pathophysiology and the underlying molecular agents, but there is also a striking similarity – most of NDDs are characterized by protein misfolding and aggregation (Bourdenx *et al*., 2015). Further elucidation of the molecular mechanisms of protein aggregation, as well as the understanding of physiological and pathological functions of the proteins involved in NDDs, are needed for developing new therapeutic approaches.

1.2. Synucleinopathies: Parkinson's disease (PD), Parkinson's disease dementia (PDD), and dementia with Lewy bodies (DLB)

1.2.1. General overview

The NDDs which are characterized by abnormal accumulation of alpha-synuclein (αS) are commonly referred as synucleinopathies. They include PD, DLB, multiple systems atrophy (MSA), neurodegeneration with brain iron accumulation (NBIA) and some other less prevalent disorders. In case of PD and DLB, αS forms so-called Lewy bodies and Lewy neurites in the cell

bodies or processes of neurons, respectively. Glial cytoplasmic inclusions of αS can be found in MSA (Spillantini *et al.*, 1998; Galvin *et al.*, 2001).

The first clinical description of PD appeared nearly 200 years ago when Dr. James Parkinson in *"An essay on the shaking palsy"*, 1817, described 6 individuals with the distinctive motor symptoms: tremor, lessened muscular power, a characteristic leaned posture, as well as decrease in intelligence (Parkinson J, 2002 reprint). All these symptoms, with exception of cognitive impairment, remain valid for PD diagnosis nowadays, although many nuances were added to our understanding of the disease manifestation and progression and a variety of neurologic disorders with Parkinsonism were distinguished as individual disease entities (Goedert *et al.*, 2017).

PD, PDD, and DLB are disorders of the parkinsonian spectrum which share many pathological features. Some clinicians and scientists even recognize these related conditions as "diagnostic categories" which represent a biological continuum of Lewy body disease rather than single pathologies (Donaghy and McKeith, 2014; Jellinger and Korczyn, 2018). However, the differences in the clinical manifestation of PD, PDD and DLB indicate that neurons of different regions may be specifically vulnerable to these disorders (Surmeier and Sulzer, 2013).

1.2.2. Prevalence of PD, PDD, and DLB

PD is the second most common neurodegenerative disorder, outnumbered only by AD. In the general population, the prevalence of PD amounts to 0.3%, and it increases up to 1% for over 60-year-old (y/o) individuals, and to 3% for people above 80 y/o. The incidence of the disease is 8–18 cases per 100 000 person per year. Males receive PD diagnosis 1.5 – 2 times more often than females. The mean age of disease onset is 60 y/o, and life expectancy after the diagnosis is ~15 years. Nearly 30% of PD patients develop PDD, and the incidence of this dementia increases with the duration of the PD (Erkkinen *et al.*, 2018).

DLB is the second most common disorder among neurodegenerative dementias. Its prevalence is estimated to be between 4.2% (Vann Jones and O'Brien, 2014) to 30% (Zaccai *et al.*, 2005) of all dementia cases depending on the diagnostic inclusion criteria (Hogan *et al.*, 2016). The overall incidence of DLB is 3.5 – 5.9 cases per 100 000 person per year with higher numbers for men than for women (Savica *et al.*, 2013). The mean age of onset also varies greatly in different populations: from 59 to 78 years. The disease lasts on average approx. 7 years but its duration can

vary from 2 to 20 years in individual patients (Erkkinen *et al.*, 2018).

1.2.3. Clinical manifestation of PD, PDD, and DLB

Typical symptoms of PD include motor symptoms (resting tremor, bradykinesia, rigidity, and postural instability) and a variety of non-motor symptoms such as anosmia, REM sleep behavioural disorder, orthostatic hypotension, constipation, mood and sensory disturbances etc. (Barker and Williams-Gray, 2016).

PDD and DLB share many common symptoms. Besides parkinsonian motor and non-motor symptoms, they are characterized by the progressive cognitive decline (dementia), recurring visual hallucinations, fluctuations in alertness and attention, depression, delusions etc. These patients also show severe sensitivity to neuroleptics, and cannot be treated against psychosis with pharmaceutical methods. They are usually responsive to the "golden standard" PD medication L-DOPA, but due to the side effects, such as hallucinations and other psychotic manifestations, levodopa is often omitted. Subsequently, even the symptomatic treatment of PDD and DLB is limited which has drastic effects on the quality of life of patients and caregivers (Donaghy and McKeith, 2014; Snyder, 2015).

According to the international consensus, the diagnosis PDD is given if movement symptoms precede dementia at least for 1 year. In DLB, dementia is present before parkinsonism, or cognitive impairment and motor symptoms appear at the same time (McKeith *et al.*, 2005).

1.2.4. Histopathology and molecular basis of PD, PDD, and DLB

Two major histopathological hallmarks of PD have been known since the beginning of the 20th century. First, the distinctive protein aggregates in neuronal cell bodies were discovered by the German neurologist Frederic Lewy in 1912. These pathological structures were named after him Lewy bodies (LB), and, by analogy, Lewy neurites (LN). Second, in the year 1919, Konstantin Tretiakoff postulated a hypothesis that the loss of dopaminergic neurons in the Substantia nigra (SN) is related to PD pathology. Only decades later this idea was accepted and until now remains to be one of the cardinal hallmarks of PD (Drew, 2016). How Lewy pathology relates to the loss of dopaminergic neurons is still not clearly understood.

In 2003 Braak and colleagues proposed that Lewy pathology in PD develops in 6 consequent stages, ascending from the enteric part of PNS to neocortex (as described in Figure 1.1. E) and correlates with the progression of the disease and the severity of the symptoms (Braak *et al.*, 2003). In DLB brains, αS-positive LBs and LNs can be found in various regions, including SN and hippocampus (Figure 1.1. A-D; Spillantini *et al.*, 1998), but also in the olfactory pathways, brainstem, limbic and cerebral cortex which probably can explain heterogeneity of the DLB symptoms (Harding *et al.*, 2002; Snyder, 2015). Postmortem analysis of the DLB brains usually shows an advanced form of the disease with massive cortical involvement corresponding to the Braak's stages 5 or 6 and does not provide any information about the initial phases of the disease. At the Braak's stages 5 and 6 there are no histopathological differences in Lewy body pathology between PD and DLB, despite the differences in symptomatology (Donaghy and McKeith, 2014). Histopathological analysis of 88 PD brains showed that widespread cortical LBs do not necessarily lead to dementia or cognitive decline (Braak *et al.*, 2005).

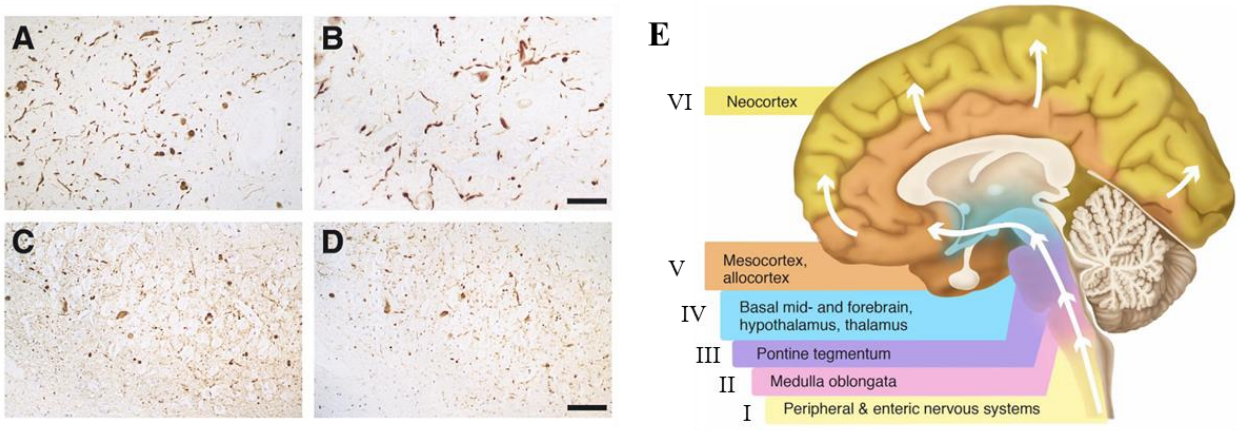

Figure 1.1. Lewy body pathology.

Lewy bodies and Lewy neurites in the Substantia nigra (A, B; scale bar: 100 μm) and in the hippocampus (C, D; scale bar: 80 μm) of the DLB brain (reproduced from Spillantini *et al.*, 1998). (E) Braak's stages of Lewy body pathology (modified from Donaghy *et al.*, 2014).

The discrepancies between symptoms and LB pathology in PD and DLB might be explained by involvement of different molecular agents in the pathophysiology of the disorders. Although the main component of LB and LN, αS, probably plays the central role in the pathophysiology of PD and DLB, other proteins may modulate αS properties and aggravate its toxicity or act as the

independent pathological factors.

In addition to its major component αS, the LBs and LNs are composed of neurofilaments (Trojanowski and Lee, 1988), proteolytic marker ubiquitin (Lowe *et al.*, 1988), autophagy marker p62 (Kuusisto *et al.*, 2003), heat-shock proteins (Uryu *et al.*, 2006), synphilin 1 (Wakabayashi *et al.*, 2000), chaperon-like protein 14-3-3 (Kawamoto *et al.*, 2002) etc. These proteins may interact with αS and influence LB formation. A close homologue of αS – beta-synuclein (βS) was not found in LB, but it is present in the axonal spheroid-like structures in PD and DLB (Galvin *et al.*, 1999). So far, no apparent differences in the immunostainings were revealed between LBs of PD and DLB (Galvin *et al.*, 1999; Kawamoto *et al.*, 2002; Trojanowski and Lee, 1988; Uryu *et al.*, 2006).

Markers of AD pathology (β-amyloid Aβ and tau) are also often present in DLB brains, though there are DLB cases without any signs of Aβ or tau aggregations as revealed by amyloid PET imaging (Donaghy *et al.*, 2015). Aβ-plaques are present also in PD and healthy aged brains, but the load of Aβ is statistically higher in DLB (Halliday *et al.*, 2011).

Compared with PD, DLB brains have more abundant αS depositions in the hippocampal CA2/3 area (Jellinger *et al.*, 2012), a higher density of the serotonin 1A receptor in the frontal cortex (Francis *et al.*, 2007), and virtually no upregulation of D2-dopamine receptor in the striatum (Piggott, 1999). A close homologue of αS, βS might be also involved in PD and DLB pathology, since a genetic link between DLB and βS was identified (Ohtake *et al.*, 2004; see section 1.2.6.).

Also, it was suggested that different strains of αS can produce a number of αS macromolecular assemblies (oligomers, ribbons, fibrils) with different pathological potential and seeding capabilities. E.g., fibrils were more toxic to the dopaminergic neurons, while ribbons were more prone to aggregation and formation of LB-like structures when different structural strains of αS were injected into the rat's brain. Such variability might explain the heterogeneity in the symptomatology of different synucleinopathies (Peelaerts *et al.*, 2015).

1.2.5. Genetics of PD, PDD, and DLB

Most cases of synucleinopathies are sporadic, where some environmental factors and aging probably trigger the conversion of αS into a toxic species. Genetic predispositions play an important role in approx. 5 – 10% of PD cases. The genome-wide association studies (GWAS)

identified the association between PD and over 20 human genes and this number will probably increase in the future (Peeraully *et al.*, 2012; Nussbaum RL, 2017). Familial PD forms with autosomal dominant and autosomal recessive inheritance were described. Besides, some alleles are characteristic for the age of the PD onset: juvenile (under 20 y/o), early (20-40 y/o) or late (above 40 y/o) (Sekiyama *et al.*, 2014). Mutations in the LRRK2 (PARK8) gene are the most common causes of familial PD. LRRK2 (leucine-reach repeat kinase 2) is a GTPase/kinase protein which is involved in cell proliferation, differentiation and survival (Funayama *et al.*, 2002; Funayama *et al.*, 2005). Several monogenic conditions with autosomal recessive inheritance were described. These genes include but are not limited to: parkin (PARK2) coding for E3 ubiquitin protein ligase (Kitada *et al.*, 1998); PINK1 (PARK6) coding for PTEN-induced putative kinase 1 which is important for sustaining mitochondria (Rogaeva *et al.*, 2004; Valente *et al.*, 2004; Exner *et al.*, 2007), DJ1 (PARK7) coding for protein and nucleotide deglycase involved in the protection against oxidative stress (Bonifati *et al.*, 2003), ATP13A2 (PARK9) coding for a lysosomal ATPase (Ramirez *et al.*, 2006).

Several missense mutations were also identified in the SNCA gene (PARK1/4) coding for αS. Single amino acid substitutions A53T, A30P, H50Q, and G51D were identified in rare familial PD cases (Polymeropoulos *et al.*, 1996; Polymeropoulos *et al.*, 1997; Kruger *et al.*, 1998; Proukakis *et al.*, 2013; Kiely *et al.*, 2013). The E46K mutation was reported causal in PD and DLB cases (Zarranz *et al.*, 2004). The A53E mutation was described in a MSA case (Pasanen *et al.*, 2014). A18T and A29S mutations were associated with sporadic PD (Hoffman-Zacharska *et al.*, 2013). Duplication and triplication of the SNCA gene were also identified in PD patients (Ibanez *et al.*, 2004; Singleton *et al.*, 2003).

Although no specific mutations of SNCA gene were identified in DLB so far, several mutations mentioned above are associated with poor prognosis and progression to dementia: E46K, duplication, and triplication of the SNCA gene (Obi *et al.*, 2008; Farrer *et al.*, 2004). In two familial cases with A53T mutation of αS cognitive impairment was also described, although the patients did not meet the consensus criteria for DLB diagnosis (Tsuang *et al.*, 2004). Besides, the MAPT gene coding for tau, the GBA gene coding for a lysosomal enzyme glucocerebrosidase and the Apoε4 gene for apolipoprotein are associated with DLB (Nussbaum RL, 2017).

1.2.6. Genetic link between βS and DLB

Ohtake *et al.*, 2004 suggested that genetic alterations in the βS gene may contribute to the pathophysiology of DLB. The authors sequenced the *SNCB* gene from 33 human subjects with sporadic DLB, 10 patients from DLB families and over 330 control individuals. As a result, 2 single-amino-acid mutations were identified: P123H in familial and V70M in sporadic cases of DLB. These mutations were absent in all 660 *SNCB* alleles of the control individuals of Caucasian and Japanese origin.

The 64-year old patient with P123H mutation initially demonstrated an atypical clinical picture for DLB: dementia, language and cognitive dysfunctions and was diagnosed with fronto-temporal lobar degeneration (FTLD). Only 3 years after the first diagnosis, he developed characteristic for DLB audio and visual hallucinations and, later, parkinsonian symptoms. Besides, 7 members of his family had dementia, 4 of these cases were consistent with DLB (Figure 1.1). Autopsy confirmed both Lewy bodies and AD pathology (Bonner *et al.*, 2003). Further neuropathological examination revealed a high amount of Lewy bodies in hippocampus, amygdala, and Substantia nigra with immunoreactivity to αS. Positive diffuse staining for βS was also present in these brain regions, but no aggregates of βS were detected (Ohtake *et al.*, 2004).

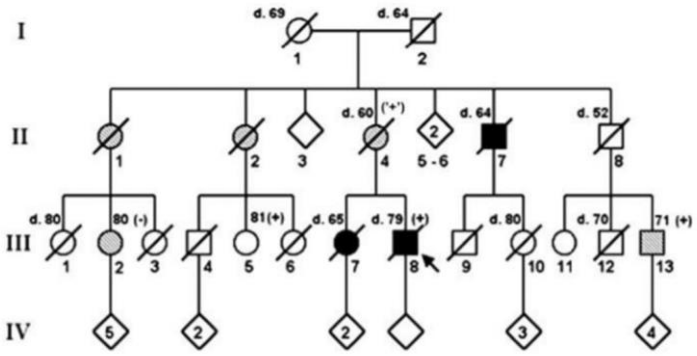

Figure 1.2. Pedigree of the patient with P123H *SNCB* allele (Ohtake *et al.*, 2004).

The P123H mutation is an autosomal dominant trait with incomplete penetrance. Four generations of the family with P123H *SNCB* allele are shown. The proband is marked with an arrow. Individuals marked with (+) are heterozygous for P123H *SNCB* allele, those who have a (-) mark do not carry the mutation. Ages of family members at the time of ascertainment are provided in the figure. Black symbols indicate diseased individuals, gray symbols stand for probable DLB case, and white symbols are assigned to healthy family members.

The 83-year old patient with V70M *SNCB* allele was a sporadic case of DLB. His disease manifested at the age of 78 with visual hallucinations, cognitive impairment, and parkinsonian gait. Bradykinesia, rigidity, and tremor, as well as dysarthria and dysphasia, developed later. Unfortunately, the autopsy was not permitted in this case (Ohtake *et al.*, 2004).

1.3. Synuclein family of proteins

1.3.1. The proteins of the synuclein family: αS, βS, and γS

The synuclein family of proteins includes 3 members: alpha-, beta- and gamma-synuclein (αS, βS, and γS), which were so far described only in vertebrates. The genes coding for the synuclein proteins are highly conserved between species, so that, for example, human and rodent αS are 95.3 % identical, and human and rodent βS share 97.8 % of the amino acid sequence (Surguchov, 2008).

αS was discovered nearly 30 years ago in neurons of the electric lobe of the Pacific electric ray *Torpedo californica*. Due to its subcellular localization in presynaptic terminals and adjacent to the nuclear envelop the protein was called synuclein (Maroteaux *et al.*, 1988). Later, two other highly homologous to αS proteins were discovered: first, neuronal phosphoprotein PNP14 from bovine brain (Nakajo *et al.*, 1990; Nakajo *et al.*, 1993) and, second, BCSG1 from the advanced breast carcinoma or presyn from PNS (Ji *et al.*, 1997; Ninkina *et al.*, 1998). For the consistency, they were later called βS and γS respectively.

In the human genome, the αS gene SNCA was mapped to chromosome 4q21.3-q22 (Campion *et al.*, 1995), the SNCB gene coding for βS was mapped to chromosome 5q35 (Spillantini *et al.*, 1995), and the SNCG coding for γS was mapped to chromosome 10q23 (Lavedan *et al.*, 1998). Human αS is composed of 140 amino acid residues, βS and γS consist of 134 and 127 amino acid residues (AA), respectively (Von Bohlen und Halbach O, 2004).

The synuclein proteins share many structural similarities. They are composed of 3 common domains: N-terminal region, central NAC-domain (non-amyloid component of Alzheimer's disease amyloid) and C-terminal region (Figure 1.3.). The N-terminal region is the most conserved between the 3 synuclein species and contains five to seven imperfect motif repeats KTKEGV. This part of the molecule (AA 1-60) is positively charged due to the high amount of

basic amino acid residues. It forms an α-helix which is able to bind to lipids and membranes. The central part of the molecule, AA 60 – 95 in αS, comprises the NAC domain (non-amyloid-component of Alzheimer's disease β-amyloid). This highly hydrophobic region is thought to be involved in fibrillation of αS. In βS, 11 AA of the core NAC domain are naturally deleted which leads to a lower aggregation propensity of this protein. The NAC domain of γS is less hydrophobic than in αS which results in the decreased ability to form fibrils (Biere *et al.*, 2000; Surguchov, 2013). The acidic C-terminal region of synucleins is the least conserved part of the molecule. This region in αS is relatively stable to proteolysis and it might regulate aggregation (Hoyer *et al.*, 2004; Surguchov, 2008).

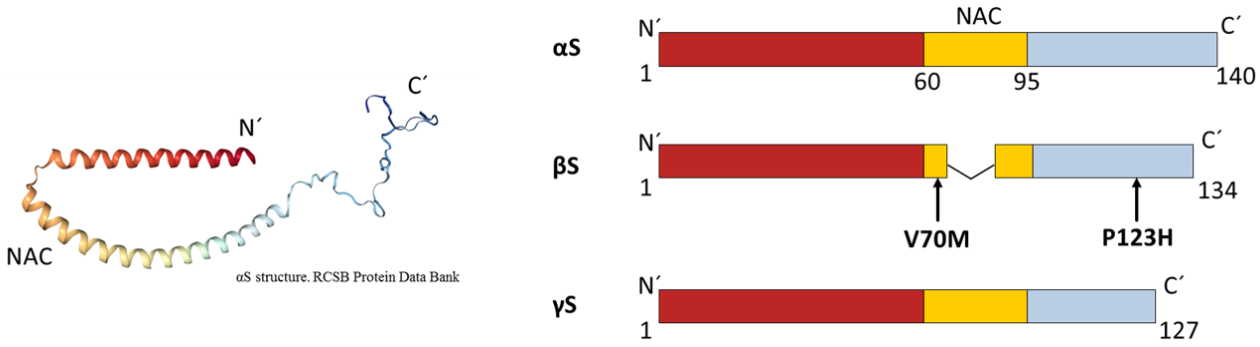

Figure 1.3. Structure of synuclein proteins.

αS, βS, and γS are composed of 3 structural domains: highly conserved basic N-terminal region, hydrophobic NAC domain, and highly flexible C-terminal region. The DLB-associated mutations of βS, V70M and P123H, lie in NAC domain and C-terminus respectively.

1.3.2. Physiological functions of synuclein proteins

Synucleins are highly abundant proteins. Thus, αS comprises 0.1% of the protein in the brain homogenate (Shibayama-Imazu *et al.*, 1993) or 1% of the soluble protein in cytosolic brain fractions (Iwai *et al.*, 1995). Additionally, αS is present in CSF, blood plasma, saliva, as well as erythrocytes, lymphocytes, and platelets (Galvin *et al.*, 2001; Surguchov, 2008). Similarly to αS, its close homologue βS is also highly abundant in CNS, especially in the presynaptic terminals. The highest expression of βS in the rat brain was observed in the olfactory bulb, the CA3 region

of the hippocampus, cortical layer IV, as well as in basal and thalamic nuclei (Mori *et al.*, 2002). γS was shown to be predominantly expressed in PNS: in primary sensory neurons, motor neurons, and sympathetic neurons (Buchman *et al.*, 1998).

So far, physiological functions of synuclein proteins were not clearly defined but numerous studies suggest that these proteins may be involved in several important cellular processes (Surguchov, 2013; Lashuel *et al.*, 2013; Gallegos *et al.*, 2015). A great level of homology between the synuclein species and their frequent co-localization may indicate functional redundancy of these proteins.

Presynaptic location of αS and βS indicates their involvement in the regulation of the synaptic function. Burré *et al.* showed that the C-terminal region of αS can bind to synaptobrevin-2/VAMP2 and that αS can catalyze SNARE complex assembly in HEK293 cells and transgenic mice (Burré *et al.*, 2010). αS may participate in synaptic vesicle traffic and maintenance of the synaptic vesicle pool (Chandra *et al.*, 2004), in regulation of dopamine release (Abeliovich *et al.*, 2000; Larsen *et al.*, 2006; Hara *et al.*, 2013), and synaptic plasticity (Jin and Clayton, 1997). Although single KO of αS, βS or γS genes do not impair animals' survival or normal activities of the brain (Lashuel *et al.*, 2013), triple KO mice are characterized by a progressive age-dependent neuronal dysfunction and impairments of synaptic structure and transmission which shows the importance of synucleins for the long-term maintenance of the nervous system (Greten-Harrison *et al.*, 2010).

A physical link between αS and mitochondria was found: the N-terminus of αS directly binds to the mitochondrial outer membrane which leads to changes in the shape of mitochondria. αS also interacts with mitochondria complex I and may regulate mitochondria homeostasis (Hashimoto *et al.*, 2004; Li *et al.*, 2007; Mullin and Schapira, 2013).

Moreover, all three synuclein proteins may be implicated in regulation of the proteasomal function (Snyder *et al.*, 2005), chaperon-like activity (Ahn *et al.*, 2006), and phospholipase D 2 (PLD2) inhibition (Payton *et al.*, 2004).

1.3.3. Mechanisms of neurotoxicity of αS and βS

Pathophysiological mechanisms of αS were extensively studied, numerous cellular processes leading to neuronal cell death and to propagation of synuclein pathology were reported but the exact molecular mechanisms of pathogenicity and the nature of toxic species are far from being completely understood and are often the subject of disputes in the research community (Surguchov, 2013; Lashuel *et al.*, 2013; Gallegos *et al.*, 2015). Even less is known about neuropathology of βS and γS. Misfolding and aggregation of synuclein proteins and their role in pathogenicity will be further discussed in the section 1.3.4. Here, just a few cellular pathways involved in synucleinopathies will be mentioned. Major subcellular targets of toxic αS are summarized in Figure 1.4.

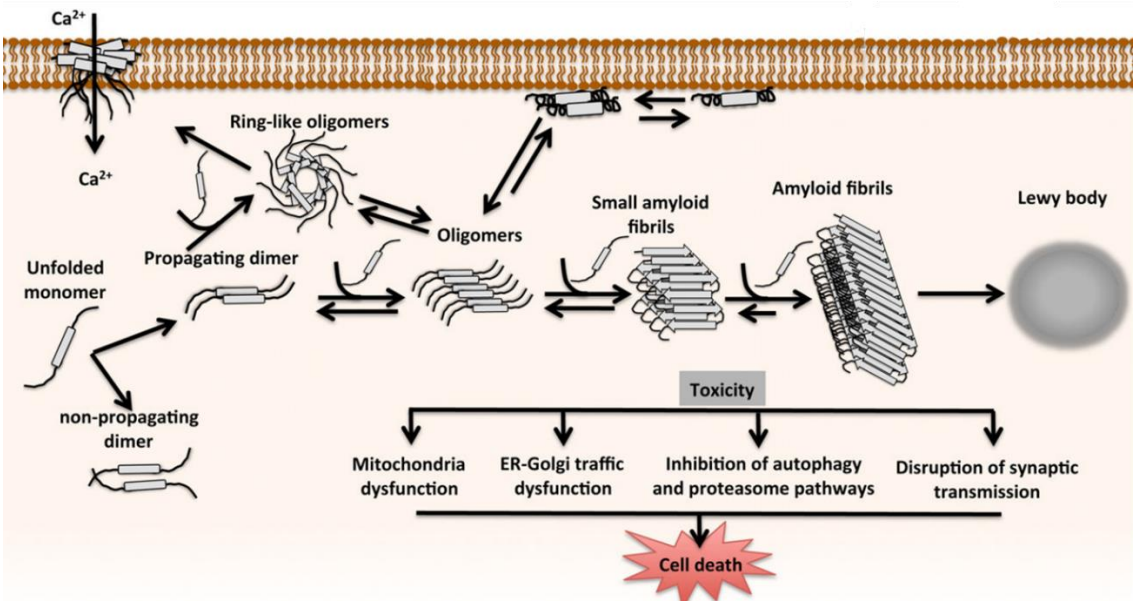

Figure 1.4. Mechanisms of αS aggregation and toxicity (modified from Lashuel *et al.*, 2013).

Under physiological conditions, αS persists as an intrinsically disordered monomer. Misfolded αS can propagate to dimers, oligomers, pre-fibrils, and amyloid fibrils which then make up LB and LN. Although the nature of a toxic species is still under debate, several cellular pathways are involved in the αS pathology including mitochondrial, ER, Golgi and proteasomal dysfunctions, inhibition of autophagy etc.

Mitochondrial dysfunction is considered to be one of the major pathological mechanisms underlying both sporadic and familial PD. αS can directly interact with mitochondrial outer

membrane and influence fission/fusion homeostasis of mitochondria. A53T-αS transgenic mice were characterized by deformed mitochondria and damages of mitochondrial DNA (Martin *et al.*, 2006). Incorporation of αS into mitochondrial membrane can lead to an intervention in mitochondrial fusion and subsequent impairment of mitochondrial motility in neurites, and mitophagy, the process through which damaged mitochondria are removed (Mullin and Schapira, 2013). Besides, αS inhibits mitochondrial complex I (Devi *et al.,* 2008) and may induce apoptosis by caspase activation (Parihar *et al.,* 2008). Our lab showed that overexpression of αS, as well as βS, in primary cultured cortical neurons can induce morphological abnormalities of mitochondria: condensation to swollen rounded structures (Taschenberger *et al.,* 2013), and αS can increase thiol oxidation, permeabilization of mitochondrial outer membrane and caspase activation (Tolö *et al.,* 2018).

ER and Golgi stress due to accumulation of misfolded αS can lead to the activation of the neuronal death cascade. Abnormal ER morphology and activation of caspase 12 and subsequent apoptosis were reported in A53T-αS tg mice (Colla *et al.,* 2012). Oxidative stress and proteasomal dysfunction are also typical for PD and DLB pathology and were described in several cell culture and animal models in association with αS. Increased intracellular ROS levels may be one of the reasons for the selective vulnerability of dopaminergic neurons in PD brains (Puspita *et al.,* 2017). Pore formation in the cellular membrane and disruption of ion homeostasis was also suggested as one of the synucleins pathological mechanisms (Tsigelny *et al.,* 2007). Not only αS but also wild type βS (WT-βS) was shown to form transient channels in artificial membranes (Taschenberger *et al.,* 2013).

Besides recent publication on βS toxicity in primary cortical cells and rats SN with some mechanisms mentioned above (Taschenberger *et al.,* 2013), βS axonal pathology was also detected in hippocampi of PD and DLB patients (Galvin *et al.,* 1999). βS accumulations in form of axonal spheroids but not in LB were found in NBIA type 1, rare synucleinopathy characterized by the combination of parkinsonism and cognitive impairment (Galvin *et al.,* 2000). Extensive βS accumulations were described in Purkinje cells of MSA patients (Mori *et al.,* 2003). βS was found to be toxic and formed cytosolic inclusions in a similar way as αS in the yeast model of PD (Tenreiro *et al.,* 2016). βS may also cause inflammation in NDDs (Mor *et al.,* 2003).

1.3.4. Aggregation properties of synuclein proteins

In solutions, αS is usually present as a natively unfolded intrinsically disordered monomer. Alternatively, Bartels *et al.* suggested that endogenous αS may persist in form of a 58 kDa helical tetramer, a stable physiological form of αS which resists aggregation (Bartels *et al.,* 2011), though this hypothesis remains under debate (Fauvet *et al.,* 2012). Upon binding to lipid membranes or SDS-micelles with its N-terminal region, αS can obtain a more stable conformation with 2 canonical α-helices (Alderson and Markley, 2013).

Once αS is misfolded, it can aggregate into dimers, oligomers, and fibrils (Figure 1.4). The mechanisms of conversion of αS into a toxic species, the molecular basis of aggregation and nucleation, and the nature of such toxic species are not yet clearly understood. Growing evidence indicates that soluble αS oligomers or protofibrils of certain confirmation may be the pathogenic species which could initiate seed formation or nucleation, while the large filamentous aggregates in LBs and LNs are rather cytoprotective side products of the aggregation process (Karpinar *et al.,* 2009; Paleologou *et al.,* 2009; Winner *et al.,* 2011).

Numerous factors can influence αS aggregation. Thus, increase in αS concentration, such as observed with familial duplication or triplication of SNCA gene, promotes fibrillation. Besides, the missense mutations of αS, associated with rare familial PD and DLB cases may induce the pathological cascade of αS aggregation (see section 1.2.5.). Post-translational modifications (PTM) also regulate αS aggregation propensities, e.g. phosphorylation of serine 129 promotes fibrillation (Fujiwara H*et al.,* 2002) while nitration reduces aggregation of αS (Yamin *et al.,* 2003). Environmental factors, such as metals (Fe^{2+}, Cu^{2+}) and pesticides (paraquat, rotenone) can accelerate fibrillation of αS (Deleersnijder *et al.,* 2013).

Previous studies have demonstrated that βS and γS may reduce αS aggregation *in vitro* under certain conditions (Uversky *et al.,* 2002; Leitao *et al.,* 2018), thus, a role of βS as a negative regulator of αS and as a neuroprotective factor was suggested (Hashimoto *et al.,* 2001). The differences in aggregation propensities are connected not only to the 11-AA deletion in the NAC domain in βS but also lies in the structure of the C-terminal region and intramolecular electrostatic interactions between N- and C-termini. Such interactions are stronger in βS than in αS which leads to a more stable monomeric form of βS (Allison *et al.,* 2014). However, certain conditions can stimulate βS aggregation. Yamin *et al.* showed that βS fibrillation can be triggered by the presence of macromolecular crowding agents, heavy metals (Zn^{2+}, Pb^{2+}, and Cu^{2+}), and

pesticides while organic solvents cause the formation of the amorphous βS aggregates (Yamin *et al.,* 2005). βS can also form a high-affinity complex with Cu^{+}-ion which changes the conformation of βS to an α-helix (Miotto *et al.,* 2017). Moreover, a switch of pH to the more acid one (pH 5.8) which is characteristic for some compartments of the cell, e.g. lysosomes, can promote βS aggregation (Moriarty *et al.,* 2017; Landau, 2017). Previously our group showed that βS could form PK-resistant aggregates also *in vivo* which correlated to a dramatic loss of dopaminergic neurons in rats SN (Taschenberger *et al.,* 2013).

Although βS was not found in LB or LN, some histopathological findings showed that it might aggregate also in patients' brains. βS was accumulated in axonal spheroids in PD, DLB and NBIA type 1 brains (Galvin *et al.,* 1999; Galvin *et al.,* 2000). WT-βS was found in Triton X detergent-insoluble fractions but not in LBs of the DLB brains (Wei *et al.,*2007).

1.3.5. P123H and V70M mutants of βS

Although P123H-βS and V70M-βS were discovered in 2004 there are just a few publications devoted to these DLB-associated synuclein species.

Ohtake *et al.,* 2004 suggested that P123H and V70M mutations of βS may have an effect on its tertiary structure and aggregation propensities. Amino acid residues at positions 123 and 70 of βS are highly conserved between vertebrate species. They are identical in human, rat, mice, pig etc (UniProt search). P123H, the proline to histidine substitution at codon 123 results in the reduction of negative charge at the C-terminal region of βS since histidine, unlike proline, has a basic side chain at physiological pH. Proline, in its turn, is uncharged and sterically constrained due to the pyrrolidine ring. The valine to methionine substitution at codon 70 is located to the NAC-domain, which was shown to be important for αS fibrillation. Bulky sulfur group of methionine might also influence confirmation properties of βS with consequent functional implications (Ohtake *et al.,* 2004).

In 2007 Wei *et al.,* showed that stable overexpression of P123H-βS and V70M-βS in the neuroblastoma cell line B103 caused an increase in lysosomal activity and formation of lysosomal inclusion bodies where mutant βS accumulated. These effects were greatly enhanced when αS was co-expressed with the βS mutants (Wei *et al.,* 2007). Addition of gangliosides, inhibited such accumulation of P123H-βS and lysosomal pathology in cultured cells (Wei *et al.,*

2009). Recombinant P123H-βS and V70M-βS were more prone to aggregation than WT-βS under cell-free conditions which suggested a possible connection between toxicity and aggregation properties of these proteins (Wei *et al.*, 2007).

A P123H-βS transgenic mouse line was recently generated. These animals were characterized by neuritic pathology (axonal swellings), astrogliosis, and memory deficits. Histopathological analysis revealed an age-dependent accumulation of insoluble P123H-βS. The double transgene animals obtained by the cross-breeding ofP123H-βS-tg mice and αS-tg mice were characterized by enhanced loss of hippocampal neurons and striatal dopaminergic fibers. Altogether these data suggested a putative causative role of P123H-βS in familial DLB pathology (Fujita *et al.*, 2010). Ultrastructural analysis of axonal swellings in P123H-βS-tg and αS-tg mice revealed the accumulation of autophagosome-like membranous structures in both conditions but only axonopathies of αS-tg mice were positive for LRRK2 and mitochondrial factors cytochrome c, VDAC1, and COX IV (Sekigawa *et al.*, 2012; Sekigawa *et al.*, 2013). However, no mouse line with overexpression of WT-βS or double transgene of WT-βS and αS were generated in these studies for control. One cannot exclude that the observed neuropathology arisen not due to the P123H mutation but due to mere increase in βS concentration due to overexpression.

Already during this Ph.D. project, some conformational propensities of P123H-βS were characterized by Janowska and Baum with biophysical methods on recombinant proteins *in vitro*. ESI-MS experiments revealed more compact conformation of the C-terminal region in P123H-βS than in WT βS acetylated recombinant proteins. Thioflavin T (ThT) spectroscopic assay showed increased fibril formation of co-incubated P123H-βS and αS in contrast to a "WT-βS + αS" condition where fibril formation was delayed. Further biophysical investigation showed that the P123H mutation renders the C-terminus of βS more flexible and more similar in its conformation properties to αS (Janowska and Baum, 2016). Recently, an attenuation of autophagy associated with accumulation of βS was described in the brains of DLB patients. Confirmatory *in vitro* experiments of this study showed that WT-βS can inhibit the autophagy flux, and V70M-βS can cause an even more dramatic reduction in autophagy which might potentially lead to the impairment of protein degradation pathways and neuronal cell death (Evans *et al.*, 2018).

Overall, the extent to which WT-βS, P123H-βS, and V70M-βS are causative for DLB is largely unknown. This work aimed to elucidate if P123H and V70M mutations increase the neurotoxicity of the WT-βS.

1.4. Viral vector-mediated models of neurodegenerative disorders

1.4.1. AAV vectors

Adeno-associated viruses (AAV) are small single-stranded DNA non-enveloped viruses of the *Parvoviridiae* family. AAV is classified as a dependovirus because it cannot autonomously replicate without a so-called helper virus, such as adenovirus, herpesvirus or papilloma virus (Grieger *et al.*, 2012).

The AAV genome consists of only ~4.7 Kb which is one of a few limitations for AAV use. The AAV genome includes 3 major regions: the *rep* gene which encodes 4 replication and integration proteins, the *cap* gene which encodes 3 proteins of the viral capsid, and the inverted terminal repeats (ITR) which flank the *rep* and *cap* genes and serve as the origins of replication. In recombinant AAV vectors, both *rep* and *cap* genes are removed, so these viruses are not able to replicate. A transgene cassette can be then introduced into the AAV genome in place of *rep* and *cap* genes (Ortolano *et al.*, 2012).

AAV vectors have numerous advantages for application in research and gene therapy. AAV is not pathogenic, it has not been associated with any known disease so far. AAV viruses have very low immunogenicity in most experimental animal species. They infect both dividing and quiescent cells and can provide stable long-term transgene expression without causing inflammatory or toxic side-effects. AAV persist mostly in the episomal state which reduces the risk of mutagenic insertions in the DNA. A simple structure of the AAV genome allows straightforward vector design whereby transgene expression can be modulated with simple approaches. For instance, the strength of a promoter can be regulated by changes in the non-coding sequences of 3´-untranslated region (UTR), 5´UTR, enhancer or polyadenylation sites. Cell type-specific promoters can be employed to restrict a transgene expression to a desired cell type, e.g. the human synapsin 1 promoter controls strictly neuron-specific expression (Gray, 2012). Besides, diverse serotypes of AAV viruses have different cellular tropism and transduction properties, which makes them a useful tool for targeting specific cells or tissues, for focal or global gene delivery (Weinberg *et al.*, 2013).

rAAV-mediated gene delivery has demonstrated success in a variety of animal species and tissues. The viral vectors can be applied at any age of the animal which allows studying the role

of a transgene without developmental interference. AAV vectors allow simultaneous delivery of multiple genes and have the potential to expand transgenic research to a variety of model organisms (Burger *et al.*, 2004).

1.4.2. Advantages of AAV animal models for synucleinopathies.

The animal models of NDDs are created in order to recapitulate and study the role of pathophysiological aspects of these diseases. Although not all features of PD or DLB can be recreated in a single animal model, a combination of various model species and approaches can facilitate the completion of the mosaic of synucleinopathies' etiology and pathogenesis.

The main hallmarks of PD are the aggregation of αS in form of LBs and LNs and the progressive loss of dopaminergic neurons in SNpc. Over 30 transgenic mouse lines were generated for overexpression of WT αS (Kahle *et al.*, 2000; van der Putten *et al.*, 2000; Rockenstein *et al.*, 2002), its missense mutations A53T (Giasson *et al.*, 2002), A30P (Neumann *et al.*, 2002), etc., and other PD-related genes such as LRRK2 (Tong *et al.*, 2009), parkin (Lu *et al.*, 2009), DJ1 (Chen *et al.*, 2005) to name a few. These models showed some neuropathological features of PD and DLB such as αS accumulation or aggregation, motor, and cognitive phenotypes, but none of the described so far genetically engineered mouse models shows progressive loss of dopaminergic neurons (Crabtree and Zhang, 2012). Here, AAV animal models appeared to be very useful because time-dependent progressive neurodegeneration in SNpc can be recapitulated in them (Decressac *et al.*, 2012a, b; Taschenberger *et al.*, 2012).

The viral models provide several advantages over genetically engineered mice in addition to the described loss of dopaminergic neurons in SNpc:

- The viral animal models can be produced easier, faster and cheaper than transgenic mouse lines, since a complex cross-breeding is not needed here.
- The expression of a transgene can be – to some extent – restricted to the area of interest by the stereotaxic injection of AAV vectors. The virus can be applied unilaterally and the injected and contralateral sides can be compared. This is especially important for some behavioural tests, which depend on the lesion asymmetry, e.g. the apomorphine test.
- A variety of the AAV serotypes with different cell tropism could be employed.

- The expression level of a PD-related protein can be adjusted simply by changing the viral dose, a promoter, or other regulatory elements in the expression cassette.
- The experiments with viral models can be transferred relatively easy to other species: from rat to mouse or to non-human primates. This gives additional flexibility with experimental design.
- The AAV vectors can be delivered at any age so that even developmentally lethal genes can be studied.

Some possible disadvantages of the AAV viral vectors lie in the variability of results between the laboratories which can be caused even by slight changes of the experimental design, different structure of the expression cassettes, by usage of different AAV serotypes or differences in viral production and titration protocols (Löw and Aebischer, 2012; Volpicelli-Daley *et al.*, 2016). Besides, AAV viral vectors have to be injected into each experimental animal individually using stereotaxic surgery techniques.

1.5. The aim of the project

200 years after the first description of PD patient and 20 years after the recognition of αS as the major component of Lewy bodies, many aspects of synucleinopathies remain unknown. Extensive studies of the disease-associated αS mutations brought many valuable insights into our understanding of molecular processes leading to a toxic conversion of αS, despite these mutations being present in the very rare familial cases. Research on the DLB-associated mutations of βS could shed light on this still elusive and controversial homologue of αS. Although it was claimed before that βS may inhibit αS aggregation and possibly act as a neuroprotective factor in some experimental models (Hashimoto *et al.*, 2001), our lab described the conditions under which βS can induce neurotoxicity *in vitro* and *in vivo* (Taschenberger *et al.*, 2013).

Here, I aimed to study further the abilities of βS to aggregate and induce neurodegeneration *in vitro* in cultured cortical neurons and *in vivo* in rat's Substantia nigra and compare the respective properties with those of the disease-associated mutants of βS: P123H-βS and V70M-βS. I wanted to elucidate if these mutations are indeed causative to neuropathological effects or if they are just coincidental with DLB.

2. Materials and Methods

2.1. Materials

2.1.1. Chemicals

0.9 % NaCl	B.Braun (Melsungen, Germany)
2-log DNA ladder	New England BioLabs (Ipswich, MA, USA)
αSyn, recombinant protein	rPeptide (Bogart, USA)
βSyn, recombinant protein	rPeptide (Bogart, USA)
Aceton	Roth (Karlsruhe, Germany)
Acetic acid	Roth (Karlsruhe, Germany)
Agarose	Sigma Aldrich (Taufkirchen, Germany)
APS	Sigma Aldrich (Taufkirchen, Germany)
Acrylamide	Roth (Karlsruhe, Germany)
B-27 Supplement	Gibco (Karlsruhe, Germany)
Bepanthene	Bayer (Leverkusen, Germany)
Boric acid	Roth (Karlsruhe, Germany)
Braunol	B.Braun (Melsungen, Germany)
Bromphenol Blue	Sigma Aldrich (Taufkirchen, Germany)
BSA	Sigma Aldrich (Taufkirchen, Germany)
Carprieve	Bayer (Leverkusen, Germany)
Coomassie Brilliant Blue R250	Merck (Darmstadt, Germany)
CutSmart buffer	New England BioLabs (Ipswich, MA, USA)
DAPI	Sigma Aldrich (Taufkirchen, Germany)
DMEM	Sigma Aldrich (Taufkirchen, Germany)
DMSO	Sigma Aldrich (Taufkirchen, Germany)
DNAseI	Roche (Basel, Switzerland)
dNTPs	New England BioLabs (Ipswich, MA, USA)
DPX	Fluka (Steinheim, Germany)
EDTA	Merck (Darmstadt, Germany)

Ethanol absolute	Applichem (Darmstadt, Germany)
FCS	Biochrom (Berlin, Germany)
Glycerin	Roth (Karlsruhe, Germany)
Glycine	Applichem (Darmstadt, Germany)
Glucose	Roth (Karlsruhe, Germany)
HBSS 10x	Gibco (Karlsruhe, Germany)
HEPES	Sigma Aldrich (Taufkirchen, Germany)
H_2O_2	Merck (Darmstadt, Germany)
KCl	Roth (Karlsruhe, Germany)
Ketamine	Medistar (Ascheberg, Germany)
L-Glutamine	Lonza (Cologne, Germany)
Laminin	Sigma Aldrich (Taufkirchen, Germany)
Luminol	Calbiochem (Darmstadt, Germany)
LB-agar	Roth (Karlsruhe, Germany)
LB-medium	Roth (Karlsruhe, Germany)
Metapyrin	Serumwerk (Bernburg, Germany)
Methanol	Roth (Karlsruhe, Germany)
$MgCl_2$	Sigma Aldrich (Taufkirchen, Germany)
$MgSO_4$	Roth (Karlsruhe, Germany)
Mineral oil	Sigma Aldrich (Taufkirchen, Germany)
Mowiol - 488	Calbiochem (Darmstadt, Germany)
NaCl	Roth (Karlsruhe, Germany)
$NaHCO_3$ 7.5%	Gibco (Karlsruhe, Germany)
NaH_2PO_4	Roth (Karlsruhe, Germany)
NaN_3	Sigma Aldrich (Taufkirchen, Germany)
NaOH	Applichem (Darmstadt, Germany)
Neurobasal medium	Gibco (Karlsruhe, Germany)
NGS	Biochrom (Berlin, Germany)
Nonfat dried milk	Applichem (Darmstadt, Germany)
p - cumaric acid	Applichem (Darmstadt, Germany)
PageRuler™ Plus, protein ladder	Thermo Scientific (Waltham, MA, USA).

PBS	Applichem (Darmstadt, Germany)
PFA	Roth (Karlsruhe, Germany)
Phusion HF buffer	New England BioLabs (Ipswich, MA, USA)
Phusion HF DNA polymerase	New England BioLabs (Ipswich, MA, USA)
PK	Invitrogen/Thermo Scientific (Darmstadt, Germany)
PLO	Sigma Aldrich (Taufkirchen, Germany)
PSN	Gibco (Karlsruhe, Germany)
Restriction enzymes	New England BioLabs (Ipswich, MA, USA)
Rymadil	Zoetis (Parsippany-Troy Hills, NJ, USA)
SDS pellets	Roth (Karlsruhe, Germany)
Sodium acetate	Sigma Aldrich (Taufkirchen, Germany)
Sucrose	Roth (Karlsruhe, Germany)
TEMED	Roth (Karlsruhe, Germany)
Transferrin	Sigma Aldrich (Taufkirchen, Germany)
Tris base	Applichem (Darmstadt, Germany)
Tris HCl	Applichem (Darmstadt, Germany)
TritonX 100	Roth (Karlsruhe, Germany)
Trypan blue	Sigma Aldrich (Taufkirchen, Germany)
Trypsin	Sigma Aldrich (Taufkirchen, Germany)
Tween20	Applichem (Darmstadt, Germany)
Xylariem	Ecuphar (Greifswald, Germany)
Xylene	Sigma Aldrich (Taufkirchen, Germany)

2.1.2. Antibodies

Table 2.1 Primary antibodies

Antigen	Host species, clonality	Product number	Company	Application	Concentration
6xHis	mouse mono	ab18184	Abcam	WB	1:5000
AU1	mouse mono	MMS-130R	HiSS	WB	1:500
αSyn (Syn211, human)	mouse mono	32-8100	Invitrogen	WB	1:1000
				IHC-IF	1:1000
αSyn (C-20, human)	rabbit poly	sc-7011-R	Santa Cruz	WB	1:1000
				IHC-IF	1:500
Bcl-xL	rabbit mono	2764	Cell Signalling	WB	1:1000
β-Tubulin	mouse mono	T-4026	Sigma	WB	1:5000
βSyn (C-terminal)	rabbit poly	ab6165	Abcam	WB	1:1000
βSyn (aa 81-95)	rabbit poly	SAB1100305	Sigma	WB	1:1000
				IHC-IF	1:1000
βSyn (N-terminal)	rabbit mono	ab76111 (EP1537Y)	Abcam	WB	1:3000
γSyn	rabbit poly	ab6169	Abcam	WB	1:1000
GFP	mouse mono	11814460001	Roche	WB	1:5000
panSyn	rabbit poly	ab6176	Abcam	WB	1:1000
TH	rabbit poly	ab152	Abcam	WB	1:5000
				IHC-DAB	1:3000
TH	mouse mono	T1299	Sigma	IHC-IF	1:1000

Table 2.2 Secondary antibodies

Conjugate	Species	Product number	Company	Application	Concentration
DyLight488	goat-anti- rabbit	115-485-072	Dianova	IHC-IF	1:250
Cy3	goat-anti- mouse	115-165-003	Dianova	IHC-IF	1:250
Biotin	goat-anti-rabbit	BA-1000	Vector Laboratories	IHC-DAB	1:250
HRP	goat-anti- rabbit	sc-2004	Santa Cruz	WB	1:4000
HRP	goat-anti- mouse	sc-2005	Santa Cruz	WB	1:3000

2.1.3. Plasmids

pAAV6-s-SEWB (kindly provided by Dr. Sebastian Kügler)

pAAV6-s-αSyn-SEIS-WB (kindly provided by Dr. Sebastian Kügler)

pAAV6-s-WT-βSyn-SEIS-WB (kindly provided by Dr. Sebastian Kügler)

pAAV6-s-P123H βSyn-SEIS-WB (kindly provided by Dr. Sebastian Kügler)

pAAV6-s-ɣSyn-SEIS-WB (kindly provided by Dr. Sebastian Kügler)

pT7.7-αSyn–Amp (subcloned by Anupam Raina)

2.1.4. Oligonucleotides

5'-αSyn-AU1-Asc:

AAAAAAGGCGCGCCAAACCACCATGGATGTATTCATGAAAGGACTTTCAA

3'- αSyn-AU1-Sbf:

TTTTTTCCTGCAGGTTTCTATTAACCTATATATCGGTATGTATCTCCGGCTTCAGGTTC
GTAGTCTTGA

5'-βSyn-AU1-Asc:

AAAAAAGGCGCGCCAAACCACCATGGACGTGTTCATGAAGGGCCTGTCCA

3'- βSyn-AU1-Sbf:

TTTTTTCCTGCAGGTTTCTATTAACCTATATATCGGTATGTATCTCCCGCCTCTGGCTCATACTCCTGATA

5'-γSyn-AU1-Asc:

AAAAAAGGCGCGCCCCACCATGGATGTCTTCAAGAAGGGCTTCTCCATCGC

3'- γSyn-AU1-Sbf:

TTTTTTCCTGCAGGTTTCTATTAACCTATATATCGGTATGTATCTCCGTCTCCCCCACTCTGGGCCTCCT

5'-αSyn-6xHis-NdeI:

CGGTGTAATCATATGGATGTATTCATGAAAGGACTTTCAAAGGCCAAGGAG

3'- αSyn-6xHis-HindIII:

GCGTTGAAGCTTTTAATGATGATGATGATGATGGGCTTCAGGTTCGTAGTCTTGATACC

5'-βSyn-6xHis-NdeI:

CGGTGTAATCATATGGACGTGTTCATGAAGGGCCTGTCC

3'- βSyn-6xHis-HindIII:

GCGTTGAAGCTTTTAATGATGATGATGATGATGCGCCTCTGGCTCATACTCC

T7 (for sequencing):

TAATACGACTCACTATAGGG

2.1.5. Buffers and Solutions

aCSF(1x): 128 mM NaCl, 30 mM HEPES, 3 mM KCl, 1 mM $MgSO_4$, 1 mM NaH_2PO_4, 10 mM Glucose, pH 7.45; filtered and autoclaved.

Blocking solution for IHC: 5% NGS, 0.1% Triton X-100 in PBS (pH 7.4).

Blocking solution for WB: 5% non-fat dry milk in TBS-T (pH 7.6).

Borate buffer: 150 mM boric acid in was diluted in ddH_2O, pH was adjusted with NaOH to 8.4, then sterile filtered.

CMF-medium: dilute HBSS 1:9 in ddH_2O, add sodium bicarbonat 7.5% until pH 7.2-7.4. The color of solution should be red, not orange or pink.

Coomassie staining solution: 0.1% Coomassie Brilliant Blue R-250, 7.5% acetic acid, 25% methanol, in H_2O.

Coomassie destaining solution: 20% isopropanol, 7.5% acetic acid, in H2O.

DNA loading buffer (6x): 15% Ficoll 400 DL, 100 mM LiCl, 2% glycerol, 100 mM EDTA (pH 8.0), 0.6% SDS, 0.03% BPB in H_2O.

DNAseI: 5 mg of DNAse were dissolved in 1 ml of Ca^{2+}/Mg^{2+} free medium (CMF), aliquoted (100 µl) and stored at -20°C. Final concentration was 5 mg/ml.

ECL 1: 2.5 mM Luminol, 0.4 mM p-Coumaric acid, 0.1 M Tris-HCl; pH 8.5.

ECL2: 18% H_2O_2, 0.1 M Tris; pH 8.5.

Electrophoresis buffer 10x: 1.9M Glycine, 1% SDS, 250 mM Tris-HCl. 1x solution prepared fresh before the SDS-PAGE.

FCS (for cell culture): FCS was thawed, pre-warmed at 37°C and heat inactivated for 30 min at 56°C. 1ml aliquots were stored at -20°C.

HCN medium:5 µg/ml Transferrin, PSN (Penicillin 50 µg/ml, Streptomycin 50 µg/ml, Neomycin 100 µg/ml), 2 mM L-Glutamin, 2% B-27 supplement in Neurobasal medium (NBM).

Incubation solution for primary antibody for IF: 2% NGS, 0.02% NaN_3 in PBS (pH 7.4) with, 0.1% Triton X-100.

Incubation solution for secondary antibody for IF: 2% NGS in PBS (pH 7.4) with 0.1% Triton X-100.

Laminin: Laminin aliquots were stored at -80^{0}C. Laminin was diluted 1:1000 (1 µg/ml) in DMEM before use.

LB medium: 25 g of LB powder was dissolved in 1L H_2O, autoclaved and stored at 4° C. 10 mg/ml ampicillin was added right before the use.

LB agar: 40 g of LB agar was dissolved in 1L H_2O. Solution was aliquoted to 100- or 200-ml portions, autoclaved and stored at 4^{0}C. Upon necessity, an aliquot of LB agar was heated up to 60°C, 10 mg/ml ampicillin was added, and the solution was poured into sterile Petri dishes in a clean bank. Plates were dried o/n, then stored no longer than 2 weeks at 4°C.

Lysis buffer I: 0.5% SDS, 1 mM DTT, 50 mM Tris-HCl pH 8.0, proteinase and phosphatase inhibitors.

Lysis buffer II (PK digestion): 0.5% SDS in PBS, pH 7.4.

Mowiol: 4.8 g Mowiol 4-88 was mixed with 12 g glycerol. Then 6 ml of water was added and solution was stirred for 3h at RT. After Mowiol dissolved the solution was clarified by centrifugation at 5000 x g for 15 min. Then Mowiol was aliquoted and frozen (-20°C) for long-term storage or kept at 4° C for short-term storage. Mowiol was warmed up at 37^0C for 30 min before each use.

PFA 4%: 40 g PFA, 9.55 g PBS powder in 1L ddH_2O, add 1 ml NaOH for better dissolving of PFA, gently heat to 60° C for ~1 h (until PFA is completely dissolved). Adjust pH to 7.4, filter. Keep at 4^0C no longer than 1 week.

PBS: 9.55 g PBS powder in 1L ddH_2O; filtered, autoclaved.

Poly-D-ornithine (10x): 50 mg of poly-D-ornithine was dissolved in 50 ml of sterile and filtered borate buffer. 1x solution (0.1 mg/ml) was prepared before use by dilution in sterile H_2O.

SDS-Sample buffer (6x): 350 mM Tris-HCl, pH 6.8; 10% SDS, 0.6 M DTT, 30% Glycerol, 0.03% BPB.

SOC++ medium: 2% bacto-tryptone, 0.5% yeast extract, 2.5 mM KCl, 10 mM $MgCl_2$, 10 mM $MgSO_4$, 10 mM NaCl, 20 mM glucose, pH 7.0.

TE (1x): 10 mM Tris-HCl (pH 7.4) and 1 mM EDTA (pH 8.0).

TBE (1x): 42 mM boric acid, 10 mM EDTA, 50 mM Tris-HCl, set to pH 8.0.

TBS (antigen retrieval): 150 mM NaCl, 10 mM Tris-HCl, pH 9.0

TBS (DAB staining protocol): 0.1MTris-HCl and 150 mM NaCl, pH 7.4.

TBS-T (10x): 1.5M NaCl, 200 mM Tris, 0.1% Tween 20, pH 7.6. 10x solution was stored at 4^0C.

Transfer buffer (1x): 192 mM Glycine, 25 mM Tris-HCl, 20% Methanol. The buffer has to be automatically at pH 8.3, pH cannot be adjusted. Addition of Methanol here is exothermic; therefore, the buffer has to be prepared 1 day in advance and to be cool down to 4^0C.

Trypsin 0.25%: 25 mg Trypsin in 10 ml CMF, sterile filtered

Tris pH 6.8(4x): 0.5 M Tris-HCl, 100 ml H_2O, pH 6.8.

Tris pH 8.8 (4x): 1.5 M Tris-HCl, 100 ml H_2O, pH 8.8.

2.1.6. Kits

BCA protein assay kit, Pierce	Thermo Scientific (Rockford, IL, USA)
DNA gel extraction kit	Quiagen (Hilden, Germany)
DAB Peroxidase Substrate Kit SK-4100	Vector Laboratories (Burlingame, USA)
Gel Extraction Kit	Quiagen (Hilden, Germany)
HRP Substrate Pico, Immobilon Western	Millipore (Billeria, USA)
HRP Substrate Femto, SuperSignal West Femto	Thermo Scientific (Rockford, IL, USA)
Miniprep kit	Quiagen (Hilden, Germany)
Megaprep kit	Macherey Nagel (Düren, Germany)
PCR purification kit	Quiagen (Hilden, Germany)
VECTASTAIN ABC Peroxidase Standard Kit PK-4000	Vector Laboratories (Burlingame, USA)
VECTASTAIN ABC Peroxidase Elite Kit PK-6100	Vector Laboratories (Burlingame, USA)

2.1.7. Animals, cell lines and electrocompetent cells

Wistar rats, Janvier (for *in vivo* experiments)

Wistar rats, Central Animal Facility, University of Göttingen (for primary cell culture)

DH5α*E. Coli* strain, ElectroMAX

BL21 (DE3) *E. coli* strain, Invitrogen

SURE®*E. coli* strain, Stratagene

HEK293 cells, Stratagene

2.1.8. Equipment and consumables

24-well sterile cell culture plates	Greiner bio-one (Frickenhausen, Germany)
96-well micro-test plate	Sarstedt (Nümbrecht, Germany)
Autoclave	Systec (Linden, Germany)
Bacterial incubator, Certomat IS	B.Braun (Melsungen, Germany)
Bead mill homogenizer Precellys 24	Peqlab (Erlangen, Germany)
Biophotometer	Eppendorf (Hamburg, Germany)
Capillary pipet tips for gel wells	Biozym Scientific (Oldendorf, Germany)
Cell culture incubator, Hera	Unity Lab Services, part of Thermo Fisher Scientific GmbH (Schwerte, Germany)
Centrifuge, Heraeus Megafuge 1.0R	Unity Lab Services, part of Thermo Fisher Scientific GmbH (Schwerte, Germany)
Clean bank, Hera guard, Heraeus	Unity Lab Services, part of Thermo Fisher Scientific GmbH (Schwerte, Germany)
Cover slides, 24 x 60 and 24 x 55 mm	Menzel (Braunschweig, Germany)
Cover slides, diameter 12 mm	Menzel (Braunschweig, Germany)
Cryostat CM 3050S	Leica Microsystems (Mannheim, Germany)
Cryomatrix	Thermo Scientific (Waltham, CA, USA)
DNA electrophoresis chamber	Bio-Rad (Munich, Germany)
Drill tip 0.8 mm	Dremel (Breda, Netherlands)
Electrophoresis power supply, E835	Consort (Turnhout, Belgium)
Freezer -80^{0}C, Herafreeze	Unity Lab Services, part of Thermo Fisher Scientific GmbH (Schwerte, Germany)
Gel Documentation 2000TM UV Transilluminator	Bio-Rad (Munich, Germany)
Glass capillaries, 3.5 nanoliter	World Precision Instruments (Sarasota, FL, USA)

High temperature cautery kit	Bovie medical corporation (Clearwater, FL, USA)
Ice machine	Zigra (Isernhagen, Germany)
Insulin syringes, U-100, BD Micro-Fine	BD Medical (Franklin Lakes, NJ, USA)
Microcentrifuge 5415R	Eppendorf (Hamburg, Germany)
Micro drill	Proxxon (Wecker, Luxemburg)
Micro injector Nanoliter 2000	World Precision Instruments (Sarasota; Fl, USA)
Micro pipette puller P97	Satter Instruments Company (Novato, CA, USA)
Micro syringe pump controller, Micro4	World Precision Instruments (Sarasota; Fl, USA)
Micro tube 2 ml, PP	Sarstedt (Nümbrecht, Germany)
Microscope Axio Observer.Z1	Carl Zeiss Microscopy (Jena, Germany)
Microscope Axioplan 2	Carl Zeiss Microscopy (Jena, Germany)
Microscope Imager D2	Carl Zeiss Microscopy (Jena, Germany)
Mini-PROTEAN Tetra Cell system	Bio-Rad (Munich, Germany)
Mini Trans-Blot Cell system	Bio-Rad (Munich, Germany)
Neubauer counting chamber	Brand (Wertheim, Germany)
Nitrile examination gloves, Micro-Touch	Ansell (Brussel, Belgium)
Nitrocellulose membrane, 0.22 µm pore size	AppliChem (Darmstadt, Germany)
Parafilm M	Bemis NA (Neenah, WI, USA)
Pasteur capillary pipettes	Sigma Aldrich (Taufkirchen, Germany)
Peristaltic perfusion pump	Ismatec (Wertheim, Germany)
Pipette controller, acu-jet pro	Integra (Bibertal, Germany)
Precellys 24 Zirconium oxide beads 1.4 mm	Bertin instruments (Hamburg, Germany)
Protein LoBind tube, 0.5 and 1.5 ml	Eppendorf (Hamburg, Germany)

Purple nitrile-XTRA exam gloves	Halyard (Zaventem, Belgium)
Sterile bank, LaminAir HB 2448	Unity Lab Services, part of Thermo Fisher Scientific GmbH (Schwerte, Germany)
Sterling nitrile exam gloves	Halyard (Zaventem, Belgium)
Spacer plates and short plates	Bio-Rad (Munich, Germany)
Spinal needle diameter 1.2 mm	Vygon (Ecouen, France)
Stereotactic frame, rat jaw holder, ear bars	David Kopf Instruments (Tujunga, CA, USA)
SuperFrost Plus Microscope Slides	Menzel (Braunschweig, Germany)
Surgical instruments	Fine Science Tools (Essen, Germany)
Tecan Spark 10M plate reader	Tecan Group Ltd (Männedorf, Switzerland)
Thermocycler PTC-150 MiniCycler	MJ Research Inc. (St. Bruno, Canada)
Transilluminator, Chemi Doc XRS+	Bio-Rad (Munich, Germany)
Ultrasonic homogenizer UW 2070	Bandelin electronics (Berlin, Germany)
Water bath GFL	Schütt Labortechnik (Göttingen, Germany)
Whatman blotting paper	GE Healthcare (Chalfton St. Gilles, UK)

2.1.9. Software

AxioVision 4.8 (Carl Zeiss Microimaging)
Clone Manager 6 (Scientific & Educational Software, NC, US)
Finch TV 1.4.0 (N.I.H.)
G*Power version 3.0.10. (University of Düsseldorf)
GraphPad Prism 7.02 (GraphPad Software, Inc.)
ImageJ 1.50e (N.I.H.)
Image Lab (Bio-Rad)
Leica Application Suite Advanced Fluorescence 2.7.3.9723 (Leica Microsystems CMS)
MS Office (Microsoft)

Quantity One 4.6.9 (Bio-Rad)

Spark Control Magellan 1.2 (Tecan)

Stereo Investigator 9.14.5 (Micro Bright Field Inc.)

Zen 2.3 (Zen pro and Image processing) (Carl Zeiss Microimaging)

2.2 Methods

2.2.1. Molecular cloning

In terms of the doctoral research project, the next cloning procedures were performed:

- cDNA for V70M-βS was cloned into the pAAV6-s-synuclein-SEIS-WB and pAAV2-s-synuclein-WB plasmisds via MluI and SphI restriction sites.
- The AU1 tag was introduced at the C-terminal of αS, WT-βS, P123H-βS, and γS, and the cDNAs were cloned into pAAV6-s-synuclein-SEIS-WB plasmid via Asc and Sbf restriction sites.
- The 6xHis tag was introduced at the C-terminal of αS, WT-βS, P123H-βS, V70M-βS and γS and the cDNAs were cloned into T7.7 plasmid via NdeI and HindIII restriction sites

All procedures were performed according to the standard molecular cloning protocols as described in «Molecular Cloning: A Laboratory Manual» Green MR and Sambrook J, 2012. Primers were designed and all cloning procedures were simulated with Clone Manager 6 software (Scientific & Educational Software, NC, US).

2.2.1.1. PCR amplification

PCR amplification of the sequences of interest was carried out in a thermocycler PTC-150 MiniCycler (MJ Research Inc., Canada). The 100 µl reaction mix contained: 1 µl of Phusion HF DNA Polymerase, 20 µl of 5x Phusion HF buffer (New England BioLabs, USA), 2 µl of 10 mM dNTPs (dATP, dCTP, dGTP, dTTP), 5 µl of 10 µM forward primer, 5 µl of 10 µM reverse primer (Sigma, see section 2.1.4. Oligonucleotides), 5 ng DNA, 3% DMSO and 2 mM $MgCl_2$, filled to 100 µl with ddH_2O. The PCR reaction was performed following the next steps:

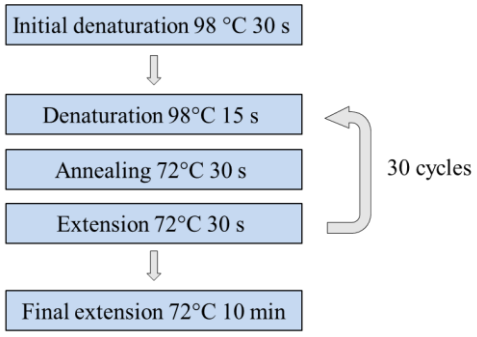

Then the reaction mix was placed on ice, PCR purification was performed (PCR purification kit, Qiagen), and the products of the PCR amplification were analyzed for their size with electrophoresis on 1.7% agarose gels (see section 2.2.1.4).

2.2.1.2. DNA precipitation

DNA precipitation was performed in order to increase the concentration and purity of DNA samples before the next molecular cloning procedures. A DNA eluted from the agarose gel or a purified PCR product was mixed with 2.5 volumes of ice-cold 100% ethanol and 1/10 volume of 3M sodium acetate (pH 5.0). The mixture was briefly vortexed and left for precipitation o/n at -20^{0}C. Next, the mixture was centrifuged 30´ at 13 000 rpm at 4^{0}C, 100% ethanol supernatant was removed, and ice-cold 70% ethanol was added. The mix was centrifuged again 30´ at 13 000 rpm at 4^{0}C. Then the 70% ethanol supernatant was carefully removed, the pellet was dried at RT and DNA was resuspended in 1x TE buffer.

2.2.1.3. Quantification of DNA concentration

DNA concentration was determined by the spectrophotometric method using Eppendorf Biophotometer. Optical density (OD) of a sample was measured at 260 nm to determine a DNA concentration. Additionally, the ratio OD_{260}/OD_{280} was used to evaluate protein contamination (an expected value for the pure DNA is ~1.8). Absorbance reading at 230 nm was performed in order to evaluate possible contamination with ethanol or salts (a value for OD_{260}/OD_{230} was expected to be above 1.5).

2.2.1.4. DNA restriction and agarose gel electrophoresis

For a restriction digest reaction, 5 to 10 µg of a plasmid DNA and 500-600 ng of a PCR product were used. Restriction enzymes and CutSmart buffer (New England BioLabs, USA) were added to DNA and incubated for 2h in a 37^{0}C water bath. The sizes of the obtained DNA fragments were verified on an analytical agarose gel. The gels with 0.8% of agarose were used to verify the size of a backbone construct (~3000 bp), and the 1.7% gels were used to determine the exact size of an insert (~500 bp). To prepare the gel, agarose was dissolved in 1x TBE buffer by boiling in a

microwave oven for 2 min, and 3 µl of EtBr was added to the solution before pouring the gel. For an analytical gel, the samples were prepared by mixing ~100 ng of DNA, DNA loading dye (6x) and 1x TE buffer to the final volume of 10 µl. DNA samples were loaded onto the polymerized gel in parallel with the 2-log DNA ladder. Gels were run at 80 V in 1x TBE buffer long enough to obtain good separation of the bands. DNA bands were visualized with UV-light at the Gel Documentation 2000TM UV Transilluminator (Bio-Rad) using Quantity One software.

If DNA fragments had the expected size, the rest of the restricted DNA samples were run on preparative 0.8 or 1.7% agarose gels as described above. The desired bands were cut out under UV illumination and the gel extraction was performed according to the instructions to the QIAGEN gel extraction kit.

2.2.1.5. DNA ligation and E. coli transformation

To perform a ligation, a vector and an insert DNA were mixed in 1:3 molar ratios. After the DNA mixture was incubated 5´at 45^0C, 1 µl T4 DNA Ligase and T4 ligation buffer were added (final volume of the reaction mix = 10 µl). The ligation reaction mix was incubated for 25´at 16°C, then for 10´ at 25°C. Afterwards, the reaction mix was placed on ice and used for transformation into *E. coli* cells.

In case of all pAAV plasmids for viral vector production, SURE® *E. coli* cells (Stratagene, La Jolla, USA) were transformed via electroporation. The name of the strain - SURE®- means Stop Unwanted Rearrangement Events. These electrocompetent cells were used in order to prevent the corruption of ITR sequences in pAAVs. For the transformation, 80 µl of SURE® cells glycerol stock was thawed on ice, mixed with 2 µl of a DNA ligation product, transferred to a pre-cooled cuvette and subjected to the 1.8 kV electroporation pulse in Bio-Rad Gene Pulser II. Immediately after the electroporation, 800 µl of SOC++ medium (pre-warmed in the water bath to 37^0C) was added to the cuvette, cells were transferred to a sterile tube and then incubated for 45´ at 37^0C incubator with moderate shaking.

DH5α *E. coli* strain (ElectroMAX) was used for transformation when several pre-cloning steps were necessary. Chemically competent DH5α *E. coli* cells provide easier transformation and a higher number of colonies than SURE® *E. coli* cells.

BL21 DE3 competent *E. coli* cells (Invitrogen, Karlsruhe, Germany) were used for the transformation of pT7.7 plasmids and following production of recombinant proteins. Transformation of DH5α and BL21 DE3 *E. coli* cells was performed with the next steps: 50 µl of thawed *E. coli* cells were mixed with 1 ng of a plasmid DNA from the ligation reaction on ice. The mix was kept on ice for 30´ without stirring. Then bacteria were heat-shocked for exactly 30 sec at 42°C and placed on ice again for 5´. Bacteria were supplied with 950 µl of pre-warmed SOC++ medium and incubated at 37°C for 1h under 230 rpm shaking.

After the transformation, SURE®, DH5α and BL21 DE3 bacteria were plated onto the pre-warmed in the 37°C incubator LB agar plates. All plasmids, described in this thesis, contained the ampicillin-resistance gene, therefore LB agar always contained 100µg/ml ampicillin. LB agar plates were incubated at 37°C for 14-15 h and single clones were picked for the follow-up procedures.

2.2.1.6. Plasmid Mini- and Megaprep

Plasmid DNA was extracted and purified from the transformed *E. coli* cells on a small and large scale with Mini- and Megaprep protocols respectively. For a Miniprep plasmid purification, a single clone of bacteria was picked from the LB agar plate and inoculated to the 10 ml of ampicillin-containing LB medium which was then incubated for 14-15 h at 37^0C with vigorous shaking (190 rpm). For a Megaprep, 2 L of LB medium containing 100 µg/ml ampicillin was inoculated with 2 ml of LB bacterial culture. The culture was divided into four 2 L flasks and incubated for 15 h at 37^0C with moderate shaking (110 rpm). The bacterial cells were harvested by centrifugation at 8 000 rpm for 5´ at RT. Bacterial pellets were used for DNA plasmid extractions with the QIAprep Spin Miniprep kit (Qiagen) and NucleoBond® PC 2000 Megaprep kit (Macherey Nagel) according to the protocol of the manufacturer. The main steps of the protocol included: RNA degradation with RNAse, alkaline lysis of bacterial cell walls and membranes, removing of cellular debris with centrifugation, loading supernatant to an ion exchange column, washing out chromosomal DNA and proteins with the high-salt solution, and elution of plasmid DNA with low-salt buffer. An eluted DNA was precipitated and resuspended in 1x TE buffer as described in the section 2.2.1.2. Control digestion followed every Mini- and Megaprep of plasmid DNA.

2.2.2. AAV vector production and purification

All viruses were kindly provided by Dr. Sebastian Kügler. The vectors for the *in vitro* experiments were packaged in the AAV6 capsid. The vectors for the *in vivo* experiments were packaged in the AAV2 capsid. Vector production and purification were performed as previously published in Kügler *et al.*, 2007. In short, AAV vectors were propagated in HEK293 cells. HEK cells were seeded at 1-1.2 x 10^8 cells per cell factory in DMEM medium containing 10% FCS and 1% PS. After reaching ~50% confluency, HEK293 cells were transfected with AAV plasmid and pDG helper plasmid with the calcium-phosphate method. The cells were supplied with 2% FCS medium during the transfection and 10% FCS medium afterward. The cells were harvested and lysed using citric saline ~2 days after transfection. Viral particles were then purified by iodixanol step gradient ultracentrifugation, followed by fast protein liquid chromatography (FPLC) and dialysis against PBS. The purity of the virus was confirmed with SDS-PAGE and Coomassie staining. The virus titer (vector genome copies) was determined by qPCR. Since it was assumed that every 30th viral particle is infectious, viral concentration in transduction units corresponded to 1/30 of the concentration in vector genome copies, e.g. 1x10^8 tu = 3x10^9 vg. During all procedures dealing with AAV vectors, 0.5% SDS water solution was used for disinfection.

Genetic content of all AAV vectors used in this thesis is schematically described in Figure 2.1:

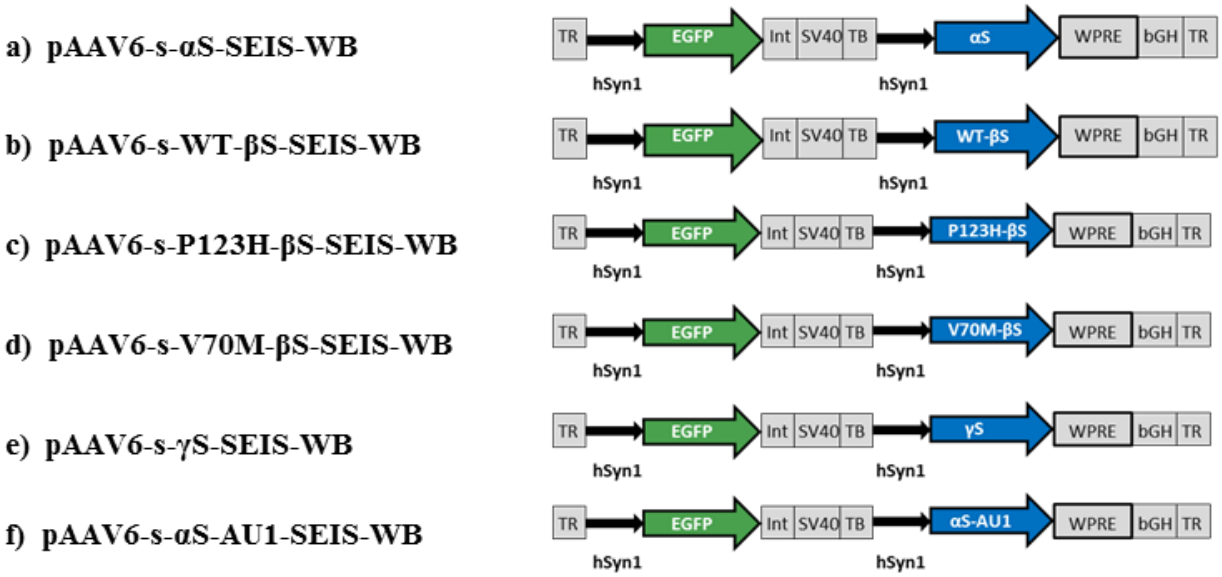

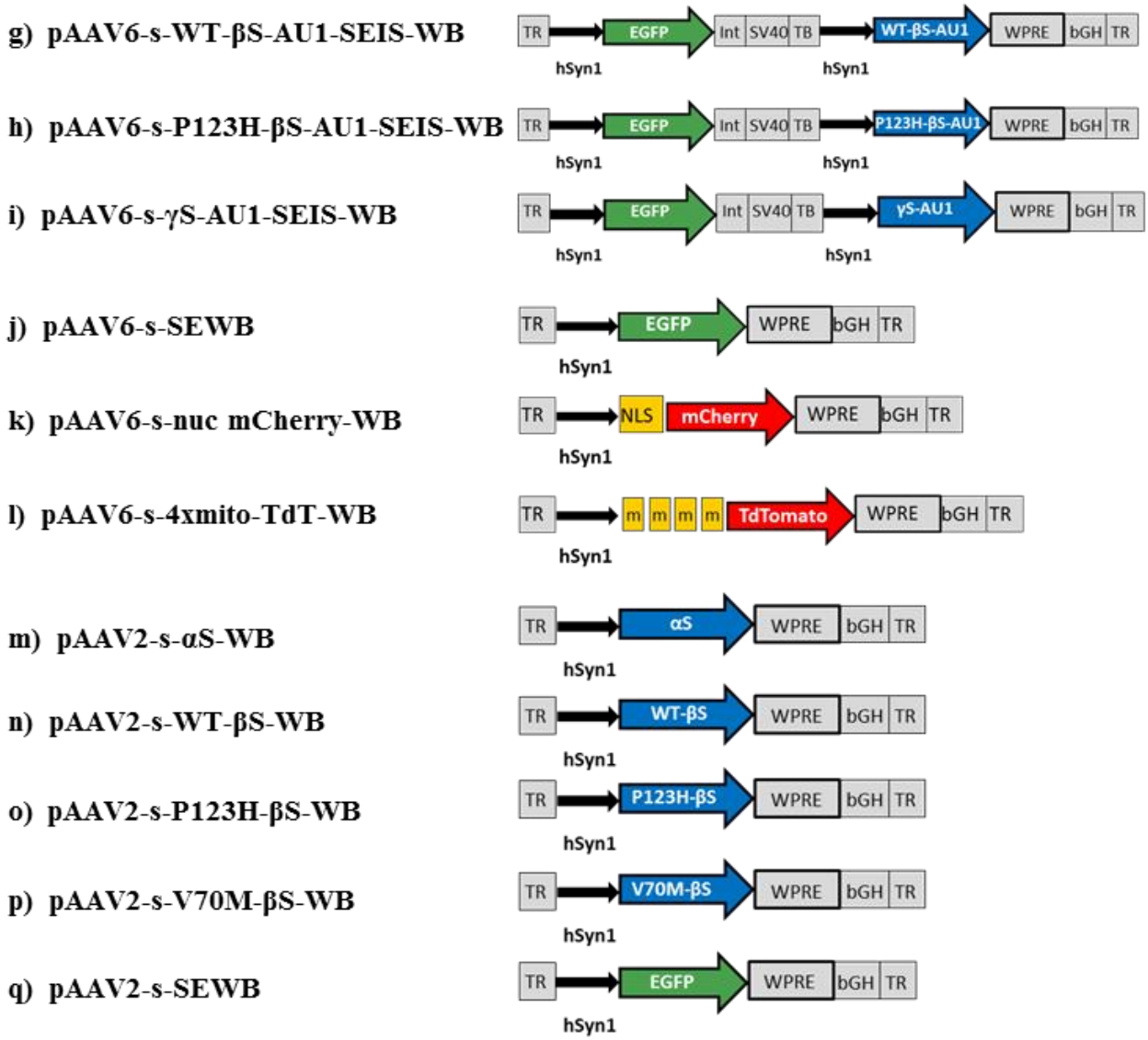

Figure 2.1.Structure of the AAV vector genomes. Bicistronic AAV6 vector which includes a cDNA for humansynuclein (either αS, WT-βS, P123H-βS, V70M-βS or γS) and the cDNA for EGFP were constructed for expression in primary cortical neuron culture **(a-e)**. cDNAs for αS, WT-βS, P123H-βS or γS with the sequence for the C-terminal AU1-tag were cloned into bicistronic AAV6 plasmids **(f-i)**. Monocistronic AAV6 vector carrying the cDNA for EGFP was used as a control in primary culture experiments **(j)**. Monocistronic AAV6 vector carrying the cDNA for mCherry with nuclear localization was used for expression in primary neurons **(k)**. Monocistronic AAV6 vector had the cDNA for TdTomato, equipped with 4 copies of mitochondrial localization sequences and was used for overexpression in primary neurons **(l)**. Monocistronic AAV2 vectors with sequences for human αS, WT-βS, P123H-βS or V70M-βS were used for targeted expression in rat's SN **(m-p)** and AAV2 vector with the cDNA for EGFP was used as a control in *in vivo* experiments **(q)**. Expression of the transgenes was controlled by neuron-specific human synapsin 1 gene promoter (hSyn1) and enhanced by Woodchuck hepatitis virus posttranscriptional regulatory element (WPRE). Int - intron; SV40 - SV40 polyadenylation site; bGH - bovine growth hormone gene polyadenylation site; TR - inverted terminal repeats; NLS – nuclear localization sequence; m - mitochondrial localization sequence.

2.2.3. Primary cell culture

2.2.3.1. Preparation of coverslips and plates coating

Preparation and maintenance of neuronal culture were performed according to Yavin *et al.*, 1973 (with modifications).

Prior to culturing of primary cortical neurons, sterile 24-well plates were coated with Poly-L-Ornithine (PLO) and laminin to ensure optimal cell growth and adhesion. PLO is a positively charged synthetic amino acid, which enhances attachment of the neurons to glass and plastic surfaces. Laminin is one of the major extracellular matrix (ECM) glycoproteins which can be found in the basement membranes. It improves cell adhesion and supports the growth of neurites.

For experiments on mitochondria morphology and motility, plates with glass coverslips were used. In all other *in vitro* experiments, neurons were plated without coverslips.

Coverslips of 12 mm in diameter (Menzel, 4003030) were cleaned in 1M HCl under agitation at RT overnight (the acid wash method). Afterward, coverslips were extensively rinsed with ddH_2O 3 times. Before being placed into a 24-well plate, each coverslip was sterilized by high temperature (backed in the oven at 200^0C for several hours).

10x PLO stock solution was diluted to 1x (0.1 mg/ml) in the sterile water right before use, and 500 µl 1x PLO was applied to each well. Plates were sealed with Parafilm and incubated at RT for 24 h. Then, plates were placed at 4^0C for 1 week. Before coating with laminin, PLO was aspirated and plates were washed twice with sterile H_2O. Laminin was diluted 1:1000 (1 µg/ml) in DMEM and 500 µl/well were applied. Plates were incubated with laminin overnight at 37^0C, 5% CO_2, and 95% humidity. On the day of cell seeding, plates were washed 2x with DMEM, 500 µl/well of 37^0C-pre-warmed HCN medium was added. Corner wells and all other empty wells were filled with sterile PBS in order to minimize evaporation of the culture medium.

2.2.3.2. Dissection and cell preparation

Primary cortical neurons were obtained from E17.5 (embryonic day 17.5) Wistar rats. All surgical procedures were performed on ice and in CMF medium. Embryos were decapitated, cortices were dissected, and hippocampi were removed (as described in Pacifici *et al.*, 2012). Pieces of cortical tissue were collected in 15 ml CMF medium, centrifuged at 800 rpm, 4 min,

and 4^0C. CMF medium was aspirated and 1 ml of 0.25% trypsin in CMF was added for cell dissociation. After 10 min trypsin incubation in 37^0C water bath, 50 µl of DNAseI was added for 1 min in order to dissolve DNA aggregates from the damaged cells. Immediately after, trypsin activity was stopped by applying 1 ml ice-cold FCS. The tissue was dissociated by gentle trituration with a specially prepared Pasteur pipette (tip of the pipette was cut off and fire-polished). After centrifugation for 4 min, 800 rpm at 4^0C cells were resuspended in the HCN medium (1 ml per embryo). An aliquot of neurons was stained with trypan blue to assess the viability of cells, and living cells were counted in the Neubauer counting chamber. Neurons were seeded at a density 250 000 cells/well in 750 µl of the HCN medium in PLO/laminin coated plates without coverslips. For plates with coverslips, a drop of the medium, containing 75 000 cells was applied onto each coverslip; then plates were placed in the 37^0C incubator for 50 min; then the volume of HCN medium was increased to 750 µl/well.

2.2.3.3. Culturing and virus transduction

Primary cultures were maintained in HCN medium at 37°C in 5% CO_2, and 95% humidity. No medium replenishment was performed for the duration of the culture (up to 30 days) since our initial experiments showed no difference in cell survival between groups with and without medium replenishment.

Neurons were transduced on the day in vitro (div) 3 with AAV vectors of serotype 6. Structure and concentrations of AAV6 vectors are described in details in the "Result" section, relevant to each experiment. AAV6 vectors were diluted to the appropriate concentration in sterile filtered ice-cold PBS so that 10 µl of dilution was applied per well. Plates were gently agitated in an 8-shape movement to provide even spreading of the viral vector in the well.

2.2.4 Preparation of lysates

2.2.4.1. Primary cortical cell culture

After careful aspiration of the medium, plates were washed twice with ice-cold PBS. PBS was completely removed, plates were covered with Parafilm and stored in the -80^0C freezer until further procedures. For the cell lysis, plates were thawed on ice for 15 min. 25 µl of lysis buffer was applied per well of 24-well plate and cells were scraped while holding the plate in a tilted

position. Lysis buffer II, which contained PBS (pH 7.4) and 0.5% SDS, was used for all lysates subjected to PK digestion assay. No proteinase inhibitors were added there. For all other applications lysis buffer, I was used (0.5% SDS, 1 mM DTT, 50 mM Tris-HCl pH 8.0, and proteinase and phosphatase inhibitors). Lysed cortical cells were collected in 1.5 ml Eppendorf tubes. Lysates were sonicated with the ultrasonic homogenizer (UW 2070 Bandelin electronics, Berlin) for 10 sec with 20% power. Then lysates were cleared by centrifugation for 10 min, at 3 400 rpm and 4^0C. Supernatants were collected into the fresh Eppendorf tubes and kept on ice until protein concentration measurement.

2.2.4.2. Rat brain

Brains of the Wistar rats were collected 3 weeks after the unilateral injection of AAV2 vectors into the left SN (see section 2.2.7. Animal procedures). Rats were sacrificed by CO_2 inhalation. Brains were surgically removed and snap-frozen on dry ice (without PBS or PFA perfusion) and stored at -80^0C. The samples of cortex, striatum and Substantia nigra were collected with spinal needles with 1.2 mm outer diameter and ~1 mm inner diameter (VYGON, REF 183.92) on the Leica Cryostat. The sharp edge of the spinal needle was removed by grinding and polishing, and needles were washed with 70% ethanol and ddH_2O. Figure 2.2 shows the sites where the pieces of tissue were collected.

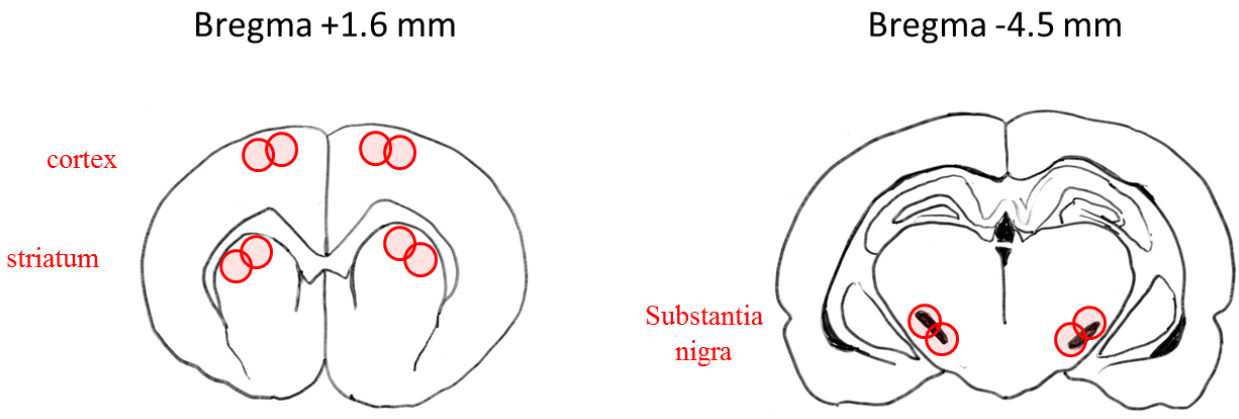

Figure 2.2. Sites of the collection of the brain tissue samples. Samples of cortex, striatum, and SN were collected from the left and right side of the brain starting from the coronal sections with coordinates +1.6 mm and -4.5 mm from bregma. Red circles represent spinal needle application sites.

Two “picks” with the needle were done for each site and sample. With each “pick” a cylinder piece of tissue with ~1.5mm length and ~1mm in diameter was collected. Such 2 small pieces of tissue from 1 site were placed into a 2 ml micro tube (Sarstedt, REF 72.694.006). The micro tubes were prepared beforehand: 100 µl of magnetic beads or ~ 35 beads (Precellys 1.4 mm bulk beads) were added to each tube, micro tubes were labeled, weighted and cooled down in the cryostat.

The tissue samples were weighted in the micro tube, and the weight of the tissue was calculated. The weight of each probe (2 small pieces of tissue from 2 picks) was approx. 5 to 10 mg (0.005 to 0.01 g). 250 µl of the lysis buffer (0.5% SDS in PBS) was added to each micro tube. No proteinase or phosphatase inhibitors were added to the buffer in order not to interfere with the following PK digestion (see section 2.2.5. Proteinase K digestion). Tissue was homogenized with a Precellys 24 homogenizer (3 cycles of 45 sec homogenization, 6 800 rpm). Micro tubes with lysates were centrifuged 10 min at 4^0C and 3400 rpm to spin down the beads. Supernatants were collected into fresh 1.5 ml Eppies and were cleared by centrifugation (10 min, 4^0C, 3400 rpm). Lysates were collected into 1.5 ml Eppies and stored at -80^0C until PK digestion and protein analysis by immunoblotting.

2.2.5. Proteinase K digestion

Proteinase K is an alkaline serine protease which shows strong proteolytic activity on a variety of native and denaturated proteins in a wide range of pH and temperatures (Ebeling *et al.*, 1974). The name of proteinase K comes from its ability to hydrolyze keratin. This enzyme was originally purified from the fungus *Tritirachium album* and is commonly used for cleaning up enzymatic reactions from protein contaminants. Although PK can hydrolyze a variety of peptide bonds, β-sheets demonstrate resistance to PK. This specificity is commonly used to analyze fibrillation state of prions and other misfolded and aggregated proteins, including α-synuclein (Neumann *et al.*, 2002; Sajnani *et al.*, 2012).

After protein concentration was calculated, lysates of primary cortical neurons and brain lysates were diluted in PBS/0.5% SDS buffer to the final protein concentration of 2 µg/µl. The same volumes of diluted lysates were taken for the PK digestion in each condition. PK solution (Invitrogen) of the original concentration of 20 mg/mL was diluted 1:200 (0.1 mg/mL) in ice-cold

PBS, and this "stock" solution was then diluted further if lower concentrations of PK were needed. PK was applied to lysates in ratio 1:10. The final concentration of PK in most experiments was 2-4 µg/mL. PK concentrations from 0.01 to 10 µg/mL were used to establish the assay. Lysates were divided into 2 equal parts: 0´ (minutes) and 5´ groups. An equal volume of PK was added to both parts. Lysates were well mixed with PK, and Eppendorf tubes were very rapidly spun down, and the test tubes which were intended for digestion were placed in the Thermomixer at 37^0C for 5´. Digested lysates were then immediately placed on ice, 6xSDS-sample buffer was added, and lysates were boiled for 5´ at 95^0C. At this temperature Proteinase K was completely deactivated. Protein samples were then analyzed by immunoblotting or stored at -20^0C.

2.2.6. Immunoblotting

2.2.6.1. BCA assay for protein concentration measurements

The concentration of proteins in the sample was determined with the BCA (bicinchoninic acid) assay. This method is based on the ability of proteins to reduce Cu^{2+} to Cu^{+} in basic condition and the formation of purple chelate complexes of Cu^{+}-ions and BCA. The amount of the colored product is directly proportional to the amount of Cu^{+} ions and to the protein concentration which can be then determined with colorimetric techniques. A chelate complex of Cu^{+} and bicinchoninic acid exhibits maximal light absorbance at a wavelength of 562 nm. Principles of the BCA reaction are described in detail in Smith *et al.*, 1987.

BCA reaction was performed in 96-well test plate. Reagents A and B of the BCA protein assay kit (Thermo Scientific) were mixed in proportion 50 to 1 according to the manufacturer's instructions. This working solution was added to the wells of 96-well plate in the way that the total volume of reagent A+B and lysate would be 200 µl in each well. Bovine serum albumin (BSA) was used as a standard. In order to generate a standard curve, BSA dilution series of 0, 0.3125, 0.625, 1.25, 2.5, 5, 10, and 20 µg/well were tested in parallel with the experimental samples. All samples were tested in duplicates. Test plate was sealed and incubated for 35´ at 37^0C. The absorbance was measured at the wavelength 562 nm with Tecan Spark 10M plate reader and Spark Control Magellan 1.2 software. Calculations of protein concentrations were performed in Microsoft Excel. The standard curve was plotted as a function of absorbance (y) to

a protein concentration (x) and had to have $R^2 > 0.998$. Protein concentrations in the samples were calculated from the mathematic equation which was drowned from the standard curve function.

2.2.6.2. SDS polyacrylamide gel electrophoresis (SDS-PAGE)

SDS-PAGE is a technique for separation of charged proteins in the electric field according to their molecular masses. Anionic surfactant SDS is used here to linearize polypeptides and to cover them with the negative charge in order to facilitate the migration of molecules towards the positive pole in the electric field. Polyacrylamide gel provided a meshwork where smaller proteins can move faster than the big ones in the electric field. In more details the principles of SDS-PAGE are described in Laemmli, 1970 and Cleveland *et al.*, 1976.

Two-phased gels (12% or 15% resolving and 5% stacking gels) were prepared as described in the table below (Table 2.3). Gels were usually pre-casted 1 day in advance to gel electrophoresis and kept maximally 1 week at 4^0C covered with wet paper.

Table 2.3 Composition of polyacrylamide gels

	Stacking Gel	**Resolving Gel**	
	5%	**12%**	**15%**
Acrylamide 30%	430 µl	4 ml	5 ml
4x Tris pH 8.8	-	2.5 ml	2.5 ml
4x Tris pH 6.8	830 µl	-	-
SDS 10%	33 µl	100 µl	100 µl
H_2O	2 ml	3.34 ml	2.34 ml
10% APS	16.5 µl	50 µl	50 µl
TEMED	3.3 µl	10 µl	10 µl

Mini-PROTEAN Tetra Cell system (Bio-Rad) and Consort electrophoresis power supply were employed for running the gel. The gel chamber was assembled according to the manufacturer's instruction and filled with 1x electrophoresis buffer (190 mM Glycine, 0.1% SDS, 25 mM Tris-HCl). The protein samples were loaded into the gel pockets in the amount of 20 – 30 µg of protein per well. The protein marker PageRuler™ Plus (Thermo Scientific) was loaded in parallel with the samples in order to analyze molecular weight of the detected proteins. Electrophoresis

was performed at RT, 20 min at 80 V to allow the proteins to enter the gel, then 1.5 h at 100 V for separation of the bands (until bromophenol blue reached the bottom of the resolving gel).

2.2.6.3. Immunoblotting and detection

Mini Trans-Blot Cell system (Bio-Rad) was used for transferring proteins from the gel onto the nitrocellulose membrane with the 0.22 µm pore size (AppliChem). The "transfer sandwich" was assembled in the order: cathode direction – sponge – Whatman blotting paper – gel – nitrocellulose membrane – sponge – anode direction. Prior to transfer, the nitrocellulose membrane was incubated 15´ in distilled H_20 and 1 h in transfer buffer. Blotting was performed for 1 h at 100 V at 4^0C in 1x transfer buffer containing 20% Methanol. The current did not exceed 180 mA when 1 chamber was used and 360 mA with two chambers. After the transfer, the membrane was briefly washed with TBS-T and blocked with 5% non-fat dried milk in TBS-T (1 h, RT).

The primary antibodies were applied o/n at 4^0C (most of the antibodies) or for 1 h at RT (anti-EGFP and anti-β-tubulin antibodies). All primary antibodies and needed concentrations are listed in Table 2.1. After incubation with the primary antibodies, the membrane was washed 3x10´ with TBS-T and secondary antibodies coupled to horseradish peroxidase (HRP) were applied for 1 h at RT (list of the secondary antibodies and respective dilutions are given in Table 2.2). The membrane was washed again 3x10´ with TBS-T and chemiluminescent HRP substrate was applied. Lab-made ECL was used for detection of TH, EGFP, and β-tubulin. ECL1 and ECL2 solutions were mixed in equal proportions and applied to the membrane right before the imaging. For synuclein protein detection and all bands which are harder to detect, we used 2 commercial kits: HRP Substrate Pico, Immobilon Western (Millipore) and HRP Substrate Femto, SuperSignal West Femto (Thermo Scientific). In each case, the reaction was based on the interaction of HRP with chemiluminescent substrate luminol. The HRP-enzyme oxidizes luminol in presence of H_2O_2, creating a reaction product which emits light at 425 nm. The signal was visualized with ChemiDocXRS+ Transilluminator (Bio-Rad) and captured by CCD camera. QuantityOne 4.6.9 software (Bio-Rad) was used to obtain the images and Image Lab software (Bio-Rad) was used for analysis of the detected bands.

2.2.7. Animal procedures

Adult female Wistar rats (Janvier Labs) were used in the experiments. All animal experiments were conducted according to the approved experimental animal license No. 11/0409 and controlled by the local animal welfare committee of the University Medicine Göttingen. All procedures were performed in accordance with the local regulation and the Directive 2010/63/EU of the European Parliament and of the Council on the protection of animals used for scientific purposes.

2.2.7.1. Animal housing, preparation for the operation and anesthesia

Wistar rats were housed in cages in groups of 5 with 12h/12h dark/light cycle and access to food and water *ad libitum*. Animals were delivered to the laboratory at least 1 week before the operation. During this time they were weighted and handled every day in order to adapt to the experimenter before the surgery. At the time of surgery, the weight of animals was 220-250 g. Before, during and after the operation rats were provided with anesthetics and analgesics.

The next drugs were used for anesthesia and analgesia:

- Ketamine 10% (Medistar), active substance – ketamine hydrochloride, provides short-term surgical anaesthesia combined with analgesic action.
- Xylariem 20 mg/ml (Ecuphar), active substance – xylazin hydrochloride, is a powerful analgesic drug, alpha-2-agonist. In combination with ketamine, it provides deeper anaesthesia (as described in Van Pelt LF, 1977)
- Rymadil (Zoetis) or Carprieve (Bayer) 50 mg/ml, active substance – carprofen, are non-steroidal anti-inflammatory drugs (NSAID) which provide analgesia and reduce fever and inflammation.
- Metapyrin 500 mg/ml (Serumwerk), active substance – Metamizole-Natrium 1 H_2O, is an analgesic drug with a weak NSAID action.

Rymadil and Metapyrin were given as pre-emptive analgesics 2 days before and 2 days after surgery. Rymadil was administered intraparietally once a day at concentration 5 mg/kg. Metapyrin was given in a drinking water (1.5 mg/ml) in our initial experiments, but we noticed that rats tend to drink less water in this case due to a bitter taste of Metapyrin. Therefore, in the next experiments, Metapyrin was injected subcutaneously as 100 µl of 5 mg/ml Metapyrin

solution. Drugs were diluted to the appropriate concentrations with sterile saline (0.9% NaCl solution). During the surgery, animals were deeply anesthetized with ketamine/xylazine mixture (150 mg/kg and 10 mg/kg body weight, respectively) which was administered via intraparietal injection. Before starting the surgery, it was made sure that toe pinch and eyelid reflexes are negative.

Prior to the surgery, the glass capillaries (World Precision Instruments) were prepared. Glass capillaries were pulled with the micro pipette puller P97 (Satter Instruments Company), using the program with the next characteristics: Pressure setting P = 500, Heat = 520^0C, Pull = 20, Velocity = 135. The thin tip of the pulled capillary was broken off with the forceps while examined through binocular. It was important that the tip was not too narrow (since then the liquid did not flow through the tip efficiently and it tended to break easily) and not too bright (in this case a big part of the injected virus would spread around needle track and would not target SN properly). The tip with the best size is shown in Figure 2.3 (a). The glass capillary was filled with mineral oil and attached to the micro injector Nanoliter 2000 and micro syringe pump controller, Micro4 (World Precision Instruments). The surplus of mineral oil was removed, and the tip was rinsed and filled with sterile filtered PBS. Mineral oil and PBS were separated by the air bubble. The glass capillary was aligned with the stereotaxic frame.

2.2.7.2. Stereotaxic injection into the rat's substantia nigra

Stereotaxic surgery was performed as described in Cetin *et al.*, 2007. A deeply anesthetized rat was shaved and fixed in the stereotaxic frame with non-traumatic ear bars and jaw holders (David Kopf Instruments). Eyes were protected from drying by application of Bepanthene (Bayer) for the whole duration of anesthesia. The skin of the head was disinfected with iodine (Braunol, B. Braun) and cut longitudinally along the midline. Skin and connective tissues were removed from the skull so that bregma and lambda were exposed. Occasional bleeding was rapidly stopped with the high-temperature cautery pen (Bovie Medical Corporation).

The coordinates of lambda and bregma were measured, a proper horizontal position of the animal in the stereotaxic frame was confirmed, and the coordinates of the stereotaxic injection were calculated. A piece of bone above the place of injection was removed by careful drilling with the mini drill (Praxxon) with 0.8 mm drill tip (Dremel), any bleeding at this step had to be avoided.

The skull was cleaned with sterile filtered PBS to remove any small pieces of bones. PBS was ejected from the glass capillary, and it was filled with AAV vector solution instead, the tip of the capillary was rinsed in sterile PBS. Prior to the surgery AAV vectors were diluted in sterile and filtered with 0.22 µm syringe filter PBS so that 2 µl of the solution contained the destined amount of viral transduction units (tu). The glass capillary was injected into the left SN according to the coordinates AP: −5.3 mm; ML: +2.2 mm; DV: −7.75 mm relative to bregma as shown in Figure 2.3. (b) (Paxinos and Watson, 1986).

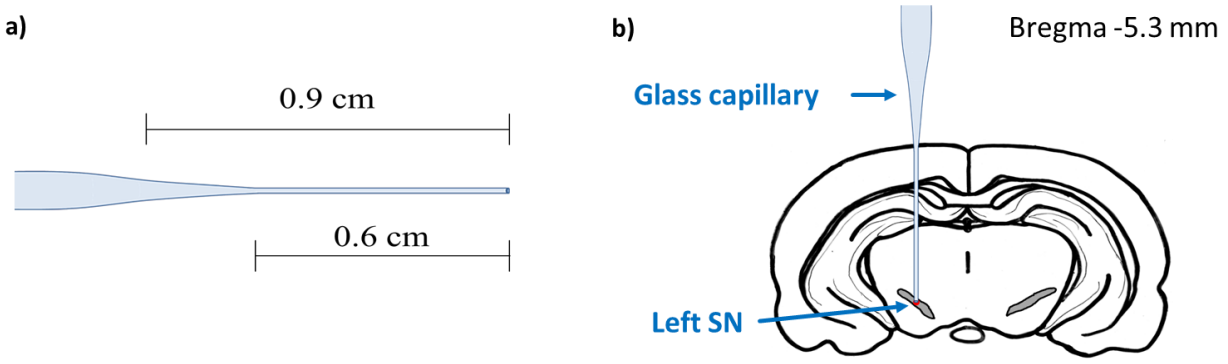

Figure 2.3. Stereotaxic injection into the rat's SN. (a) Glass capillary with the indicated dimensions provided the most efficient and well-targeted injection into the rat's SN. **(b)** Left SN was stereotaxically injected according to the coordinates AP: −5.3 mm; ML: +2.2 mm; DV: −7.75 mm relative to bregma (Paxinos and Watson, 1986). The red circle indicates the location of the injection.

The glass capillary was left to rest in the tissue for 3 min. Then, 2µl of AAV dilution containing a total of 1.2 x 10^8 tu were injected with the speed of 500 nl/min. The injection was controlled by micro syringe pump controller Micro4 (World Precision Instruments). After injection of the virus the glass capillary was left in the tissue for additional 3 min, then removed and cleaned with PBS. The skin above the skull was stitched.

After the surgery, 3 ml of sterile saline were injected subcutaneously to compensate for the dehydration of the rat during anesthesia. Warming pads were used to keep the animal warm until the awakening. During the first two days of recovery after the surgery rats received softened food and were housed singly in the cages.

2.2.7.3. Transcardial perfusion and tissue processing

Wistar rats were sacrificed by CO_2 inhalation 2 and 8 weeks after virus injection. For transcardial perfusion an animal was fixed on the rack, the abdominal cavity was opened; diaphragm and ribs were carefully cut in order to expose the heart. A blunt-ended needle connected to the perfusion tube was inserted through the left ventricle into the aorta. The position of the needle was secured by clamping. The abdominal aorta and caudal vena cava were closed with the hemostat (Fine Science Tools) above the liver in order to provide faster perfusion of the anterior part of the body. Perfusion was controlled with peristaltic perfusion pump (Ismatec) and the speed of perfusion was set to 55 ml/min. First, the body was perfused with ice-cold sterile filtered PBS (pH 7.4) until the liquid, exiting the cut nose of the rat, was clear from the blood. Then, perfusion was continued with the fixative, ice-cold 4% PFA in PBS (pH 7.4). The PFA-perfused bodies were left on the rack for 15-20 min to let the tissues harden. The basics of chemical and physical processes behind the PFA fixation are explained in Thavarajah *et al.*, 2012. When the rat's body became rigid due to PFA infusion, the animal was decapitated, and the brain was surgically removed from the skull and placed for post-fixation into 4% PFA for 24 h at 4°C. Then PFA was substituted with 30% sucrose in PBS. Impregnation with sucrose served for dehydration and cryoprotection of tissue. After 3-5 days at 4°C, the brains sank to the bottom of the tube, which indicated complete impregnation in sucrose. The specimens were dried (the rest of the sucrose solution on the brain surface was carefully removed with the Kleenex) and frozen in clean 50 ml tubes at -80^0C until further processing.

30 µm serial coronal sections of the striatum (AP +2.2 mm to -1.4 mm relative to bregma) and SN (AP -4.5 mm to -6.5 mm relative to bregma) were cut on the Leica CM 3050 S cryostat (Leica, Germany). Every striatal or nigral section was collected into 24-well plates containing PBS with 0.1% NaN_3 with the free-floating method. Plates were stored at 4°C.

2.2.7.4. Immunohistochemistry

2.2.7.4.1. IHC-IF on striatal and nigral sections

Brain sections were stained with IHC-IF protocol where antibodies against dopaminergic marker tyrosine hydroxylase (TH) and a transgene were used in order to appreciate the location of injection, compare AAV transduction efficiency between and within experimental groups and

analyze anatomical changes in striatum due to the transgene expression (striatal fiber density and presence of pathological axonal structures).

The method of IHC-IF was developed by Coons, 1958. In our experiments, every 12th section of SN or striatum were stained with IHC-IF. Sections were washed 3x5´ in PBS in order to remove NaN_3. Then, sections were subjected to antigen retrieval in 1x TBS (pH 9.0) at 60^{0}C for 4-5 h. After 3x5´ wash in PBS, sections were blocked with 5% NGS and 0.1% TritonX in PBS for 2 h.

The first antibody was applied in the following incubation solution: 0.1% TritonX + 2% NGS + 0.02% NaN_3 in PBS. The dilutions and species for each primary antibody are provided in Table 2.1. Staining was performed with 500 µl of the primary antibody solution per well of 24-well plate (3-4 coronal sections) under shaking for 48 h at 4^{0}C (SN sections) or for 60 h at RT (for striatal sections).

After 3x5´wash with PBS, Cy2 and Cy3-coupled secondary antibodies (Table 2.2) of appropriate species were applied for 2 h at RT 1:250 in the incubation solution with 0.1% TritonX and 2% NGS in PBS. The unbound secondary antibodies were washed with PBS (3x5´). Finally, the brain sections were stained with the nuclear counterstain DAPI for 15 min, washed again with PBS 3x5´ and mounted onto SuperFrost Plus microscope slides. Sections were dried o/n at RT, rehydrated in PBS and covered with pre-warmed Mowiol 4-88.

2.2.7.4.2. IHC-DAB on coronal sections of SN

Serial coronal brain sections of AP -4.5 mm to -6.5 mm relative to bregma were stained according to the IHC-DAB protocol, followed by Nissl staining for stereological quantification of dopaminergic and non-dopaminergic neuronal cell loss in SNpc. Only brains with the confirmed by IHC-IF staining proper injection in SNpc and comparable level of the transgene expression were included in IHC-DAB staining and stereological analysis.

DAB (3,3'-Diaminobenzidine) is an organic chromogen, which produces a dark precipitation reaction product when oxidized by hydrogen peroxidase. DAB staining can be observed with the brightfield microscopy, the staining is permanent, heat and illumination stable which is an advantage of DAB over IF. IHC-DAB staining method was developed by Graham and Karnovsky, 1966, and Nakane and Pierce, 1967.

Every 4th section was stained. Before the staining and between each step of the protocol sections were washed 3x5´ with 0.1M TBS (pH 7.4). Endogenous peroxidases, an activity of which can lead to an unspecific staining, were deactivated by incubation for 5´ in 10% methanol and 3% H_2O_2 solution in 0.1 M TBS. Longer than 5´incubation or higher concentrations ofH_2O_2 had to be avoided, in order to keep the physical integrity of the sections. Blocking solution contained 5% NGS in 0.1 M TBS and was applied for 1 h at RT and shaking. After the blocking, SN sections were incubated 48 h at 4^0C in the primary antibody (anti-TH ab152, rabbit polyclonal, see Table 2.1) with concentration 1:3000 in 0.1 M TBS with 2% NGS. Unbound primary antibody was washed with 1x TBS and the secondary antibody (anti-rabbit-biotin) was applied for 1 h at RT at concentration 1:250 in 0.1 M TBS with 2% NGS. After washing off the unbound secondary antibody, sections were incubated with avidin and biotinylated enzyme for 1 h at RT. This incubation solution was prepared using VECTASTAIN ABC Peroxidase Standard Kit PK-4000 (Vector Laboratories) by mixing reagents A and B in 0.1 M TBS according to the manufacturer's instructions. After the following 3x5´washing in TBS, sections were stained with DAB Peroxidase Substrate Kit SK-4100 (Vector Laboratories). According to the instructions to the kit, buffer stock solution, DAB stock solution and H_2O_2 solution were mixed in ddH_2O right before the application. The sections were incubated in the substrate solution for 4 min, then intensively washed with 0.1M TBS. Positively stained structures were visible to the naked eye. DAB-containing solutions had to be treated carefully due to the high toxicity of the DAB-substrate. Brain sections were mounted onto SuperFrost Plus microscope slides and dried o/n at RT.

DAB-stained sections were then further subjected to the Nissl staining protocol. Here, the staining agent was thionine, a basophilic amine dye, which stains nuclear acids blue. Neurons cytoplasm appears dark blue after the staining and neurons can be distinguished from other cells because neurons are rich on ribosomes and have a so-called Nissl body, a tightly packed endoplasmic reticulum structure. The steps of the Nissl staining protocol were as following: 5´ddH_2O => 7´ Thionine working solution => 2´ ddH_2O => 2´ 70% ethanol => 2´ 90% ethanol => 5´ 96% ethanol => 5´ 100% isopropanol => 2x5´ xylol. Microscope slides were dried in the fume hood and sections were covered with DPX.

2.2.8. Imaging and data analysis

2.2.8.1. Neurotoxicity of synucleins in primary cortical neurons

Cell culture plates were observed with the AxioObserver.Z1 microscope (Carl Zeiss Microscopy). Images were taken with Axiocam 503 camera using Zen 2.3 pro software. For the cell counting, 10x pictures were taken, 4 pictures per well, omitting the edges and the center of the well. Edge wells of the plates were excluded from the analysis. EGFP (100 ms), mCherry (500 ms) and brightfield (50 ms) signals were recorded. Acquired files (.zvi) were semi-automatically processed in ImageJ (NIH). For the red channel (mCherry) pictures a threshold was adjusted so that most of the cells were visible but the background not apparent. The level of adjustment was the same for all pictures and groups of a given time point (dpt). Pictures were binarized, converted to masks and watershed. Cells were automatically counted using "Analyse particle" function (size of the particles 5 – 1000 microns^2, circularity 0 – 1, edges excluded). The measurements were saved in Excel and analyzed with GraphPad Prism statistics software.

2.2.8.2. Mitochondrial morphology and motility

The pictures and time-lapse videos of mitochondria were recorded with Axio.Examiner D1 microscope (Zeiss) using 63x objective. The Colibri LED light source was used to visualize EGFP (455 nm module) and mito-TdTomato (590 nm module). In a typical experiment, live neurons on the glass cover slip were placed into the imaging chamber filled with warm aCSF medium. The chamber was constantly perfused with the speed 12 ml/h which allowed keeping the temperature of the liquid at ~32-34^0 C. From each cover slip, 10 z-stack images were taken for the analysis of the mitochondria morphology in the neuronal soma and neurites, and 3 time-lapse videos of 180 sec were recorded for the studying of the mitochondrial motility in the neurites. The z-stack pictures were deconvoluted with the Zeiss software. The mitochondria in neuronal soma were classified into one of the 3 categories: elongated or tubular, partially condensed, and fully condensed (Figure 3.10). Somas of at least 200 neurons were characterized for each experimental condition. The length and width of mitochondria in the neurites were measured with ImageJ (NIH), and the ratio length/width was calculated in Excel for 100-150 mitochondria per condition. MTrackJ Plugin of ImageJ was used for tracking of the mitochondria for the motility analysis (n = 63 per condition). All data are shown as mean $\pm$ SD.

2.2.8.3. Stereological quantification of dopaminergic neurons in SN

In order to analyze the extent of dopaminergic neurons loss in SNpc, stereological quantifications of TH-positive and Nissl-positive cells in SNpc was performed. Nissl+ neurons were counted in order to confirm the loss of TH+ neurons and exclude mere downregulation of TH expression in SNpc. Examples of TH+ and Nissl+ neurons are provided in Figure 2.4. a) and b) respectively. The examiner was blinded to the experimental groups, animal ages, and identification numbers. Every 4th section was stained with IHC-DAB protocol (see section2.2.7.4.2.), and 10 sections containing SNpc were analyzed using Stereo Investigator 9 software (Micro Bright Field Inc.). SNpr and VTA regions were excluded from the cell count. The regions of SNpc were manually outlined, and program parameters were set as following: low magnification lens 2.5x (for outlining ROIs), high magnification lens 40x (for counting cells), counting frame X and Y = 50 µm, grid size X and Y = 100 µm, section cut thickness = 30 µm, and dissector height (real section thickness after the staining) = 17 µm. Counting was performed according to the Stereo Investigator users guide (MBF, 2009). An example of counting frame is provided in Figure 2.4. (c). The measurements were saved in Excel and analyzed with GraphPad Prism statistics software.

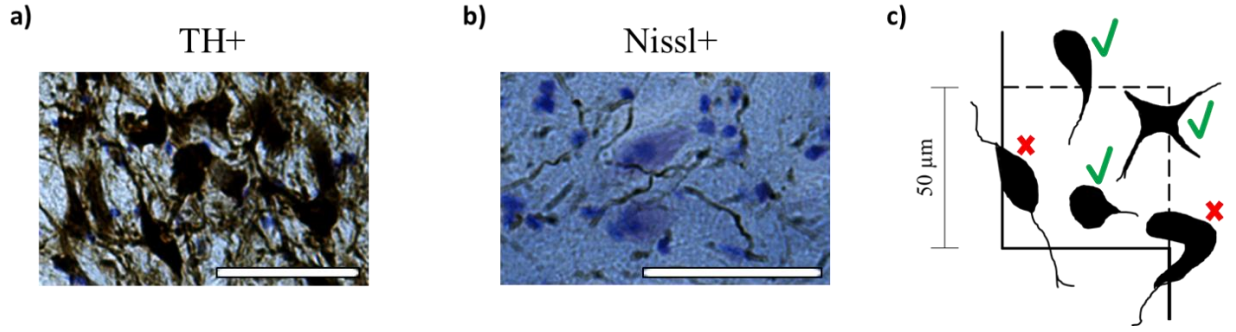

Figure 2.4. Stereological quantification of dopaminergic neurons in SN. (a) Example of TH+ cells. **(b)** Example of Nissl+ neurons; scale bar – 50 µm. **(c)** Illustration of the counting frame. Neurons, which have a green check mark are to be counted (they cross a dashed inclusion line, or can be found entirely inside the counting frame). Neurons, which have a red X are not to be counted because they cross solid exclusion line.

2.2.8.4. IHC-IF staining of SN

SN sections, stained with IHC-IF protocol were observed with Axioplan 2 microscope (Zeiss). 5x, 10x and mosaic overview pictures were recorded with Axiovision 4.8 software. The

following filter sets were selected: 20 Rhodamine filter from Zeiss (excitation: 530-570 nm; emission: 575-650 nm) was used for visualizing anti-TH-Cy3 signal, Endow GFP filter from Chroma (excitation: 450-490 nm; emission: 500-550 nm) - for EGFP or anti-synuclein-Cy2 signal, and DAPI 01 filter from Zeiss (excitation: 350-375 nm; emission: 400-1200 nm) - for DAPI. The exposure times are indicated in the result section for the respective pictures.

2.2.8.5. Quantification of the axonal bulbs in the striatum

Axonal bulbs or swollen dystrophic axons were defined as the highly immunoreactive against TH rounded structures in the rat's striatum with the Ferret's diameter of above 2 μm. These swollen axons were counted on the 40x microphotographs, taken with the Axioplan 2 microscope (Zeiss). 3 striatal sections were analyzed for each animal (the coordinates relative to bregma AP +0.8 mm, AP +0.0 mm, and AP -0.4 mm), 10 pictures were taken from each striatal section (5 on the injected and 5 on the contralateral side). The pictures were obtained from the mediolateral and dorsolateral regions of the striatum where the axons were immunopositive for EGFP or synuclein. Six to seven animals per group and time point were analysed and the obtained data were represented as a number of axonal bulbs per mm^2.

2.2.8.6. Dopaminergic fiber density in rat's striatum

For the evaluation of dopaminergic fiber density, the microphotographs of IHC-IF stained striata were taken with a laser-scanning confocal microscope Leica TCS SP5 (Leica Microsystems, Wetzlar, Germany). The 63x oil immersion objective was used for magnification, and 5x zoom was additionally applied by the LAS AF software. EGFP and Cy2 signals were visualized with help of the Argon-ion gas laser with excitation at 488 nm and emission set to 495-540 nm. Cy3 signal was visualized with 561 nm laser with emission set to 570-636 nm. For each brain, 15 pictures from 3 striatal sections were analyzed on injected and non-injected side. The density of TH-immunoreactive fibers was evaluated with ImageJ software (NIH). The pictures were thresholded using Li function, and a percentage of area covered by fibers was calculated. The values for injected and non-injected sides of the brain were compared; the fiber density of contralateral side was taken as 100% and the data were represented as mean % relative to non-injected side $\pm$ SD.

2.2.9. Statistics

Statistical analysis was performed with GraphPad Prism software (version 7.02). We assumed that the data followed the Gaussian distribution (D'Augostino-Pearson omnibus normality test). One-way ANOVA (analysis of variance) with Tukey's post-hoc test was used for multiple comparisons between groups in *in vitro* and *in vivo* experiments. The Geisser-Greenhouse correction was implemented because sphericity (equal variability of differences) was not assumed. Student's t-test with Welch correction was used when 2 groups were compared. Data are reported as mean $\pm$ SD (standard deviation). The level of significance was set at $p < 0.05$ (*), $p < 0.01$ (**), $p < 0.001$ (***), $p < 0.0001$ (****).

3. Results

3.1. Aggregation and toxicity of WT-βS, P123H-βS, and V70M-βS in primary culture of cortical neurons

3.1.1. Experimental layout

Expression of synuclein proteins in primary cortical neurons was mediated by AAV vectors of serotype 6. Bicistronic constructs were used, containing, first, a cDNA for human αS, WT-βS, P123H-βS, V70M-βS, or γS and, second, a cDNA for EGFP under control of two separate neuron-specific hSyn1 promoters. Expression of synuclein proteins was enhanced by the presence of WPRE in the 3´-end of the coding sequence in the untranslated region. WPRE is a posttranslational regulatory element which increases the level of transgene expression 5- to 8-fold (Zufferey *et al.*, 1999). The monocistronic vector expressing EGFP was used as a control for possible toxicity of AAV transduction or EGFP overexpression. In addition, neurons were co-transduced with AAV6 vector, carrying a cDNA for mCherry with a nuclear localization sequence, which was used as a reporter for neuronal cell numbers. Expression of nuclear mCherry was also driven by the neuron-specific hSyn1 promoter. The genome layout of the AAV vectors is described in detail in section 2.2.2., and Figure 3.1 b). Bicistronic AAV vectors with cDNA for WT-βS, P123H-βS, and V70M-βS were prepared in the same batch of virus production to assure the same transduction properties of these viruses and the same expression level of the proteins. Primary cortical neurons, which were seeded on PLO and laminin coated plates, were transduced with AAV6 vectors on the 3rd day *in vitro* (div 3). Bicistronic vectors coding for one of the synuclein proteins and EGFP (AAV6-s-Synuclein-SEIS-WB) or monocistronic vectors coding for EGFP alone (AAV6-s-EGFP) were applied at concentration 2 x 10^8 tu per well of 24-well plate (250 000 cells/well). The AAV vector which mediated the delivery of nuclear mCherry (AAV6-s-nuc mCherry-WB) was applied at concentration 0.25 x 10^8 tu/well in all conditions. Primary neurons were observed for 20 days after transduction (20 dpt), and microphotographs were taken every 4 days in order to compare expression levels of the transgenes and to count cell numbers to assess the toxicity of synucleins. Afterwards, neurons were lysed and subjected to Proteinase K digestion and immunoblotting analysis. The experimental layout is summarized in Figure 3.1 a).

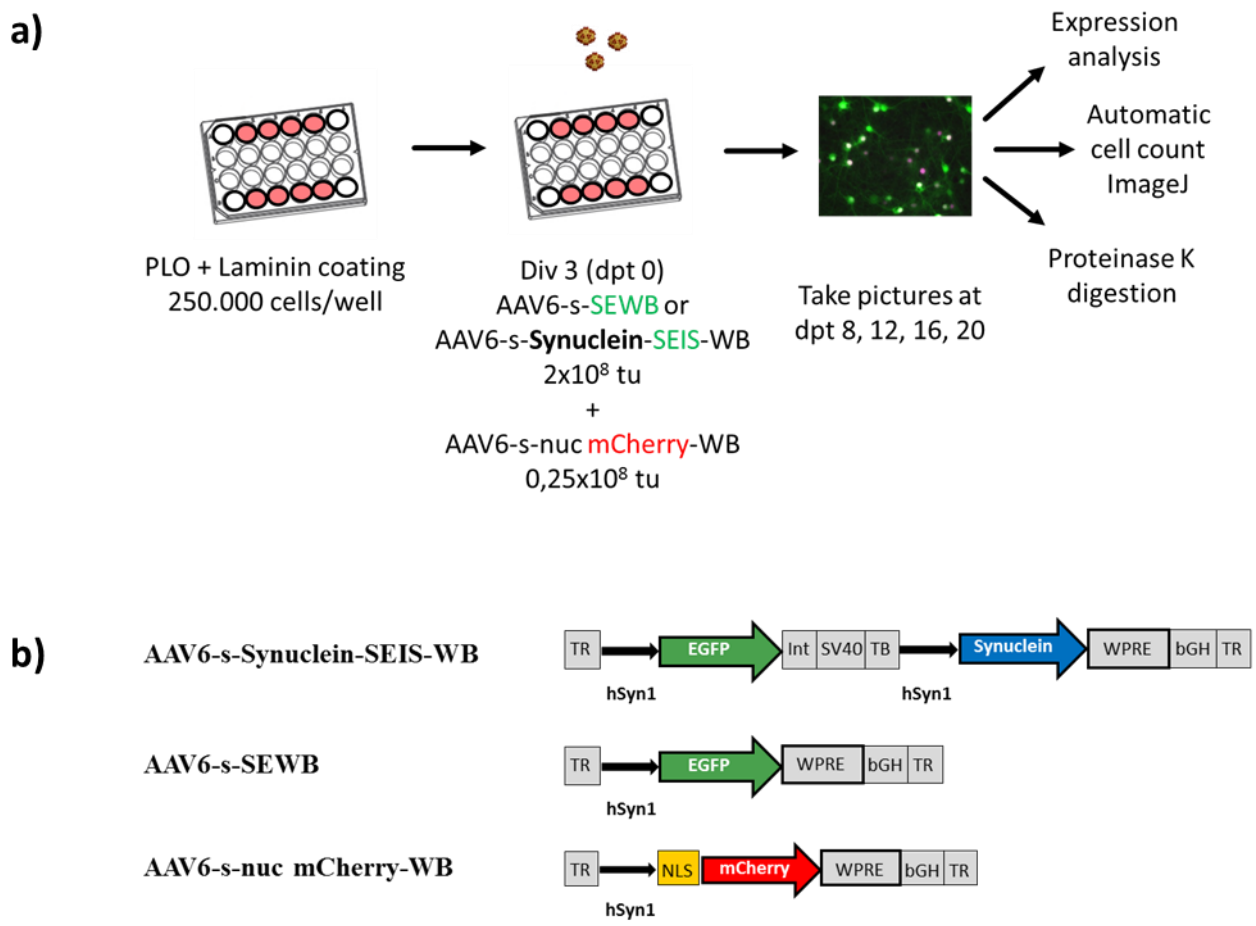

Figure 3.1. The layout of the cell culture experiments.

(a) Primary cortical neurons were seeded on poly-L-ornithine-laminin-coated 24-well plates at concentration 250 000 cells/well. AAV6 vectors were applied at the day in vitro (div) 3. Synuclein proteins were co-expressed with EGFP (bicistronic construct) and nuclear mCherry (reporter for the quantity of neurons). All proteins were expressed under control of separate hSyn1 gene promoters. Microphotographs were taken 8, 12, 16, and 20 days post-transduction (dpt) for cell count and comparison of EGFP-reporter expression. The lysates of cells (dpt 20) were used for protein expression analysis with Western blot and proteinase K digestion assay.

(b) Structure of the AAV vector genomes: bicistronic vector which include a cDNA for a synuclein (either αS, WT-βS, P123H-βS, V70M-βS or γS) and the cDNA for EGFP under control of two separate promoters; monocistronic vector carrying the cDNA for EGFP used as a control; and monocistronic vector carrying the cDNA for nuclear mCherry. Expression of the transgenes was controlled by hSyn1 - human synapsin 1 gene promoter (Kügler *et al.*, 2003) and enhanced by Woodchuck hepatitis virus posttranscriptional regulatory element (WPRE).

Int - intron; SV40 - SV40 polyadenylation site; bGH - bovine growth hormone gene polyadenylation site; TR - inverted terminal repeats.

3.1.2. Expression analysis

Expression of synuclein proteins was compared directly - by immunoblotting and indirectly – by epifluorescence microscopy (EGFP reporter was co-expressed from the same AAV vector as synuclein). Expression of EGFP reporter was observed as early as 2 days after AAV transduction in all experimental conditions. Every 4 days after transduction 10x, 20x and 40x microphotographs were taken. The edges of the well, where the concentration of cells was usually the highest, and the center of the well, where cells were much less concentrated, were excluded from analysis. Representative 10x pictures on Figure 3.2 show the gradual increase in EGFP fluorescence in γS and EGFP groups from day post transduction 8 (dpt 8) to dpt 20. EGFP fluorescence was lower in presence of WT-βS, P123H-βS and V70M-βS, and the lowest under influence of αS. A decrease of EGFP fluorescence due to the presence of αS was reported before (Taschenberger *et al.*, 2013) and it is probably caused by worsening of metabolic state in these neurons and does not indicate the decrease in synuclein expression. As concerning WT-βS, P123H-βS and V70M-βS, EGFP reporter showed the same intensity and pattern of epifluorescence increase in these 3 conditions. The lower intensity of EGFP signal in late culture (20 dpt) in case of WT-βS, P123H-βS and V70M-βS as compared to γS may indicate changes in the metabolic state due to WT-βS and mutants' toxicity, although the extent of this effect is lower than for αS.

Immunoblotting analysis of the lysates of primary cortical neurons revealed the same expression level of αS, WT-βS, P123H-βS and V70M-βS with the anti-panSynuclein antibody (ab6176) as shown in Figure 3.3 (a). This antibody detects an epitope in the highly conserved N-terminal region of αS, βS and γS: amino acid residues 11^{th} to 26^{th}. Yet, γS has 2 different amino acids in this region which resulted in the lower signal of γS with anti-panSynuclein antibody. This observation was reported before (Taschenberger *et al*, 2013). During this doctoral project, I have not found any pan-synuclein antibody with better properties. Therefore, synuclein bands were also probed with the mixture of specific antibodies: anti-αS (SC-7011-R), anti-βS (SAB1100305), and anti-γS (ab6169) which showed similar levels of expression of all synuclein proteins including γS.

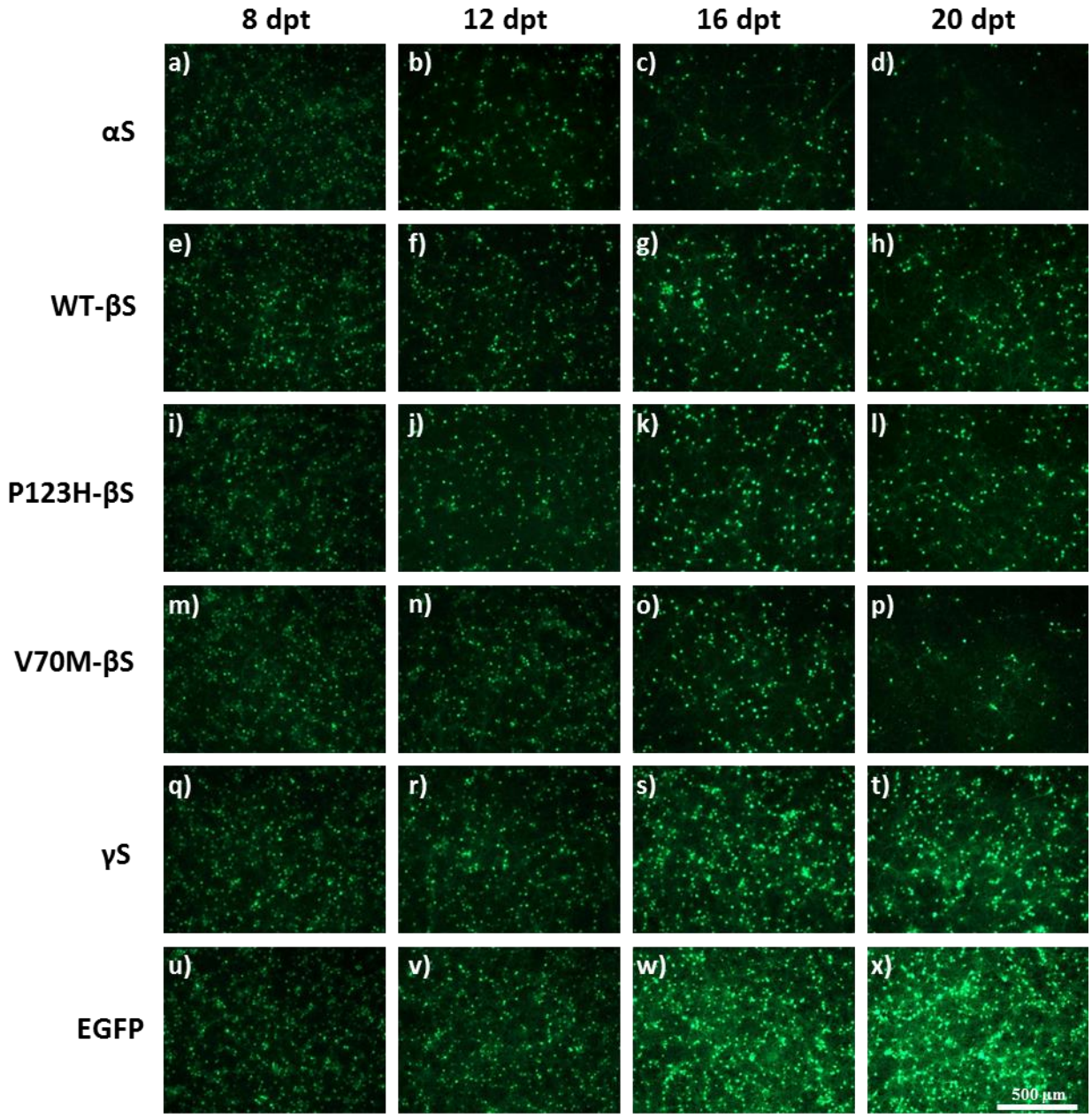

Figure 3.2. Expression analysis of synucleins in primary cortical culture.

Representative 10x pictures of primary cortical neurons which co-express EGFP with either αS, WT-βS, P123H-βS, V70M-βS or γS. Expression of EGFP alone served as a control. Microphotograph from 8th, 12th, 16th and 20th-day post-transduction (dpt) are organized in horizontal rows for each synuclein protein as indicated. Prominent cell loss can be observed starting from dpt 12 for αS **(b-d)**, and from dpt 16 for WT-βS **(g, h)**, P123H-βS **(k, l)**, V70M-βS **(o, p)**. EGFP fluorescence continues to increase in case of γS **(q-t)** and EGFP control **(u-x)** more rapidly than in case of αS, WT-βS, P123H-βS and V70M-βS. WT-βS **(e-h)**, P123H-βS **(i-l)** and V70M-βS**(m-p)** show the same level of EGFP expression at every time point. Scale bar: 500 µm. Exposure time: 100 ms.

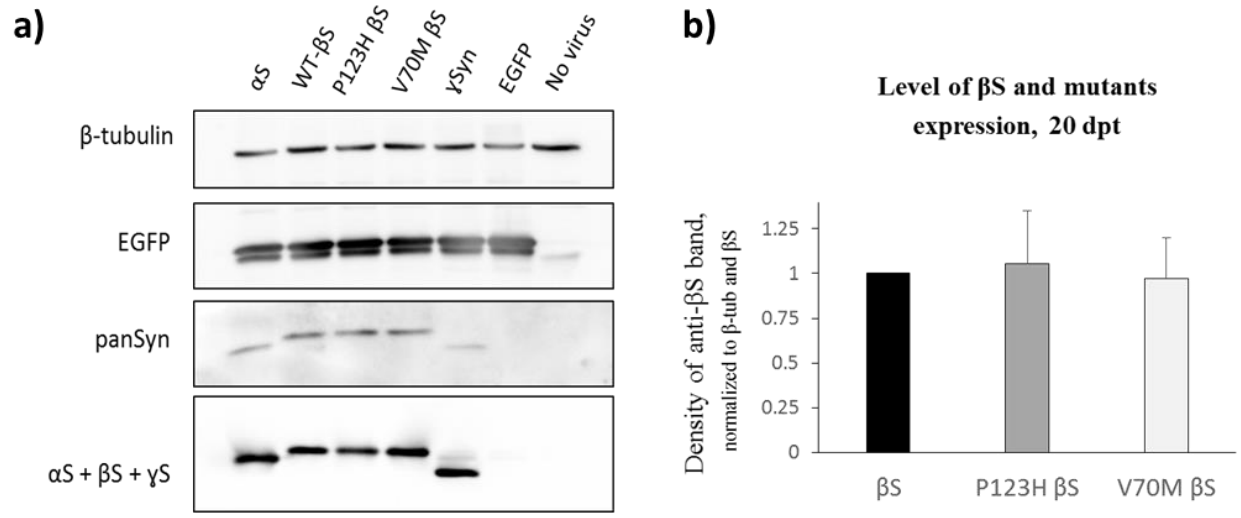

Figure 3.3. Immunoblotting analysis of synucleins in primary cortical culture.

(a) Representative Western blot of the lysates of primary neurons expressing αS + EGFP, WT-βS + EGFP, P123H-βS + EGFP, V70M-βS + EGFP, γS + EGFP, or EGFP alone, as well as untransduced control (no virus). The detected bands are β-tubulin (~55 kDa), EGFP (~27 kDa and ~25 kDa), αS (~18 kDa), βS (~20 kDa) and γS (~16 kDa).

(b) Densitometry analysis of WT-βS, P123H-βS and V70M-βS bands on 9 independent membranes showed no significant differences in expression levels of WT-βS and its mutants. Data is provided as mean ± SD.

αS was detected as a band of ~18 kDa (theoretical molecular weight 14.47 kDa). WT-βS and both mutants, P123H-βS and V70M-βS, had the same molecular weight of ~20 kDa (theoretical weight - 14.28 kDa for WT-βS). The anti-γS band had a size of ~16 kDa while 13.33 kDa was expected.

The higher than theoretical molecular weights of αS was frequently reported in numerous preceding publications (e.g., Mishizen-Eberz*et al.*, 2003) in a range of 16-19 kDa. The difference between expected and detected sizes of αS bands could be explained by the high hydrophobicity of the synuclein molecule and its interactions with SDS micelles which slows down αS movement in SDS-PAGE (Surguchov, 2008), although some posttranslational modifications cannot be excluded. The same most probably concerns βS and γS. Human and rodent βS have almost identical amino acid sequence with difference in only 2 residues. Therefore, no βS antibodies are specific for the human protein only. Despite this, endogenous rat βS was never detected in the primary cultured neurons in this project. This indicate that endogenous rat βS

might be expressed on a very low level or not expressed at all in embryonic cortical neurons of the rat.

Taken together, WT-βS, P123H-βS, and V70M-βS were expressed in primary cortical neurons on the same level as revealed by epifluorescent microscopy (EGFP reporter) and immunoblotting analysis.

3.1.3. Toxicity of WT-βS, P123H-βS, and V70M-βS in primary culture of cortical neurons

In order to analyze whether WT-βS, P123H-βS, and V70M-βS induce neurotoxicity to primary cortical cultured neurons, I counted how many cells survive during the first 20 days after transduction with the respective AAV6 vectors (as described in section 3.1.1.). Neurotoxicity of αS and WT-βS in cultured cortical neurons was reported before in Taschenberger *et al.*, 2013. At the beginning of this doctoral project, I tried to repeat the experiment described in the mentioned above article including the groups for P123H and V70M mutants of βS. Here, EGFP-positive neurons were manually counted on the 10x microphotographs. Since manual counting is a tedious and, to some extent, subjective method, I was searching for an automated procedure for estimation of the cell loss. Direct automatic cell counting of EGFP-positive neurons did not give a reliable result since due to the cytoplasmic expression of EGFP and variable and complex morphology of the neurons automatic protocols could not distinguish the cells efficiently. Therefore, I co-expressed mCherry reporter with nuclear localization alongside with synucleins and EGFP. Due to the accumulation in nuclei, the mCherry signal could be seen in form of well-separated round structures, easily distinguishable by cell counting software (Figure 3.4. (a)). The AAV6-s-nuc mCherry-WB vector was applied at concentration 0.25 x 10^8 tu/well, which provided efficient transduction of over 90% of the neurons. Besides, the presence of nuclear mCherry did not cause any apparent toxic effects in primary neurons. After the 8 dpt ~95% of all transduced neurons had both EGFP and mCherry signals.

In order to count nuc-mCherry-positive cells, I used the ImageJ macro, where a picture with mCherry signal was thresholded, binarized, converted to mask and watersheded in the way that the signal from each mCherry-positive nucleus was detected as a singular cell. In order to validate this cell counting protocol, the results of manual and automatic cell counting were

compared (Figure 3.4. (b)). Here, neurons from 16 pictures of 10x magnification were counted for each time point: 8 dpt, 12 dpt, 16 dpt and 20 dpt. The results of manual counting of EGFP-positive cells and automatic counting of mCherry-positive nuclei were not significantly different. Even though a small subset of neurons (~5%) had only mCherry or only EGFP signals, automated protocol could be reliably used for cell counting.

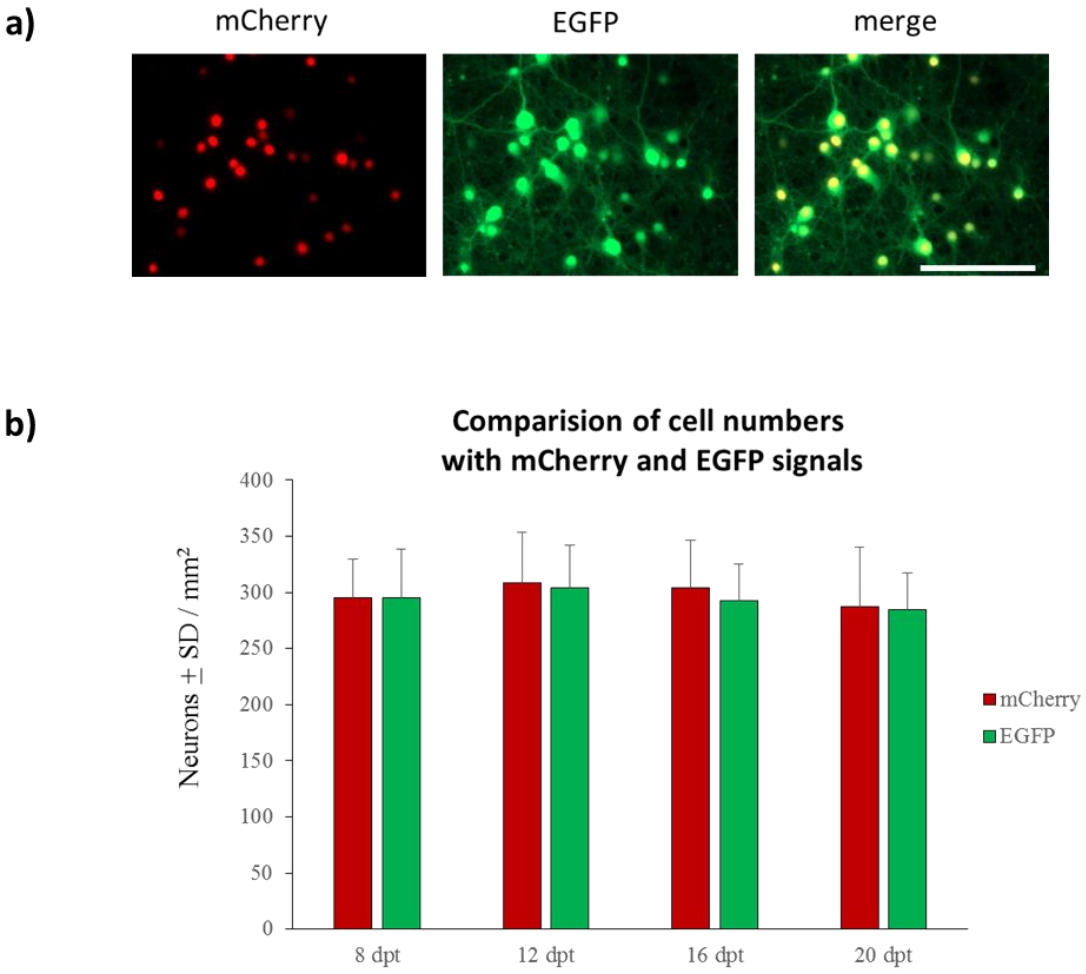

Figure 3.4. Automatic cell counting with nuclear mCherry.

(a) Representative microphotographs (40x, EGFP group, 20 dpt) show signals of nuclear mCherry, cytosolic EGFP, and their co-localization. Over 95% of neurons have both signals. Exposure time: mCherry 500 ms, EGFP 100 ms. Scale bar: 150 µm.

(b) Results of automatic (mCherry) and manual (EGFP) cell counting were compared for time points 8, 12, 16 and 20 days after transduction (div 11, div 15, div 19, and div 23, respectively). 16 pictures of 10x magnification were analyzed for each condition. No significant differences were revealed between 2 counting methods. Data is shown as the number of neurons per $mm^2 \pm$ SD.

Neurotoxicity of human αS, WT-βS, P123H-βS, V70M-βS, γS and EGFP control was assessed on 8 plates per condition (6 independent cell preparations and transductions) and results are summarized in Figure 3.5. At 8 dpt, no significant neuronal loss was observed in any condition.

Starting from 12 dpt αS, WT-βS, P123H-βS, and V70M-βS were significantly more toxic than EGFP control (p values are provided in Figure 3.5 (b)). αS appeared to be the most toxic species from 12^{th} to 16^{th} days after transduction causing the cell loss of 35.7 $\pm$ 17.1% at 12 dpt, 46.3 $\pm$ 14.6% at 16 dpt, and 57.3 $\pm$ 11.9% at 20 dpt when compared to cell numbers at 8 dpt. Expression of WT-βS resulted in neuronal loss of 24.0 $\pm$ 21.1% at 12 dpt, 35.3 $\pm$ 20.8% at 16 dpt, and 42.8 $\pm$ 16% at 20 dpt, respectively.

For P123H-βS these values amounted to 27.8 $\pm$ 20.7% at 12 dpt, 41.7 $\pm$ 22.0% at 16 dpt, and 44.0 $\pm$ 19.3% at 20 dpt. V70M-βS induced the cell loss of 30.2 $\pm$ 17.0% at 12 dpt, 44.0 $\pm$ 22.5% at 16 dpt, and 61.4 $\pm$ 15.7% at 20 dpt. Thus, there were no statistical differences between the toxicity of P123H-βS and WT-βS at any time point of the experiment, so P123H mutation did not aggravate the neurotoxicity of WT-βS in cultured primary neurons. In contrast, V70M-βS became more toxic than the WT-βS in the late culture at 20 dpt and reached the toxicity level of αS.

For the control groups γS and EGFP, the loss of neurons at the final time point 20 dpt amounted to 7.5 $\pm$ 16.0% and 15.1 $\pm$ 12.7%, respectively. The neural loss in γS and EGFP groups was significantly lower than in αS, WT-βS, P123H-βS, and V70M-βS from 16^{th} to 20^{th} day after transduction. Cell loss in primary cortical neurons expressing γS and EGFP can be attributed to the aging of the culture and possibly mild toxic effects of AAV transduction and EGFP overexpression.

In this experiment, I observed relatively high variability of the data despite optimization of culturing conditions and treating all the plates in the same way. Since primary neurons are very susceptible to evaporation, its effects were minimized by filling all the empty wells of a 24-well plate with PBS and excluding the edge wells from the analysis. Medium replenishment did not have any effect on the toxicity of the synuclein proteins. Exact initial amounts of cells and quality of the cell preparations were very important for the outcome of the experiment. The experiment was repeated with 6 independent cell culture preparations and transductions for each condition to improve the reliability of the results.

Taken together, the effects of P123H-βS were not significantly different from WT-βS at any time

points which indicated that P123H mutation did not have an additional effect on the toxicity of WT-βS, while V70M-βS significantly aggravated the toxicity of the WT-βS species in the aging culture of primary neurons.

a)

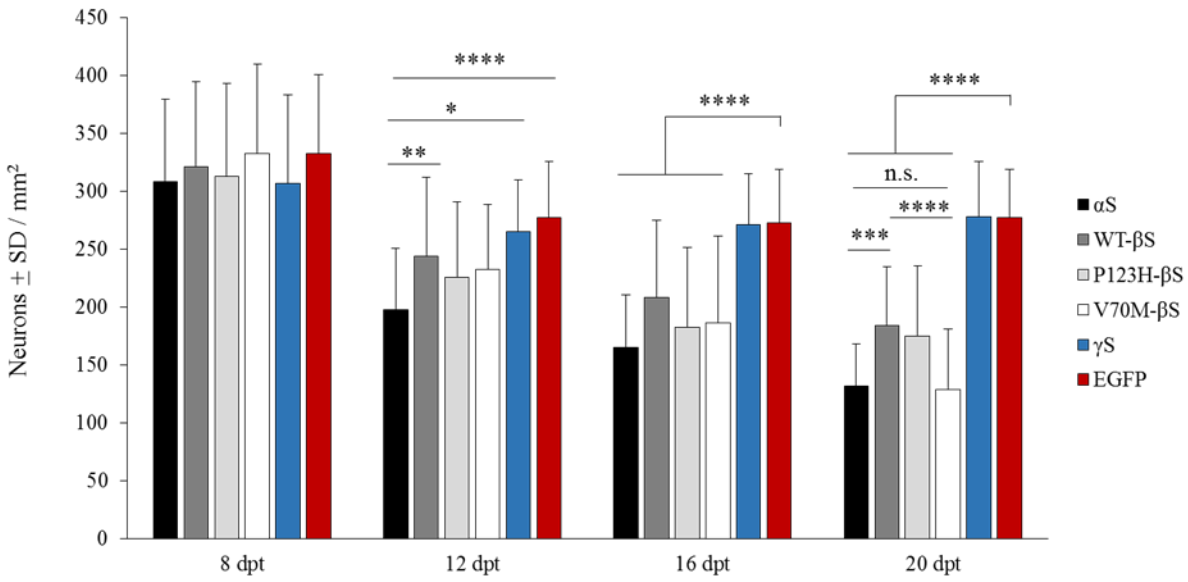

b)

8 dpt	αS	WT-βS	P123H-βS	V70M-βS	γS
EGFP	n.s.	n.s.	n.s.	n.s.	n.s.
αS		n.s.	n.s.	n.s.	n.s.
WT-βS			n.s.	n.s.	n.s.
P123H-βS				n.s.	n.s.
V70M-βS					n.s.

12 dpt	αS	WT-βS	P123H-βS	V70M-βS	γS
EGFP	****	*	**	***	n.s.
αS		**	n.s.	*	****
WT-βS			n.s.	n.s.	n.s.
P123H-βS				n.s.	n.s.
V70M-βS					n.s.

16 dpt	αS	WT-βS	P123H-βS	V70M-βS	γS
EGFP	****	****	****	****	n.s.
αS		**	n.s.	n.s.	****
WT-βS			n.s.	n.s.	**
P123H-βS				n.s.	***
V70M-βS					***

20 dpt	αS	WT-βS	P123H-βS	V70M-βS	γS
EGFP	****	****	****	****	n.s.
αS		***	**	n.s.	****
WT-βS			n.s.	****	****
P123H-βS				***	***
V70M-βS					****

*p<0.05, **p<0.01, ***p<0.001, ****p<0.0001

Figure 3.5. Toxicity of synucleins in primary cortical culture.

(a) Primary rat cortical neurons were transduced at div 3 (dpt 0) and imaged 8, 12, 16 and 20 days after transduction. Bicistronic AAV6-s-Synuclein-SEIS vectors, carrying genes for one of the synuclein species (αS, WT-βS, P123H-βS, V70M-βS or γS) and EGFP were applied as 2 x 10^8 tu/well (250 000 neurons).

Vector with nuclear reporter gene mCherry was applied as 0.25 x 10^8 tu/well. 4 picture per well of 24-well plate were analyzed, 6 independent transductions and cell culture preparations were performed. Cell numbers were acquired from the mCherry signal with automatic cell counting protocol of ImageJ software (NIH). Data is shown as number of neurons per mm^2 ± SD.

(b) Statistical analysis of the neurotoxicity was performed with 1-way ANOVA followed by Tukey's post-hoc test for multiple comparisons (GraphPad Prism software). Level of significance: *p<0.05, **p<0.01, ***p<0.001, ****p<0.0001. Statistical power (1-β err prob): 0.75 – 0.99 at 12 dpt, 0.99 – 1.0 at 16 dpt, and 0.89 – 1.0 at 20 dpt.

3.1.4. Aggregation of WT-βS, P123H-βS, and V70M-βS in primary culture of cortical neurons

In order to compare aggregation properties and stability of αS, WT-βS, P123H-βS, V70M-βS and γS expressed in the primary cultured neurons, I applied a standardized the proteinase K (PK) digestion protocol. PK is a broad serine protease which is able to efficiently hydrolyze most proteins with the exception of β-sheet-rich aggregates of prions, synucleins and some other proteins. The activity of PK depends on buffer composition, temperature, PK concentration, and time of the reaction. Here, I tested the stability of synuclein proteins under the following conditions: 37^0 C, 5 min digestion, 2 µg/ml PK and 2 µg/µl protein in PBS/0.5% SDS lysis buffer. When I referred to any of the synucleins as "PK-resistant", only a relative resistance under the mentioned above reaction conditions is meant.

While γS and β-tubulin were completely digested at given conditions, 54 ± 23% of αS remained after 5 min of PK digestion; most of it was the 18 kDa full-length form of the protein. In case of WT-βS, P123H-βS, and V70M-βS several fragments of 10-16 kDa were detected after PK digestion in addition to the minor band of ~20 kDa of the full-length protein (Figure 3.6.). Numerous repetitions of the PK digestion experiment showed that these partial fragments have the same size in WT-βS and both mutants but the total amount of resistant protein is lower in V70M-βS. The quantity of the PK-resistant material in V70M-βS, 28 ± 12%, was significantly lower than in WT-βS, 51 ± 18%,(unpaired t-test, p = 0.0016, power (1-β err prob) = 0.96), in P123H-βS, 44 ± 22% (unpaired t-test, p = 0.0403, power (1-β err prob) = 0.66), and αS 54 ± 23% (unpaired t-test, p = 0.0037, power (1-β err prob) = 0.94). The differences WT-βS vs. P123H-βS, WT-βS vs. αS, and P123H-βS vs. αS were not statistically significant.

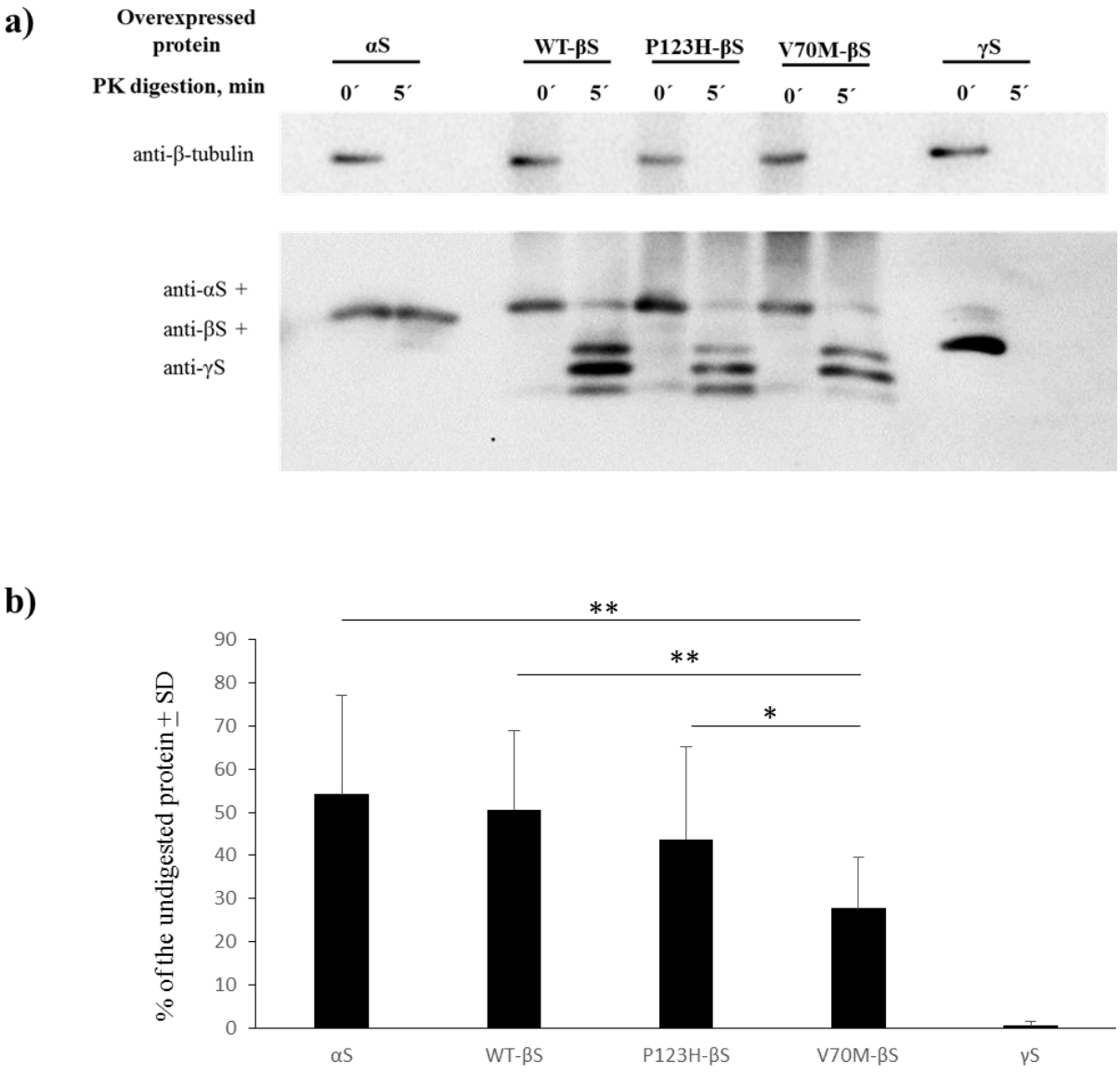

Figure 3.6. Aggregation of synucleins in primary cortical culture.

(a) Cell culture lysates werecollected 20 days after AAV6 virus transduction and digested with 2 µg/ml PK. The lanes of the immunoblot show lysates after 0 and 5 min of PK digestion. 30 µg of protein are loaded per well. In case of αS, the full-length form of the protein is the most prominent band which remains after 5 min digestion. For WT-βS and its P123H and V70M mutants, the undigested bands of 10-16 kDa in addition to the less prominent full-length protein band are detected after PK digestion. The sizes of these fragments are the same in WT-βS, P123H-βS, and V70M-βS. γS and β-tubulin are completely digested under the same conditions.

(b) The amount of protein remaining after 5 min of PK treatment is represented as a percentage of the starting material (0 min digestion). V70M-βS is digested significantly faster than αS (unpaired t-test, $p = 0.0037$), WT-βS (unpaired t-test, $p = 0.0016$), and P123H-βS (unpaired t-test, $p = 0.0403$). Data are shown as mean $\pm$ SD ($n = 11$ immunoblots from 6 independent experiments). The difference P123H-βS vs. WT-βS was not significant.

Next, I tested PK-digested material with antibodies for epitopes in different domains of αS and βS in order to determine which part of the protein remains after PK digestion (Figure 3.7.). The partial fragments of WT-βS and mutants which are produced in the PK digestion reaction could be detected with the N-terminal antibody (panS, amino acid residues 11 – 26, ab6176), antibody against epitope in the NAC domain (amino acid residues 81 – 95, SAB1100305) but were not detected with the antibody to the C-terminal region (amino acid residues 108 – 125, ab6165). Also, synucleins with C-terminal AU1-tag were PK-digested and analyzed (Figure 3.8.). Both experiments revealed that C-terminal region of βS is being cleaved off in PK reaction.

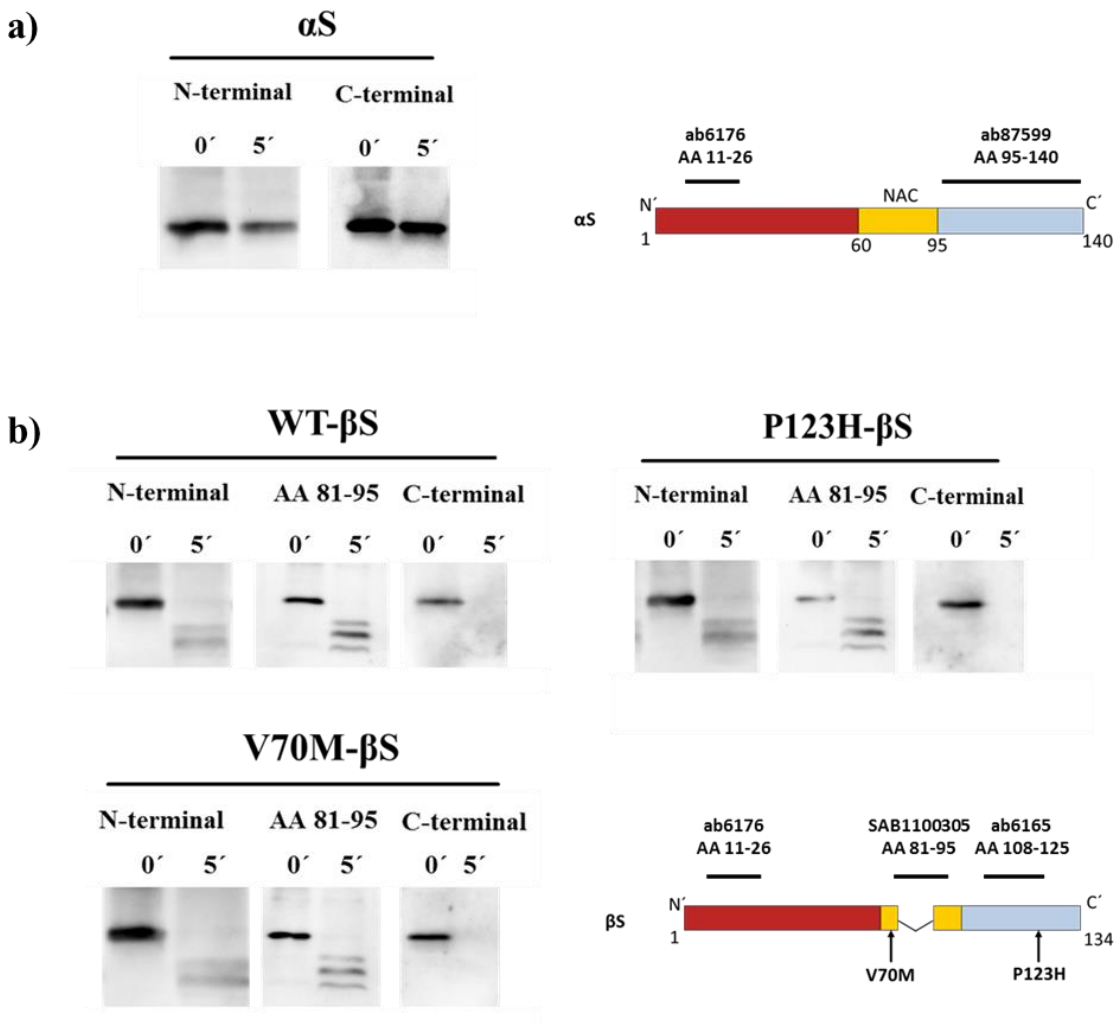

Figure 3.7. Detection of the PK-digested synucleins with various antibodies.

Lysates of αS, WT-βS, P123H-βS, and V70M-βS were digested with PK for 0 minutes (0´-lane) or 5 minutes (5´-lane) and detected with antibodies to different synuclein domains.

(a) αS was detected antibody against N-terminal region, panSynuclein (ab6176) with epitope corresponding to AA 11-26 and antibody against C-terminus, sc87599 binding to AA 95-140 in αS, as shown in the scheme. Full-length αS is detected after PK digestion.

(b) WT-βS, P123H-βS, and V70M-βS were detected with antibodies against N-terminus (ab6176, AA 11-26), central domain corresponding to αS NAC-domain (SAB1100305, AA 81-95), and C-terminus (ab6165, AA 108-125). WT-βS, P123H-βS, and V70M-βS lost the C-terminal region in the PK reaction.

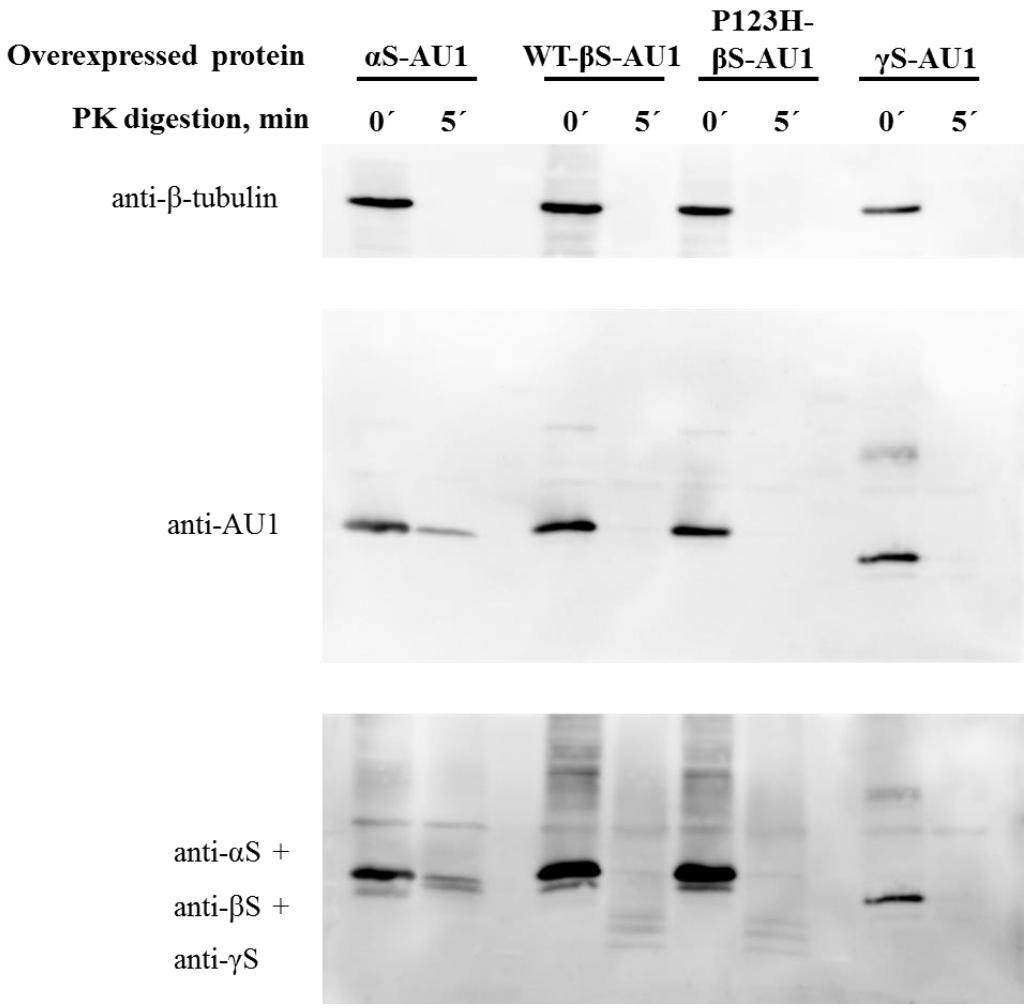

Figure 3.8. PK digestion of AU1-tagged synucleins.

The lysates of the primary cultured neurons expressing αS, WT-βS, P123H-βS, and γS with the C-terminal AU1-tag were digested with PK enzyme (37^0 C, 5 min, 4 µg PK per 1 ml lysis buffer). The panels show (from up to down) detection with β-tubulin, AU1 antibodies, and specific synuclein antibodies with N-terminal epitopes. C-terminal regions of WT-βS and P123H-βS are cleaved off by the PK.

3.1.5. Mitochondrial morphology and motility

Various impairments of mitochondrial functions were reported to be associated with the PD pathology (Schapira *et al.*, 1989; Kraytsberg *et al.*, 2006; Schapira *et al.*, 2012). Besides, αS was shown to cause mitochondrial fragmentation and deformations which interfered with the fusion/fission homeostasis of mitochondria (Kamp *et al.*, 2010; Nakamura *et al.*, 2011; Taschenberger *et al.*, 2013), and induce mitochondria-related pathological cascades leading to neuronal death (Tolö *et al.*, 2018). Recently, WT-βS was also shown to induce mitochondrial pathology (Taschenberger *et al.*, 2013).

Here, I aimed to investigate whether the disease-associated mutations of WT-βS, V70M and P123H, have an effect on mitochondrial morphology and motility which, in turn, could be one of the mechanisms underlying the neuronal loss described in the section 3.1.3. Primary cortical neurons were transduced on div 3 with 0.8 x 10^8 tu of AAV6 vectors expressing both cytoplasmic EGFP and one of the synuclein proteins (αS, WT-βS, P123H-βS, V70M-βS or γS) under control of two separate hSyn1 promoters. The AAV6 vector expressing EGFP alone was used as a control. Additionally, 0.5 x 10^7 tu of the AAV6-s-4xmito-TdTomato-WB virus was added at div 3 to each well of a 24-well plate for visualizing of mitochondria, mediated by the expression of the fluorescent protein TdTomato (Figure 3.9).

Live cultured neurons were imaged 7 and 14 days after the virus administration. According to the morphology of the mitochondria in the neuronal cell bodies, neurons were divided into the three categories: 1st – neurons with elongated or tubular mitochondria, 2nd – neurons with partially condensed mitochondria (here some mitochondria gained a rounded phenotype, and were usually smaller in size than mitochondria of the 1st category), and 3rd – neurons with fully condensed mitochondria (most of the mitochondria are rounded or swollen) as illustrated on the Figure 3.10 (a-i). Such classification of mitochondrial morphology was already reported in Taschenberger *et al.*, 2013.

Approx. 200 neurons from 4-5 cover slips were analysed for each group and time point and the percentage of neurons of each category was calculated for each cover slip. Only neurons with the high expression levels of the both fluorescent reporters, cytoplasmic EGFP, and mitochondrial TdTomato were selected for the analysis.

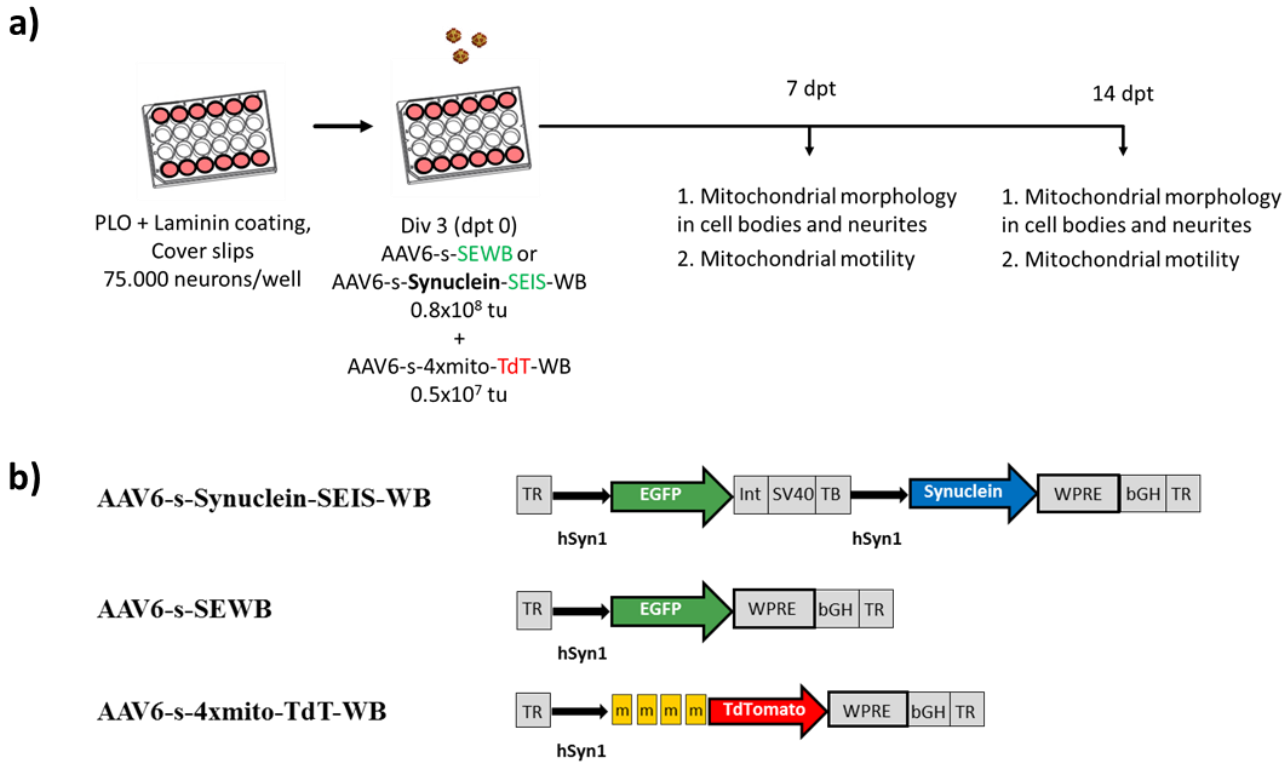

Figure 3.9. Scheme of the experiments on mitochondrial morphology and motility.

(a) Primary cortical neurons were seeded at the concentration 75 000 cells/well onto PLO/laminin coated cover slips. At div 3, AAV vectors of serotype 6 were applied for the overexpression of cytoplasmic synuclein and EGFP, and mitochondrial TdTomato. At 7 and 14 days after the virus administration, microscopic images and time-lapse videos were recorded for the analysis of mitochondrial morphology and motility.

(b) Structure of the AAV vector genomes: bicistronic vector for the expression of a synuclein (either αS, WT-βS, P123H-βS, V70M-βS or γS) and EGFP under control of two separate hSyn1 promoters; monocistronic vector expressing EGFP used as a control; and monocistronic vector carrying the cDNA for mitochondrial reporter TdTomato. Expression of the transgenes was controlled by the human synapsin 1 gene promoter (hSyn1) and enhanced by Woodchuck hepatitis virus posttranscriptional regulatory element (WPRE). Int - intron; SV40 - SV40 polyadenylation site; bGH - bovine growth hormone gene polyadenylation site; TR - inverted terminal repeats, m – mitochondrial localization sequence.

At 7 days post-transduction, the neurons overexpressing human αS and V70M-βS had significantly less frequently "healthy" elongated mitochondria in comparison with EGFP control ($p = 0.0011$, power (1-β err prob) = 0.99; and $p = 0.0054$, power (1-β err prob) = 0.98, respectively). Moreover, αS-expressing neurons significantly more often had fully condensed mitochondria than EGFP ($p = 0.0274$, power (1-β err prob) = 0.80) and γS ($p = 0.046$, power (1-β

err prob) = 0.70) groups. The differences between WT-βS vs. P123H-βS vs. V70M-βS were not significant at this time point (Figure 3.10).

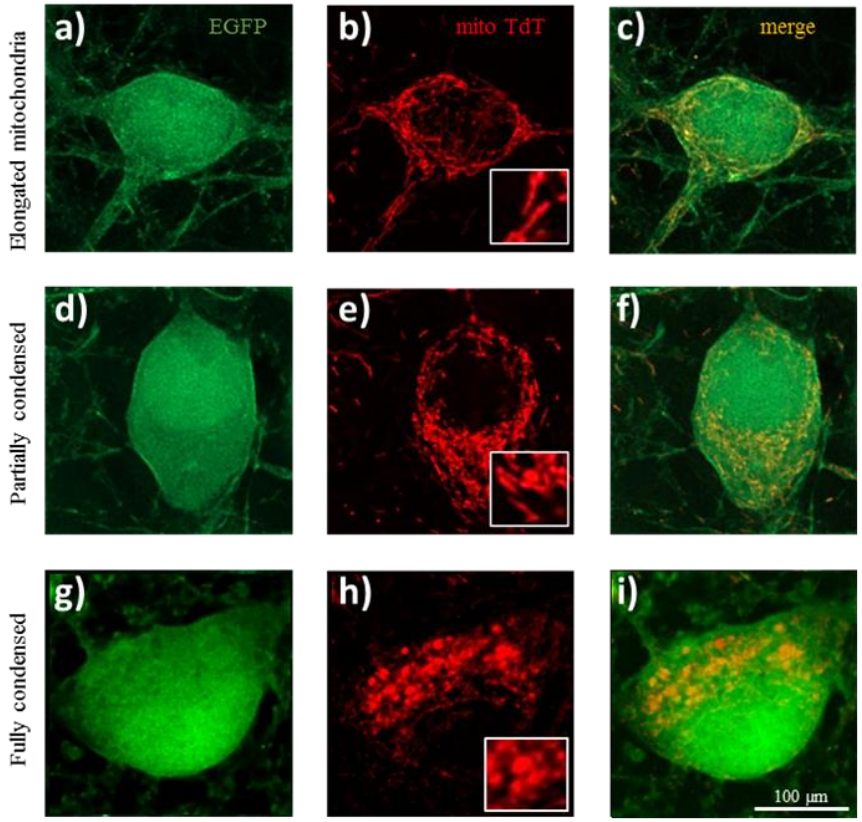

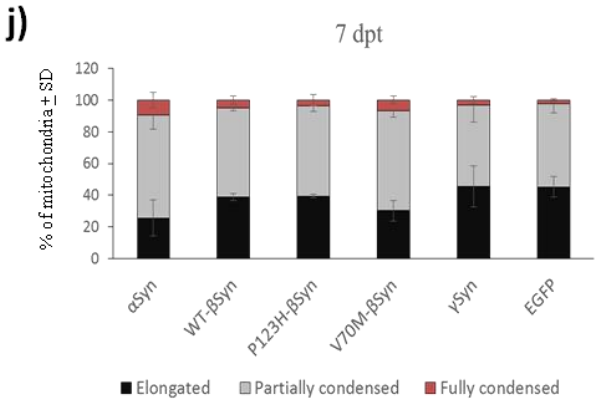

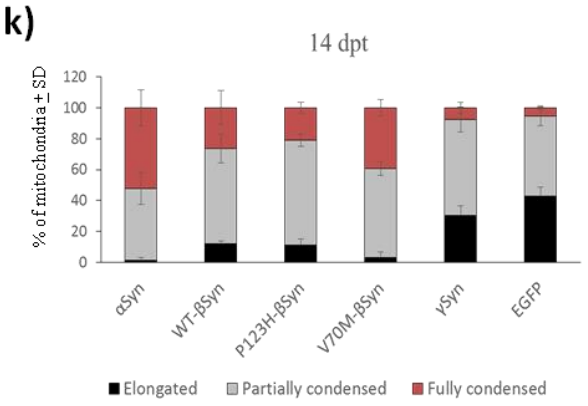

l)

Elongated mitochondria

14 dpt	αS	WT-βS	P123H-βS	V70M-βS	γS
EGFP	****	****	****	****	**
αS		*	*	n.s.	****
WT-βS			n.s.	n.s.	****
P123H-βS				n.s.	****
V70M-βS					****

m)

Fully condensed mitochondria

14 dpt	αS	WT-βS	P123H-βS	V70M-βS	γS
EGFP	****	**	*	****	n.s.
αS		****	****	n.s.	****
WT-βS			n.s.	*	*
P123H-βS				**	n.s.
V70M-βS					****

Figure 3.10. Fragmentation of mitochondria in neuronal cell bodies.

Primary cortical neurons were seeded on PLO/laminin coated cover slips with the droplet method (75 000 cells/well). Neurons were co-transduced with the respective bicistronic AAV6 vectors (synuclein+EGFP) as 0.8 x 10^8 tu/well and an AAV6 vector with cDNA for TdTomato equipped with mitochondrial localization sequence (AAV6-s-4xmito-TdT-WB) at the concentration 0.5 x 10^7 tu/well. All transgenes were expressed under control of neuron-specific promoters, hSyn1. Morphology of mitochondria was analyzed 7 and 14 days after transduction and each cell was classified in one of 3 categories according to the shape of most mitochondria in the cell: 1. Elongated mitochondria **(a-c)**; 2. Partially condensed mitochondria (both elongated and rounded mitochondria were present) **(d-f)**; 3. Fully condensed mitochondria (most mitochondria had rounded appearance) **(g-i)**. Approx. 200 neurons from 4 cover slips were classified in each condition. Percentage of the cells with elongated, partially condensed and fully condensed mitochondria was calculated at 7 **(j)** and 14 **(k)** days after transduction. Expression of αS, WT-βS, and P123H, and V70M mutants of βS leads to significant increase in fragmentation of mitochondria from day 7 to day 14 with the most dramatic effect for αS, closely followed by V70M-βS. At 14 dpt, V70M-βS had significantly more neurons with fully condensed mitochondria than WT-βS (p=0.0323), while P123H mutant was not significantly different from WT-βS. Results of 1-way ANOVA/Tukey's test are provided in Figure 3.10. **(l-m)**. Data are shown as mean % per cover slip ± SD. *p<0.05, **p<0.01, ***p<0.001, ****p<0.0001.

After 14 days of transgene expression, the percentage of neurons with mostly elongated mitochondria decreased in case of the overexpression of αS to 1.4 ± 1.8%, WT-βS to 12 ± 2%, P123H-βS to 11 ± 4%, V70M-βS to 3.4 ± 3.2%, and γS to 30 ± 6% of all analyzed neurons. For EGFP the portion of neurons with elongated mitochondria estimated 43 ± 6% which virtually did not change from the dpt 7. The differences between WT-βS and both mutants were not statistically significant in this category. P-values for the Tukey's multiple comparison test are provided in Figure 3.10 (l). The fraction of the neurons with fully condensed mitochondria at 14 dpt was significantly larger for V70M-βS (39 ± 5%) than for WT-βS (24 ± 7%) (Tukey's, $p = 0.0323$, power (1-β err prob) = 0.93) while the difference WT-βS vs. P123H-βS was not significant. For this morphological category, the V70M-βS condition was not statistically different from the αS with 52 ± 12% of the neurons with fully condensed mitochondria. For the EGFP control, the percentage of fully condensed mitochondria amounted to 6 ± 1% which was statistically lower than in αS (Tukey's, $p < 0.0001$, power (1-β err prob) = 1.0), WT-βS (Tukey's, $p = 0.0068$, power (1-β err prob) = 1.0), P123H-βS (Tukey's, $p = 0.0285$, power (1-β err prob) = 1.0) and V70M-βS (Tukey's, $p < 0.0001$, power (1-β err prob) = 1.0).

Next, the morphology of the neuritic mitochondria was analyzed by calculating length to width ratio of single mitochondria. The measurements were performed with ImageJ software (NIH). Here, at least 100 mitochondria were analyzed for each condition and time point of the

experiment. The investigator was blinded to the treatment groups. Although the mitochondria in the neurites did not have such dramatic condensed phenotype as the somatic mitochondria, we observed some rounding or decrease in length/width ratio of mitochondria compared to EGFP-control in αS, WT-βS, P123H-βS and V70M-βS conditions both at 7 and 14 days post-transduction (Figure 3.11.). Seven days after the virus administration, V70M-βS had more rounded mitochondria than P123H-βS (Turkey's, $p < 0.0001$, power (1-β err prob) = 0.99) but at 14 dpt the difference between these two groups was not significant anymore. WT-βS was not statistically different to P123H-βS and V70M-βS mutants at any time point.

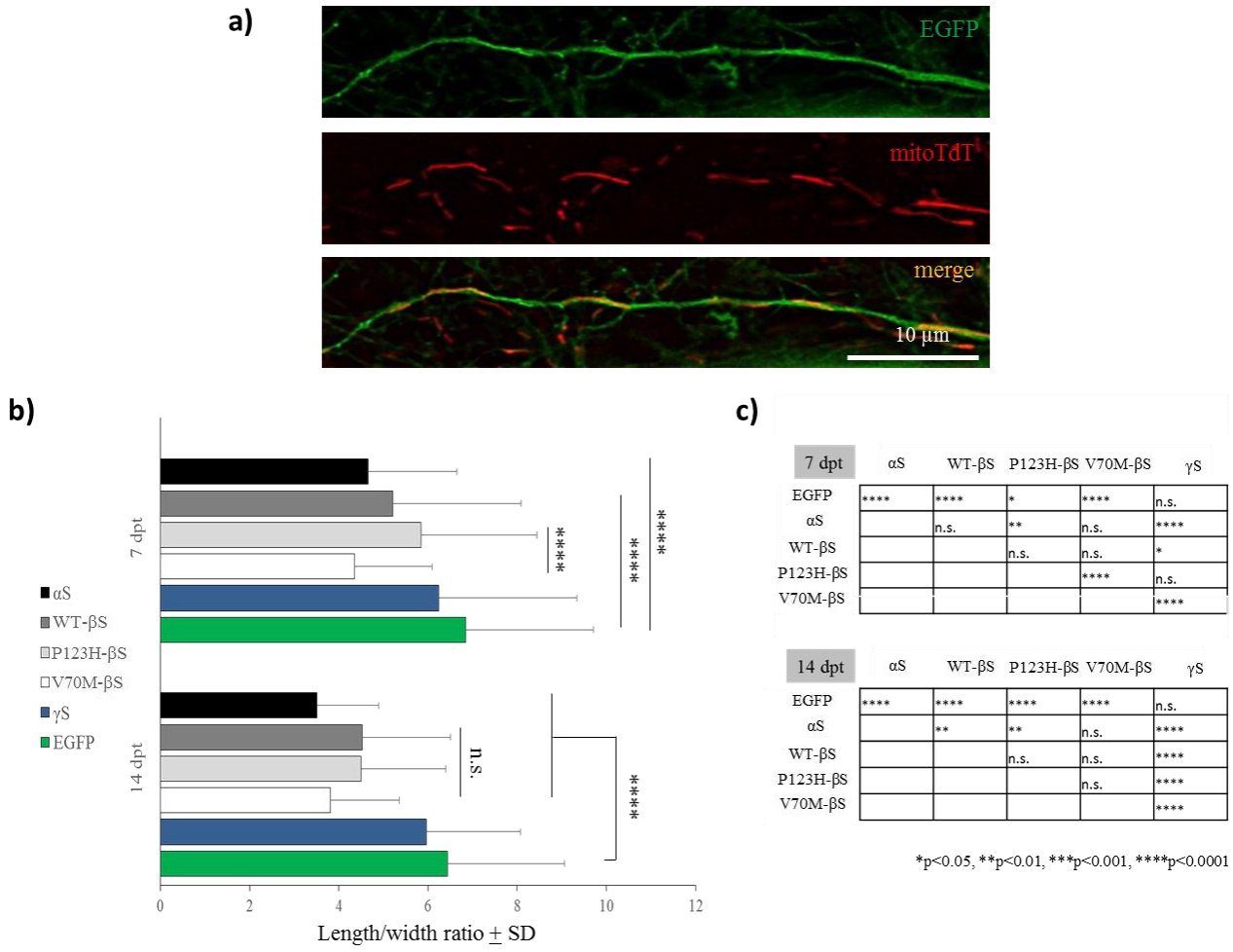

Figure 3.11. Morphology of mitochondria in neurites.

(a) Primary cortical neurons were co-transduced with bicistronic AAV constructs (synuclein + EGFP) and mitochordrial reporter (TdTomato) as described above. Only the neurites with prominent expression of EGFP were included in the analysis. Scale bar: 10 µm.

(b) Length to width ratio was calculated for 100-150 mitochondria from 4-5 cover slips per condition and time point. Mitochondrial morphology in neurites was evaluated 7 and 14 days after transduction. The

bars represent the data for αS, WT-βS, P123H-βS, V70M-βS, γS and EGFP control groups (according to the color code). Data are shown as mean length/width ratio ± SD.

(c) Statistical analysis with 1-way ANOVA/Tukey's test revealed no significant differences between WT-βS and P123H-βS or V70M-βS at 7 and 14 dpt. The mitochondria were significantly shorter in αS, WT-βS, and V70M-βS at 7 dpt and αS, WT-βS, P123H-βS and V70M-βS at 14 dpt when compared with EGFP and γS.

*p<0.05, **p<0.01, ***p<0.001, ****p<0.0001.

Next, I studied the motility of the mitochondria. To that end, time lapse videos of the neurites were taken for 180 sec and with the 63x objective magnification. Only motile mitochondria were analyzed and no distinguishment between the anterograde and retrograde direction of the movement was made. Mitochondria were traced manually with help of the MTrackJ plugin of ImageJ. At least 60 mitochondria from 3 cover slips were analyzed for each condition and time point. The results for the mean and maximal speed of mitochondria are provided in the Figure 3.12.

The mean speed of mitochondria at 7 dpt was equal to 34 ± 16 µm/min for αS, 44 ± 15 µm/min for WT-βS, 43 ± 15 µm/min for P123H-βS and 49 ± 17 µm/min for V70M-βS, 43 ± 20 µm/min for, and 49 ± 17 µm/min for EGFP conditions. The mean speed virtually did not change from 7th to 14th day after virus administration. Only αS caused a significant decrease in the speed of mitochondria in comparison with other groups.

The maximal speed of mitochondria at 7 dpt amounted to 74 ± 39 µm/min for αS, 90 ± 40 µm/min for WT-βS, 87 ± 40 µm/min for P123H-βS and 88 ± 32 µm/min for V70M-βS, 85 ± 43 µm/min for γS, and 100 ± 35 µm/min for EGFP conditions. The only statistically significant difference here was αS vs. EGFP treatments (Tukey's, p = 0.0006, power (1-β err prob) = 0.99). The maximal speed slightly increased in all the transduction groups from dpt 7 to dpt 14, with exception of V70M-βS condition where the speed stayed the same. Only αS had a statistically significant effect on the maximal speed at 14 dpt: αS vs. WT-βS (Tukey's, p = 0.0322, power (1-β err prob) = 0.92), αS vs. γS (Tukey's, p = 0.0351, power (1-β err prob) = 0.92), and αS vs. EGFP (Tukey's, p = 0.0052, power (1-β err prob) = 0.99). WT-βS and both its mutants were not significantly different from each other.

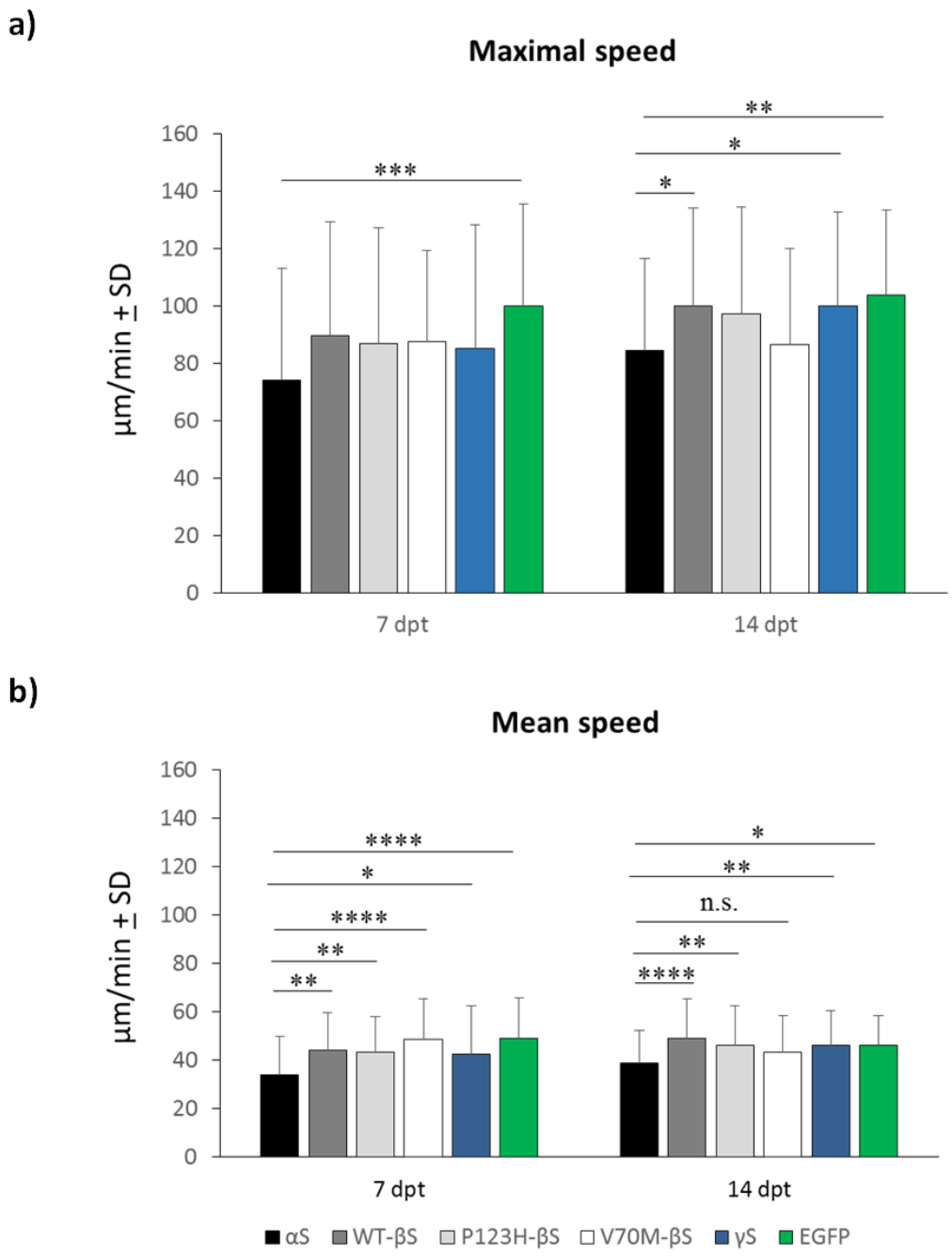

Figure 3.12. Motility of mitochondria in neurites.

Overexpression of αS + EGFP, WT-βS + EGFP, P123H-βS + EGFP, V70M-βS + EGFP, γS + EGFP or EGFP alone was mediated by AAV6 vectors (0.8 x 10^8 tu/well) in cultures of cortical neurons. Mitochondria were visualised by overexpression of TdTomato with mitochondrial localization (AAV6-s-4xmito-TdT-WB, 0.5 x 10^7 tu/well). In order to analyse the motility, mitochondria moving along the neurites were tracked on a 3 min time-lapse videos with MTrackJ plugin of ImageJ software (n=63 mitochondria from 3 cover slips). Maximal **(a)** and mean **(b)** speed of mitochondria are given in µm/min ± SD. Only αS caused significant effects on mitochondrial motility (both mean and maximal speed) after 7 and 14 days of the transgene expression.*p<0.05, **p<0.01, ***p<0.001, ****p<0.0001.

Taken together, P123H-βS did not aggravate toxic effects of WT-βS on the morphology of the somatic mitochondria, while V70M-βS expression led to less abundant neurons with “healthy” tubular mitochondria and more frequent fully condensed appearance of mitochondria. The extent of mitochondrial pathology induced by V70M-βS was virtually as strong as in αS condition. Mitochondria in the neurites were also rounded under the influence of αS, WT-βS, P123H-βS, and V70M-βS, but no difference between WT-βS and its mutants was observed. Neither WT-βS nor its mutants had an effect on the motility of mitochondria.

3.2. Aggregation and toxicity of WT-βS, P123H-βS, and V70M-βS in dopaminergic neurons of the rat's Substantia nigra *in vivo*

3.2.1. Experimental design and expression analysis

In order to study and compare the toxicity and aggregation properties of WT-βS and its P123H and V70M mutants *in vivo*, the synuclein proteins were overexpressed in SN of rats. Overexpression of human variants of αS, WT-βS, P123H-βS, and V70M-βS was mediated by AAV2 serotype vectors. The structures of the cDNAs are provided in the Figure 3.13 (b). Expression of the transgenes was controlled by the human synapsin 1 gene promoter and enhanced by WPRE sequence. AAV2-EGFP vector was used as a control.

Monocistronic AAV2 vectors were injected unilaterally into the left SNpc of adult female rats according to the coordinates AP: -5.3 mm, ML: +2.2 mm, DV: -7.75 mm relative to bregma (Paxinos and Watson, 1986). 1.2 x 10^8 tu of the virus was injected in each case. Animals were sacrificed 2, 3 or 8 weeks after the AAV2 virus administration. 2- and 8-week groups were processed for IHC stainings, stereotaxic quantifications of dopaminergic and non-dopaminergic neuronal loss in SNpc, evaluation of striatal fiber density and axonal pathology. The brains of the 3-week groups were used for the preparation of brain lysates and analysis of *in vivo* synuclein aggregation by PK digestion (Figure 3.13 (a)).

All the brains which were collected 2 and 8 weeks after the surgery were cryosectioned (Leica cryostat) and analyzed with IHC methods for the expression levels of the αS, WT-βS, P123H-βS, V70M-βS, and EGFP. Only brains with proper targeting of SNpc, a good transduction in the region AP -4.5 mm to -6.3 mm relative to bregma, and similar expression levels were selected for the further analysis (Figure 3.14.). Double immunofluorescence staining for the dopaminergic marker tyrosine hydroxylase (TH) and human αS, WT-βS, P123H-βS, and V70M-βS or EGFP control showed major localization of the overexpressed proteins in the dopaminergic neurons of SNpc. Nearly 70 – 80% of SNpc neurons on the injected side of the brain were compactly transduced 2 weeks after the virus administration. Non-injected (contralateral) SN had no expression of the transgenes (Figure 3.15). Loss of dopaminergic neurons was occasionally observed in the 2-week groups of αS, WT-βS, P123H-βS, and V70M-βS. Eight weeks post transduction the loss of TH-positive neurons resulted in the extensive lesions in the left SNpc due

to the overexpression of αS, WT-βS, P123H-βS, and V70M-βS while contralateral SN remained virtually unaffected (Figure 3.15). The loss of dopaminergic neurons was quantified with stereological methods (see section 3.2.2.).

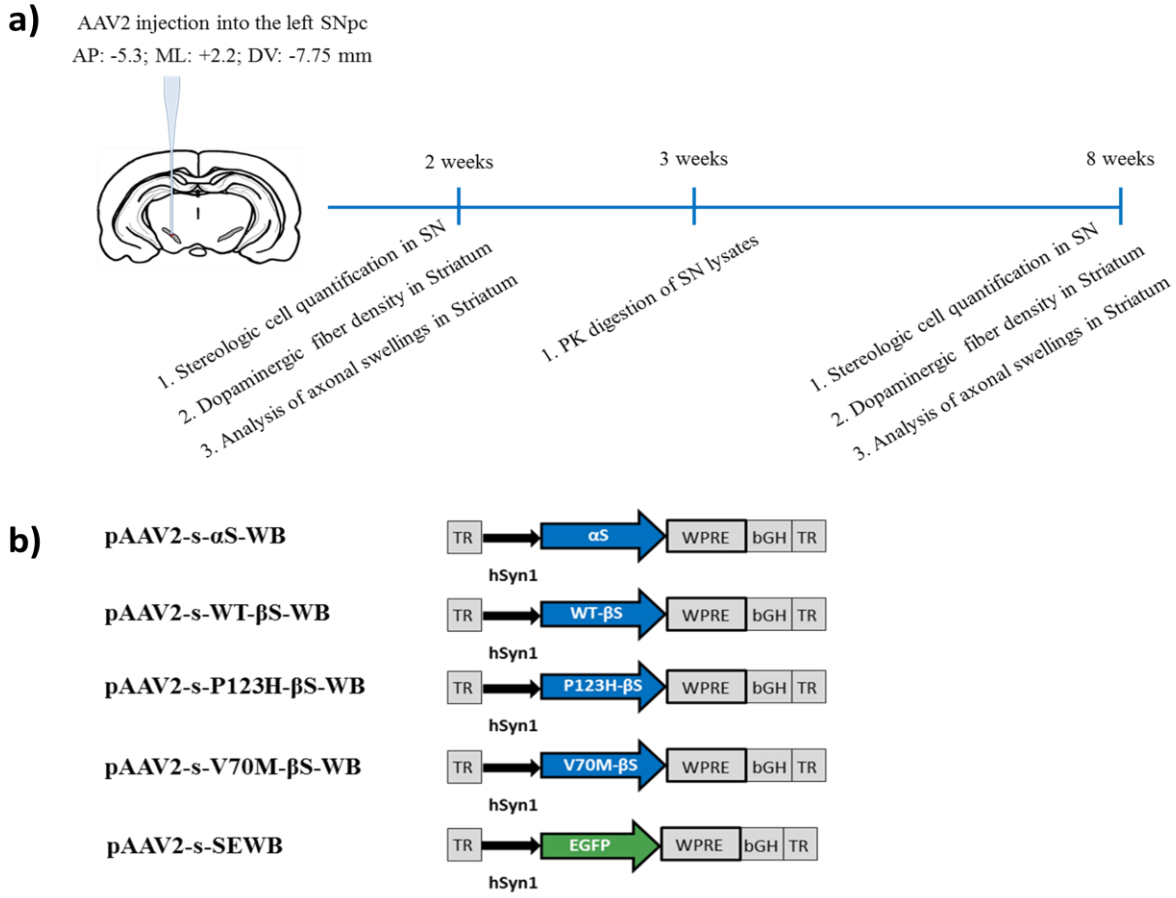

Figure 3.13. The layout of the *in vivo* experiments.

(a) Scheme of the *in vivo* experiments. AAV2 viruses expressing human αS, WT-βS, P123H-βS or V70M-βS or EGFP control were unilaterally injected into the brains of adult female rats according to the coordinates for targeting left SNpc (anterior-posterior (AP): -5.3 mm, mediolateral (ML): +2.2 mm, dorsoventral (DV): -7.75 mm relative to bregma (Paxinos and Watson, 1986) with total concentration of 1.2 x 10^8 tu per brain. Rats were sacrificed 2 and 8 weeks after surgery, and the brains were cryosectioned for IHC stainings and analysis of dopaminergic degeneration in SNpc and striatum. 3 weeks post transduction the brains were collected for preparation of lysates and studying the aggregation properties of synucleins with PK digestion and immunoblotting.

(b) Structure of the AAV2 genomes. Monocistronic AAV2 vectors with cDNAs for human αS, WT-βS, P123H-βS or V70M-βS were used for targeted expression in rat's SN and AAV2 vector with the cDNA for EGFP was used as a control in *in vivo* experiments. Expression of the transgenes was controlled by neuron-specific human synapsin 1 gene promoter (hSyn1) and enhanced by Woodchuck hepatitis virus posttranscriptional regulatory element (WPRE). bGH - bovine growth hormone gene polyadenylation site; TR - inverted terminal repeats.

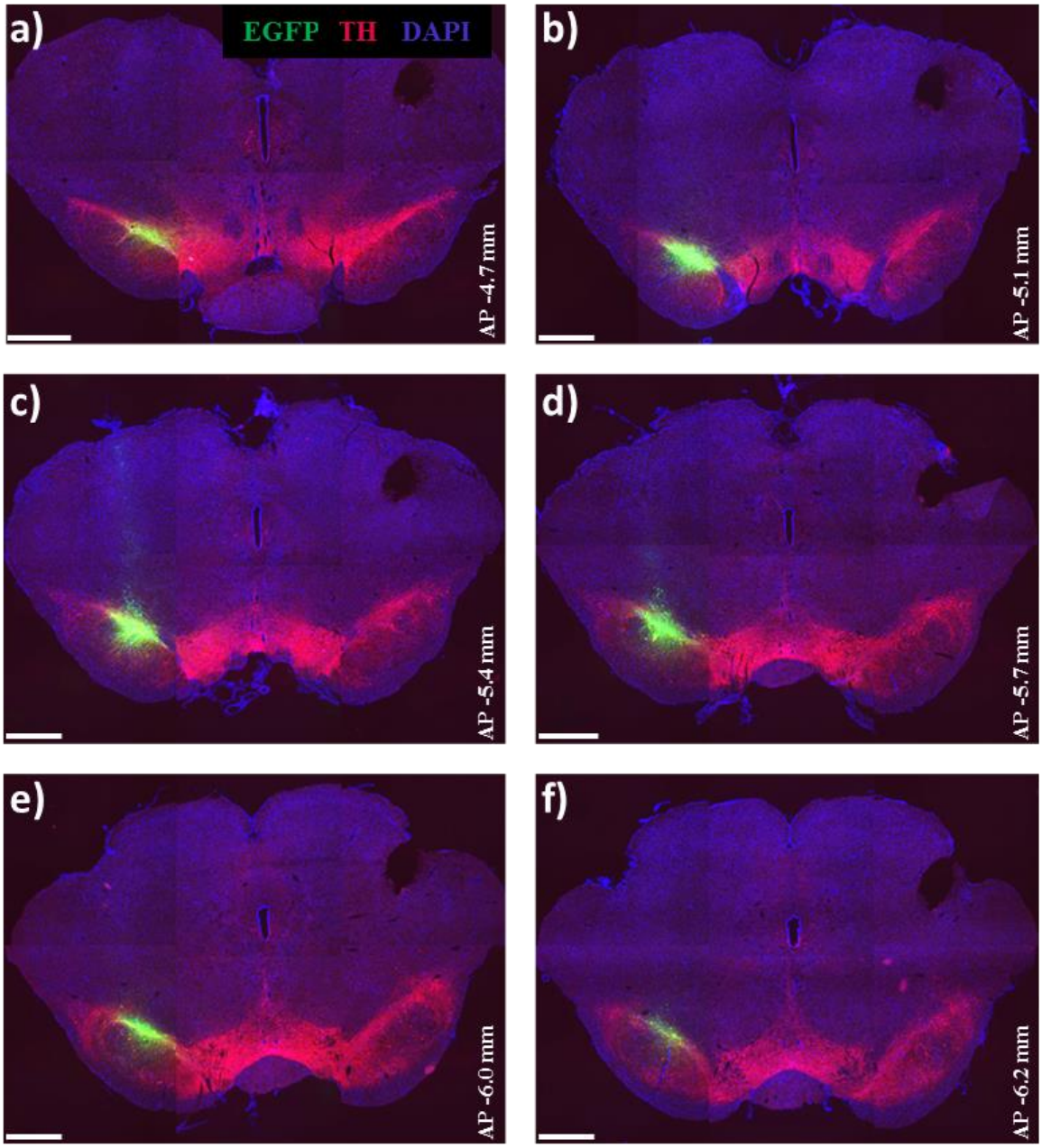

Figure 3.14. Overview of the transduced SN sections on the example of an EGFP control brain (2 weeks post-transduction).

Monocistronic AAV2 vectors were stereotaxically injected into the left SNpc of the rat's brain as described in the Figure 3.12. Representative mosaic images **(a-f)** illustrate the extent of the transduction with AAV2-EGFP vector 2 weeks after the administration of the virus. Similar transduction was also observed in other experimental groups: αS, WT-βS, P123H-βS, and V70M-βS. Only brains with proper targeting of the left SNpc and good transduction in the region AP -4.5 to -6.3 mm relative to bregma were selected for further analysis.

AP stands for anterior-posterior coordinates relative to bregma and coordinates are given in mm. Cortices were removed prior to the IHC staining and only midbrain sections are shown. Scale bar: 1 mm.

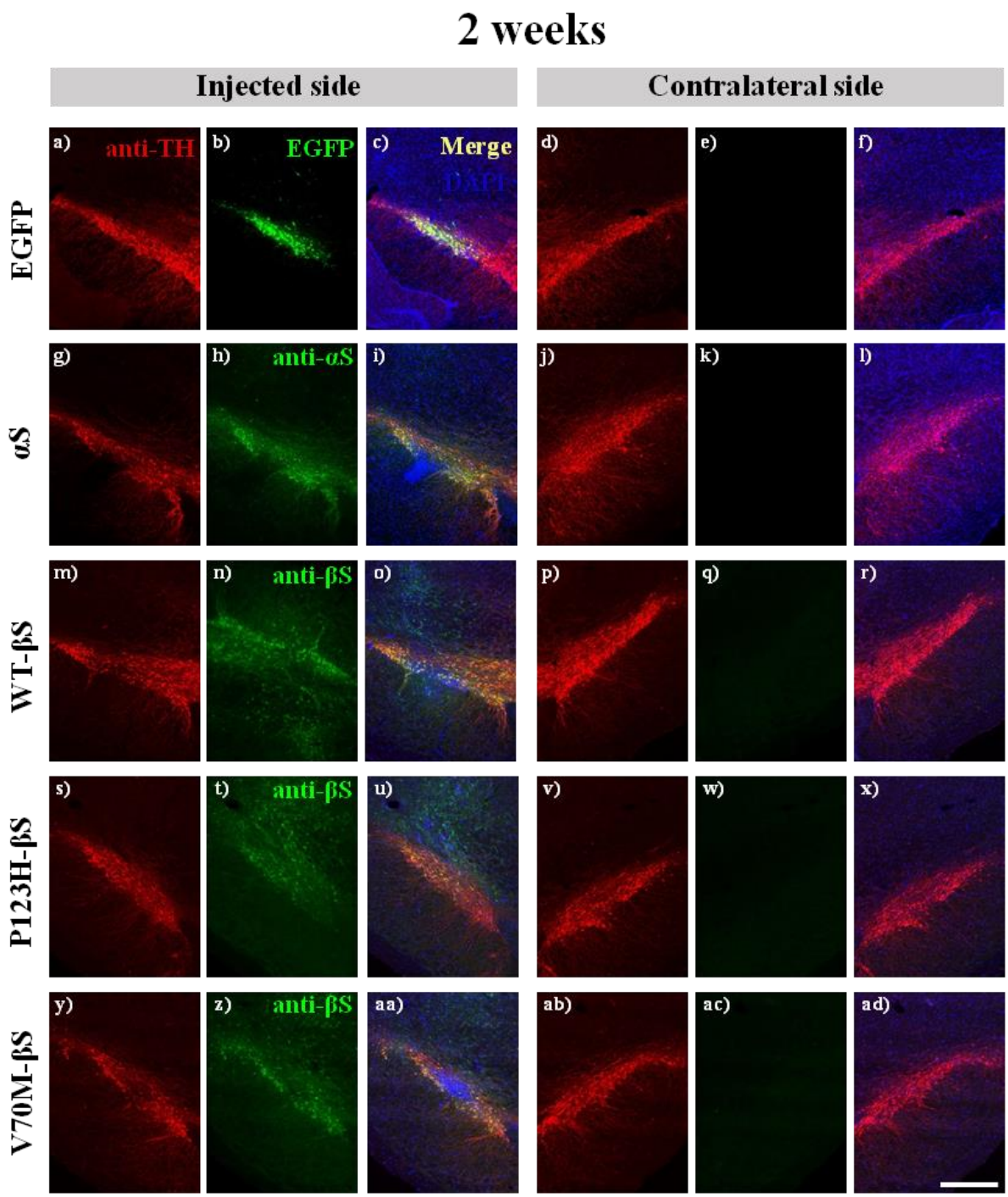

Figure 3.15. Expression of the transgenes in rats' SN, 2 weeks after AAV injection.

Stereotaxic unilateral injections of AAV2 viruses into the left SN resulted in overexpression of EGFP, αS, WT-βS, P123H-βS or V70M-βS in SNpc (pictures b, h, n, t, z, respectively). Approx. 70 – 80% of the dopaminergic (TH-positive) neurons of the injected SNpc were transduced (c, i, o, u, aa). No transgene expression was noticed on the contralateral side of the brain. Representative 5x pictures (a-ad) were taken with Axioplan 2 microscope (Zeiss). The exposure times: anti-TH-Cy3 – 4005 ms, anti-αS-Cy2 or anti-βS-Cy2 – 3567 ms, EGFP – 2267 ms, and DAPI – 432 ms. Scale bar: 500 µm.

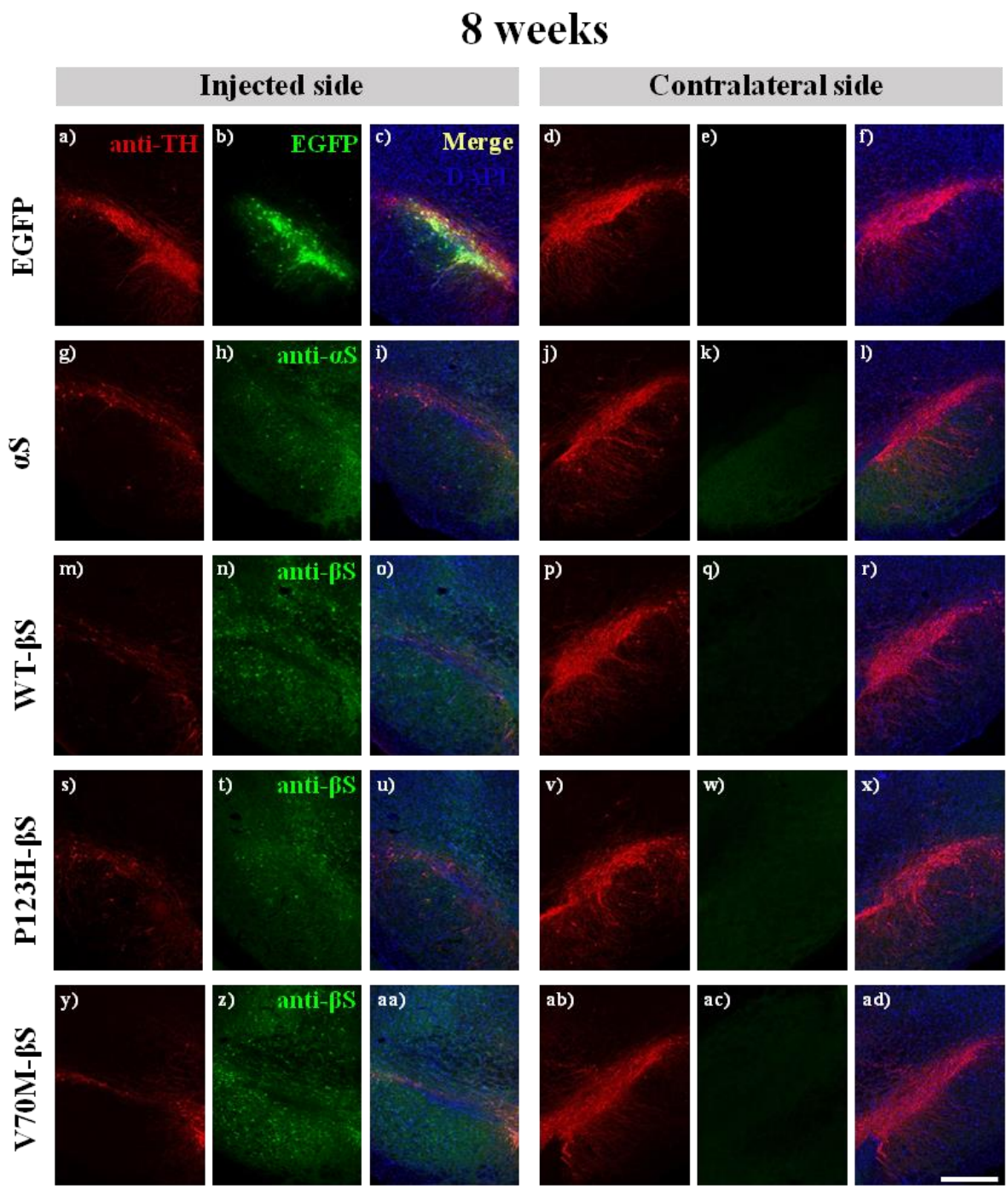

Figure 3.16. Expression of the transgenes in rats' SN, 8 weeks after AAV injection.

After 8 weeks of transgene expression, a massive loss of dopaminergic neurons of SNpc was observed on the injected side in groups of αS, WT-βS, P123H-βS, and V70M-βS as revealed by the IHC staining against TH (g, m, s, y). Overexpression of αS (h), WT-βS (n) and mutants (t, z) can be seen in a few surviving TH-positive neurons and in non-dopaminergic cells, surrounding the SNpc. SNpc on the contralateral sides and EGFP-expressing SN did not have apparent loss of dopaminergic neurons (a, d, j, p, v, ab). The exposure times: anti-TH-Cy3 – 3005 ms, anti-αS-Cy2 or anti-βS-Cy2 – 2267 ms, EGFP – 1267 ms, and DAPI – 432 ms. Scale bar: 500 µm.

3.2.2. Toxicity of WT-βS, P123H-βS, and V70M-βS in rat's SN

Progressive neurodegeneration of SNpc is one of the major hallmarks of PD and DLB. Time-dependent loss of dopaminergic neurons in SNpc was successfully recapitulated in several rAAV animal models where WT or mutant αS were overexpressed (Taschenberger *et al.*, 2012; Decressac *et al.*, 2013; Davies *et al.*, 2014). Besides, our lab has shown before that AAV-mediated overexpression of WT-βS can also lead to the direct nigral neurodegeneration in rat's brain (Taschenberger *et al.*, 2013). Here, we aimed to compare the ability of WT-βS, P123H-βS, and V70M-βS to induce neurotoxicity towards SNpc. The V70M mutant was for the first time characterized *in vivo*, and the P123H mutant was for the first time characterized in the AAV animal model.

In order to evaluate the loss of dopaminergic neurons, TH-positive neurons were stereotaxically quantified in the ipsilateral SNpc on 10 brain sections stained with the IHC-DAB protocol (Figure 3.17). Dopaminergic neurons of the VTA and SN pars reticulata were excluded from the analysis. During the stereological cell quantifications, the investigator was blinded to the injection groups and identification numbers of the animals.

At 2 weeks after virus administration, the number of TH-positive neurons in the EGFP-expressing SNpc amounted to 7653 $\pm$ 1375 cells (n = 8). In the αS group the number of dopaminergic neurons was 4751 $\pm$ 1575 (n = 8), so ~37.9% of dopaminergic neurons were lost if compared with EGFP control (Tukey's, p = 0.0015, power (1-β err prob) = 0.98). V70M-βS with 5435 $\pm$ 1440 TH-positive neurons (n = 17) also caused a significant neuronal loss (Tukey's, p = 0.0057, power (1-β err prob) = 0.97). The numbers of dopaminergic neurons in WT-βS (6139 $\pm$ 1686, n = 11) and P123H-βS (6426 $\pm$ 1067, n = 13) were not significantly reduced. The statistical differences WT-βS vs. P123H-βS vs. V70M-βS were not significant.

Eight weeks post-transduction, the quantity of surviving dopaminergic neurons was similar in αS (3235 $\pm$ 1188, n = 11), WT-βS (3481 $\pm$ 1527, n = 10), P123H-βS (3123 $\pm$ 1144, n = 16) and V70M-βS (3860 $\pm$ 1304, n = 15) groups. In comparison with EGFP group (7797 $\pm$ 1310, n = 10), the loss of dopaminergic neurons in αS, WT-βS, P123H-βS and V70M-βS estimated ~56% and was highly statistically significant ($p < 0.0001$, power (1-β err prob) = 0.99). There were no statistical differences between WT-βS, P123H-βS, and V70M-βS at this time point.

a)

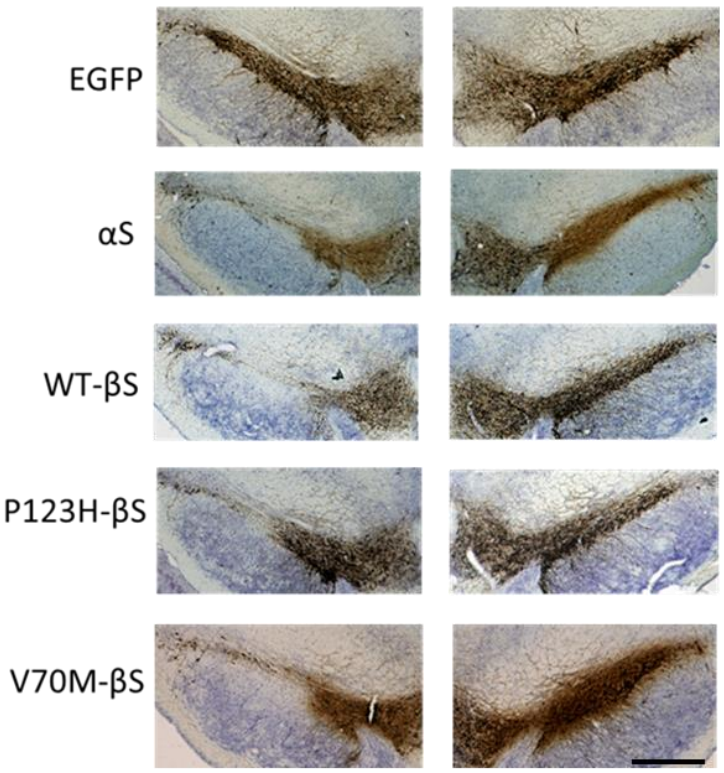

b)

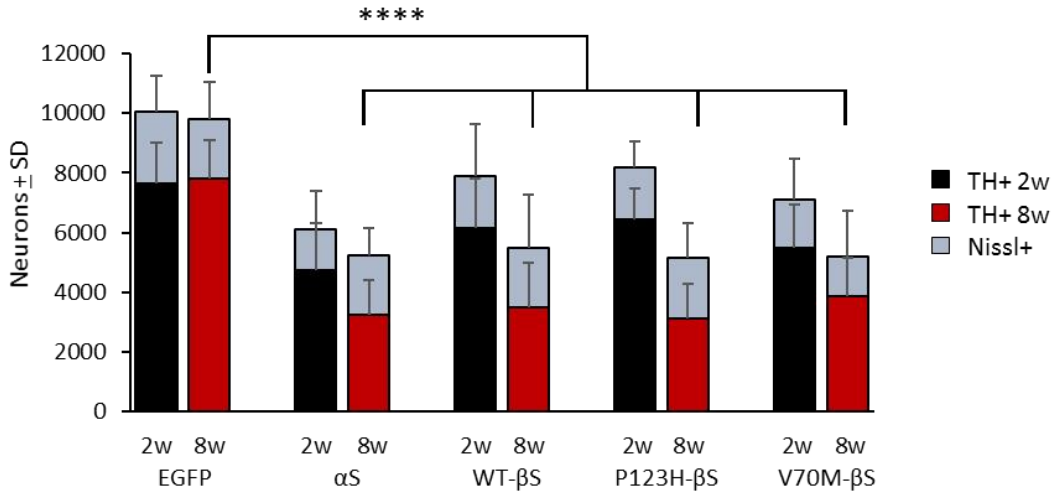

c)

TH+ neurons, 2 weeks

	αS	WT-βS	P123H-βS	V70M-βS
EGFP	**	n.s.	n.s.	**
αS		n.s.	n.s.	n.s.
WT-βS			n.s.	n.s.
P123H-βS				n.s.

TH+ neurons, 8 weeks

	αS	WT-βS	P123H-βS	V70M-βS
EGFP	****	****	****	****
αS		n.s.	n.s.	n.s.
WT-βS			n.s.	n.s.
P123H-βS				n.s.

Figure 3.17. Neurotoxicity of WT-βS, P123H-βS, and V70M-βS in rat's SN.

(a) Representative brain section of SNpc 8 weeks after unilateral injection of AAV2 vectors carrying a cDNA for EGFP, αS, WT-βS, P123H-βS, or V70M-βS. Sections were stained against TH with IHC-DAB method followed by Nissl staining. TH-immunoreactive neurons are brown, non-dopaminergic neurons are blue. On the ipsilateral (injected) side of αS, WT-βS, P123H-βS, or V70M-βS brains one can see a lesion – loss of dopaminergic neurons of SNpc. Scale bar: 500 μm.

(b) Stereological quantification of neurons in SNpc on injected side. Black bars represent numbers of TH-positive neurons 2 weeks after injection of the virus. Red bars: TH+ neurons after 8 weeks of transgene expression. Blue bars: Nissl-positive neurons (total number of dopaminergic and non-dopaminergic neurons). Data are presented as the mean number of neurons per SNpc ± SD (n = 8-17 animals per condition).

(c) Statistical analysis with 1-way ANOVA/Tukey's test. *p<0.05, **p<0.01, ***p<0.001, ****p<0.0001.

In order to test whether there is an actual loss of cells in SNpc and not mere downregulation of TH expression, non-dopaminergic neurons were counted on the Nissl-stained sections of SNpc. A basophilic amine dye – thionine – was used in the Nissl protocol to visualize the neurons. Thionine stains nuclear acids, including the abundant in neurons ribosomes, in a dark-blue color. Non-dopaminergic neurons were defined as those which had positive Nissl staining and negative TH-immunoreactivity. The sum of quantities of non-dopaminergic and TH-positive neurons gave the total number of neurons in SNpc.

Two weeks post transduction the total numbers of neurons (dopaminergic plus non-dopaminergic) in the ipsilateral SNpc were: αS 6119 ± 1283, WT-βS 7912 ± 1720, P123H-βS 8165 ± 890, V70M-βS 7092 ± 1388 and EGFP 10062 ± 1192. The differences EGFP vs. αS and EGFP vs. V70M-βS were highly statistically significant (Tukey's, $p < 0.0001$, power (1-β err prob) < 0.99). The difference in total cell numbers WT-βS vs. P123H-βS vs. V70M-βS were not significant. For the non-dopaminergic neurons only, there was no significant loss in any of the 2-week groups.

At 8 weeks after AAV injection the total numbers of neurons in left SNpc amounted to 5245 ± 925 for αS, 5564 ± 1777 for WT-βS, 5172 ± 1171 for P123H-βS, 5166 ± 1525 for V70M-βS and 9816 ± 1210 for EGFP group. The 1-way ANOVA and Tukey's multiple comparison test showed highly significant differences in the total number of neurons in pairs EGFP vs. αS, EGFP vs. WT-βS, EGFP vs. P123H-βS, and EGFP vs. V70M-βS ($p < 0.0001$, power (1-β err prob) < 0.99). The differences between αS, WT-βS, P123H-βS, and V70M-βS were not significant. There were no

significant differences in quantities of non-dopaminergic neurons between any groups including the EGFP control.

Taken together, P123H-βS and V70M-βS did not aggravate the neurotoxicity of WT-βS *in vivo* in the rat's SNpc although the neuronal loss in V70M-βS condition might manifest and reach statistical significance earlier than in WT-βS.

3.2.3. Expression of WT-βS, P123H-βS, and V70M-βS in the rat's striatum

Strong impairment of the nigrostriatal projections is characteristic for PD and DLB and correlate with the appearance of parkinsonian symptoms (Bedard *et al.*, 2011; Donaghy *et al.*, 2015). Here, I examined whether the loss of dopaminergic neurons in SNpc due to the expression of αS, WT-βS, P123H-βS, and V70M-βS would also cause an axonal pathology.

First, expression of the transgenes was analyzed in coronal striatal brain sections. According to literature, dopaminergic neurons of rat's SNpc innervate the striatum with a rough topographic localization to the lateral regions (Paxinos G, 2014). In our experiments, the overexpressed EGFP, human αS, WT-βS, P123H-βS, and V70M-βS were present practically along the entire length of the striatum in the anterior-posterior direction. EGFP had its major localization to the dorsolateral and mediolateral regions of the rat's striatum, while αS, WT-βS, P123H-βS, and V70M-βS were present also in the medial and ventral regions on the injected side of the brain (Figure 3.18). After 8 weeks of the transgene expression, a few fibers on the contralateral side of the brain were also immunopositive for the transgenes. Striatal projections of nigral dopaminergic neurons on the injected side were highly immunoreactive for αS, WT-βS, P123H-βS, and V70M-βS even 8 weeks after the administration of the virus despite the dramatic loss (~56%) of SNpc dopaminergic neurons, although many of the remaining neurites in the striatum revealed some dystrophic phenotypes which were then further analyzed.

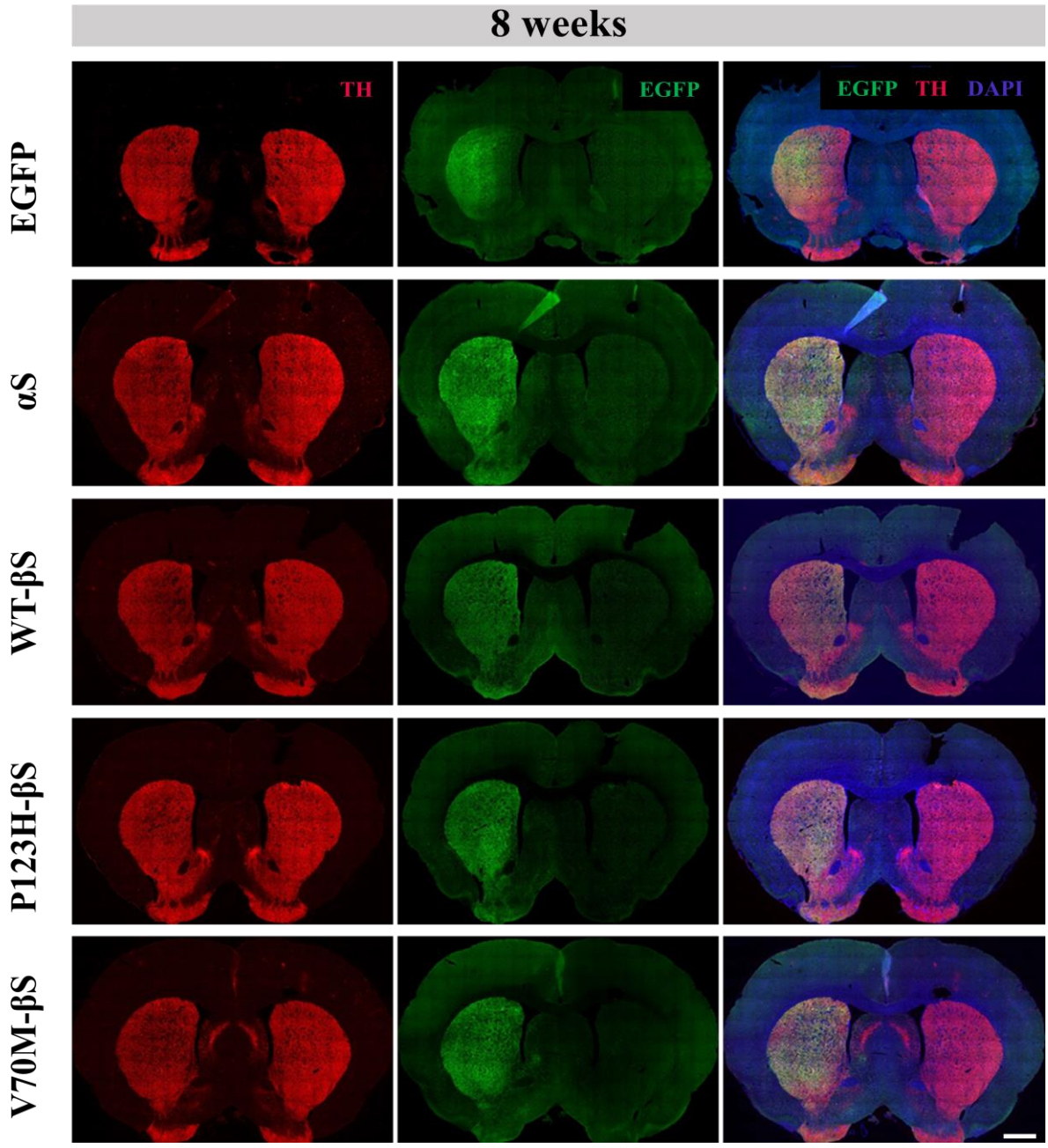

Figure 3.18. AAV2 transduction in the rat's striatum.

Representative pictures of striatal coronal sections of rats injected into the left SNpc with AAV2 vectors expressing EGFP, αS, WT-βS, P123H-βS or V70M-βS. Dopaminergic fibers were visualized with IHC staining against TH (red), αS, WT-βS, P123H-βS, and V70M-βS were visualized with immunoreactivity against human αS and βS (green). Expression of the transgenes predominates on the injected side of the brain. Loss of dopaminergic fibers can be seen in the ipsilateral striatum ofthe αS, WT-βS, P123H-βS, and V70M-βS-expressing brains. Mosaic images were taken with CCD camera on Zeiss Axioplan 2 microscope using 10x objective. Exposure times: DAPI - 632 ms, EGFP - 7267 ms, anti-βS-Cy2 or anti-αS-Cy2 - 2267, anti-TH-Cy3 - 3005 ms. Scale bar: 1.5 mm.

3.2.4. Effects of WT-βS, P123H-βS, and V70M-βS on the striatal fiber density

Dopaminergic fiber density in the rats' striata was measured on high-magnification microphotographs of coronal brain sections as a percentage of area covered by TH-immunopositive projections. The injected side of the brain was compared to the contralateral side. The representative pictures and the results of the measurements are depicted in Figure 3.19. At time point 2 weeks after virus administration no significant fiber loss was noticed in any of the injection groups. The percentages of dopaminergic fiber density compared to the contralateral side were: αS 98 $\pm$ 6%, WT-βS 98 $\pm$ 4%, P123H-βS 102 $\pm$ 5%, V70M-βS 99 $\pm$ 12% and EGFP 104 $\pm$ 3% (n = 3 rats per group).

Eight weeks post transduction axonal pathology increased in all groups except for the EGFP control which had 98 $\pm$ 3% dopaminergic fibers on the injected side. The loss of dopaminergic fibers amounted to 42 $\pm$ 8% in αS, 25 $\pm$ 9% in WT-βS, 20 $\pm$ 6% in P123H-βS, and 38 $\pm$ 6% in V70M-βS conditions (n = 7 rats per group). V70M-βS significantly reduced the striatal fiber density in comparison with WT-βS (Tukey's, $p < 0.0115$, power (1-β err prob) < 0.91) and P123H-βS (Tukey's, $p < 0.0004$, power (1-β err prob) < 0.99) and reached the level of αS toxicity, αS vs. V70M-βS (Tukey's, n.s.).

The P123H mutation did not aggravate the effects of WT-βS on the dopaminergic fiber density (Tukey's, $p = 0.7$). αS, WT-βS, P123H-βS, and V70M-βS were significantly more toxic than EGFP 8 weeks after the virus administration (Tukey's, $p < 0.0001$, $p < 0.0001$, $p = 0.0002$, and $p < 0.0001$, respectively, power (1-β err prob) = 1.0).

Taken together, the striatal pathology was observed first at 8 weeks post-transduction in groups of αS, WT-βS, P123H-βS, and V70M-βS, although the extent of the striatal fiber loss was lower than the loss of dopaminergic neurons in SNpc. V70M mutation aggravated the pathology of the WT-βS to the level of αS, and it was significantly more toxic than WT-βS and P123H-βS. The difference between WT-βS and P123H-βS was not significant.

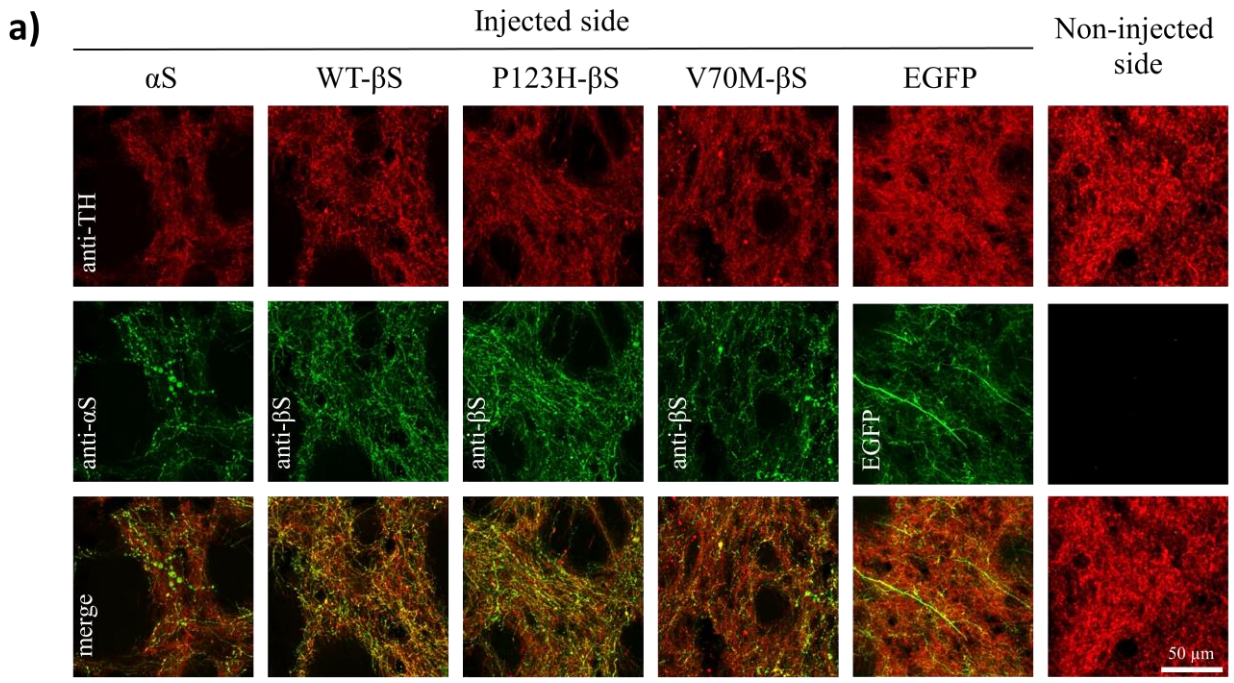

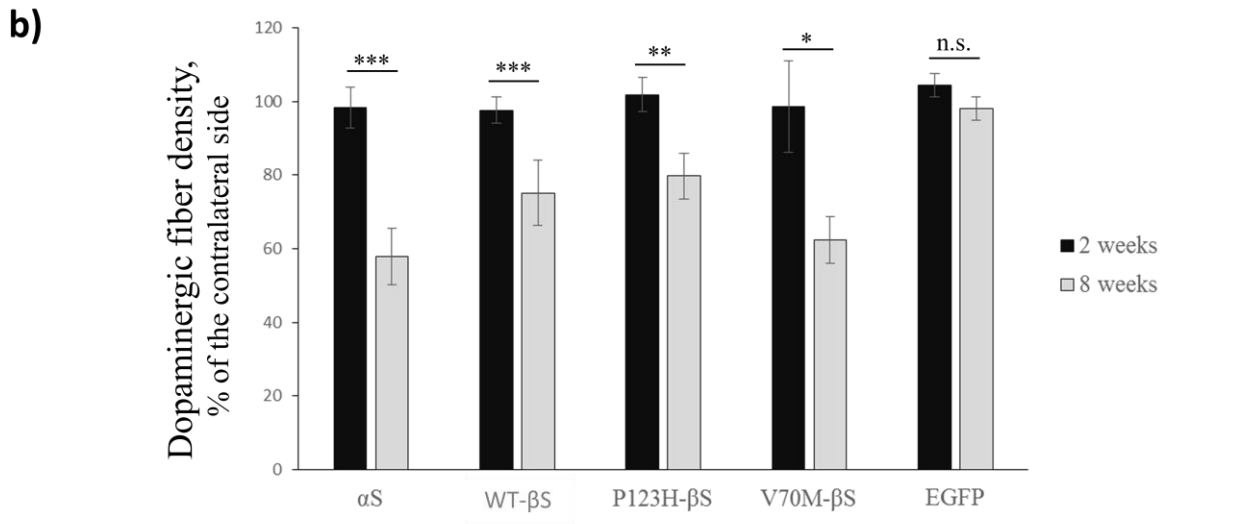

c)

2 weeks	αS	WT-βS	P123H-βS	V70M-βS
EGFP	n.s.	n.s.	n.s.	n.s.
αS		n.s.	n.s.	n.s.
WT-βS			n.s.	n.s.
P123H-βS				n.s.

8 weeks	αS	WT-βS	P123H-βS	V70M-βS
EGFP	****	****	***	****
αS		***	****	n.s.
WT-βS			n.s.	*
P123H-βS				***

Figure 3.19. Dopaminergic fiber density in rat's striatum.

(a) Representative 63x pictures of the coronal striatal sections show the loss of dopaminergic fibers in the regions of αS, WT-βS, P123H-βS, and V70M-βS expression but not for EGFP control or non-injected

side. Dystrophic axons can be observed in αS, and V70M-βS brains, and to a lesser extent in WT-βS and P123H-βS conditions.

(b) Dopaminergic fiber density was significantly reduced at 8 weeks post transduction in αS, WT-βS, P123H-βS, and V70M-βS – expressing brains, with αS and V70M-βS conditions showing the most dramatic loss of the TH-positive fibers: 42 ± 8% and 36 ± 6% respectively (n = 7 rats per group). At 2 weeks after virus administration, there was no significant loss of nigrostriatal projections in any of the conditions (n = 3 rats per group).

(c) Statistical analysis with 1-way ANOVA/Tukey's test. *p<0.05, **p<0.01, ***p<0.001, ****p<0.0001.

3.2.5. Axonal dystrophies in rat's striata

The striatal dopaminergic fibers, immunoreactive for αS, WT-βS, P123H-βS, and V70M-βS displayed axonal pathology in form of axonal retraction bulb-like structures, which were previously described in AAV-αS rat models (Taschenberger *et al.*, 2012; Decressac *et al.*, 2012b). As "axonal bulbs" the rounded structures of at least 2 μm in diameter, highly immunoreactive to TH were counted (Figure 3.20).

Two weeks post-transduction, the number of axonal bulbs per mm^2 of striatum amounted to: 37 ± 22 for αS, 20 ± 5 for WT-βS, 18 ± 2 for P123H-βS, and 34 ± 20 for V70M-βS condition, while it was 16 ± 3 in EGFP and ~10 to 15 bulbs/mm^2 on the non-injected side of the brain. The differences between these groups were not statistically significant (n = 6 animals per group).

After additional 6 weeks after the virus administration, the quantity of dystrophic axons significantly increased in the ipsilateral striata of the brains expressing αS, WT-βS and either mutant of βS. αS with 365 ± 93 axonal bulbs per mm^2 of striatum appeared to be the most toxic synuclein species, causing significantly more axonal pathology than WT-βS with 132 ± 46 axonal bulbs per mm^2 (Tukey's, $p < 0.0001$, power (1-β err prob) < 0.99), P123H-βS with 102 ± 32 axonal bulbs per mm^2 (Tukey's, $p < 0.0001$, power (1-β err prob) < 0.99), and V70M-βS with 274 ± 64 axonal bulbs per mm^2 (Tukey's, $p = 0.0363$, power (1-β err prob) = 0.64). The difference between WT-βS vs. P123H-βS was not significant, while the V70M mutant had significantly more dystrophic neurites than both WT-βS (Tukey's, $p = 0.0005$, power (1-β err prob) < 0.99) and P123H-βS (Tukey's, $p < 0.0001$, power (1-β err prob) < 0.99). The number of axonal bulbs virtually did not change from 2 to 8 weeks in EGFP-expressing brains (13 ± 4 bulbs

per mm^2), and on the contralateral sides of the brains (αS: 33 ± 18, WT-βS: 10 ± 7, P123H-βS: 14 ± 14, V70M-βS: 13 ± 8, EGFP: 7 ± 5 bulbs per mm^2).

To sum up, the striata of the brains expressing V70M-βS were characterized by the more frequent formation of dystrophic neurites/axonal bulbs in comparison with WT-βS. At the same time, P123H mutant did not produce more axonal pathology than WT-βS.

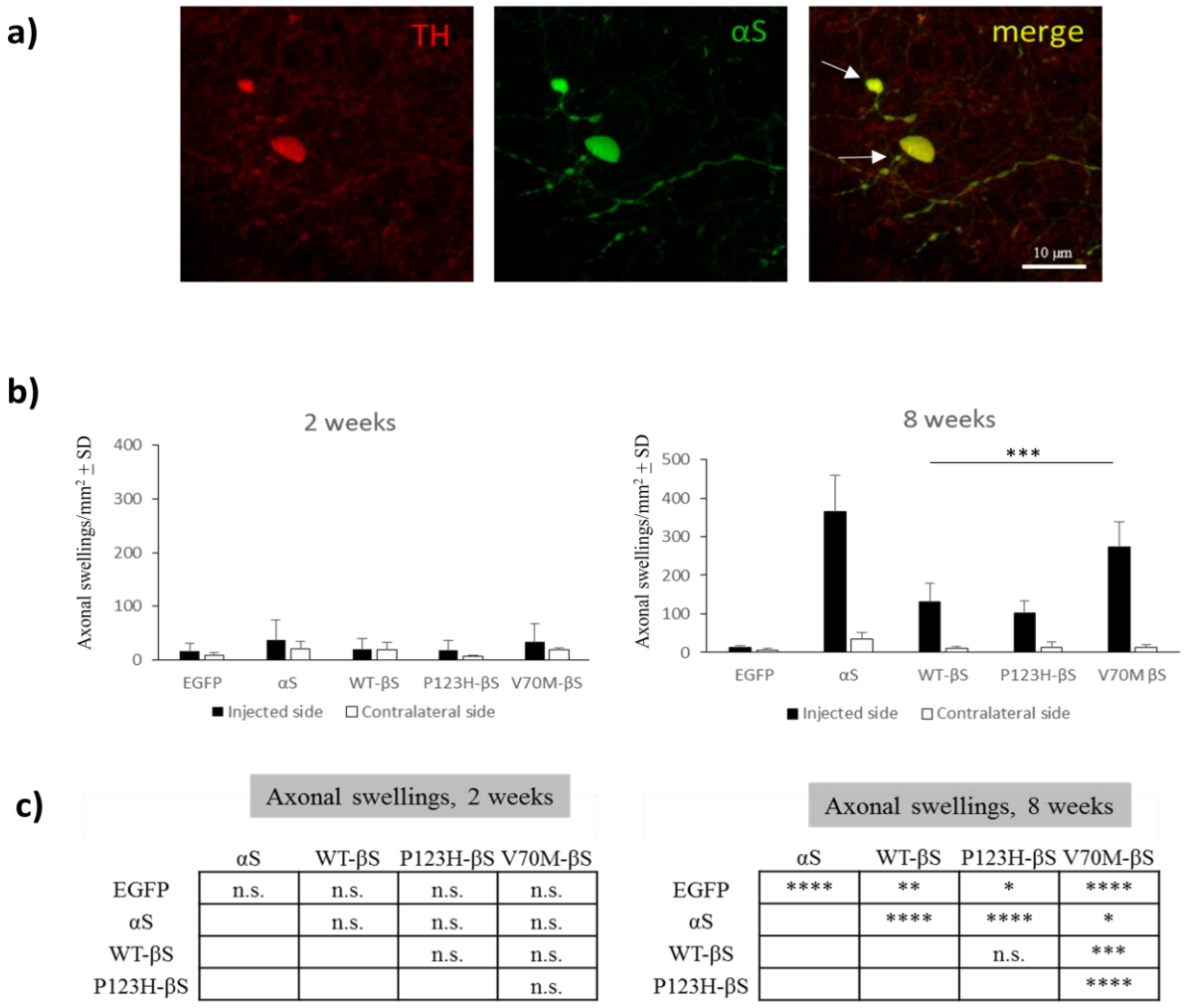

	αS	WT-βS	P123H-βS	V70M-βS
EGFP	n.s.	n.s.	n.s.	n.s.
αS		n.s.	n.s.	n.s.
WT-βS			n.s.	n.s.
P123H-βS				n.s.

	αS	WT-βS	P123H-βS	V70M-βS
EGFP	****	**	*	****
αS		****	****	*
WT-βS			n.s.	***
P123H-βS				****

Figure 3.20. Axonal swellings in rat's striatum.

(a) Axonal swellings or axonal bulbs were defined as rounded structures of at least 2 µm in Feret's diameter (ImageJ measurements) which are highly immunoreactive against TH. Immunostaining against TH (T1299) and aS (sc-7011-R) is shown. Arrows on the merged images indicate the axonal bulbs.

(b) Axonal swellings were counted on injected and contralateral sides of the brain. 3 striatal sections and thirty 40x microphotographs were analyzed for each rat. Data are presented as the mean number of axonal swellings per mm^2 ± SD (for 2-week groups n = 6, for 8-week groups n = 7 animals per condition).

(c) Statistical analysis with 1-way ANOVA/Tukey's test. *p<0.05, **p<0.01, ***p<0.001, ****p<0.0001.

3.2.6. Aggregation of WT-βS, P123H-βS, and V70M-βS in rat's SN

In order to study aggregation of WT-βS, P123H-βS, and V70M-βS in dopaminergic neurons *in vivo*, these proteins were overexpressed in rat's SN using AAV2 vectors. Overexpression of human αS was used as the positive control for the aggregation. EGFP was used as a non-toxic control. Monocistronic AAV2 vectors were unilaterally injected into the left SN, and 3 weeks after the virus administration the samples of cortex, striatum, and SN were collected for each animal.

Immunoblotting analysis revealed a 5 to 7-fold overexpression of WT-βS, P123H-βS, and V70M-βS in the injected SN (Figure 3.21. (c)). Approx. $1/10^{th}$ of the transgene proteins was present in the striatum on the injected side of the brain due to the anterograde transport in nigrostriatal projections.

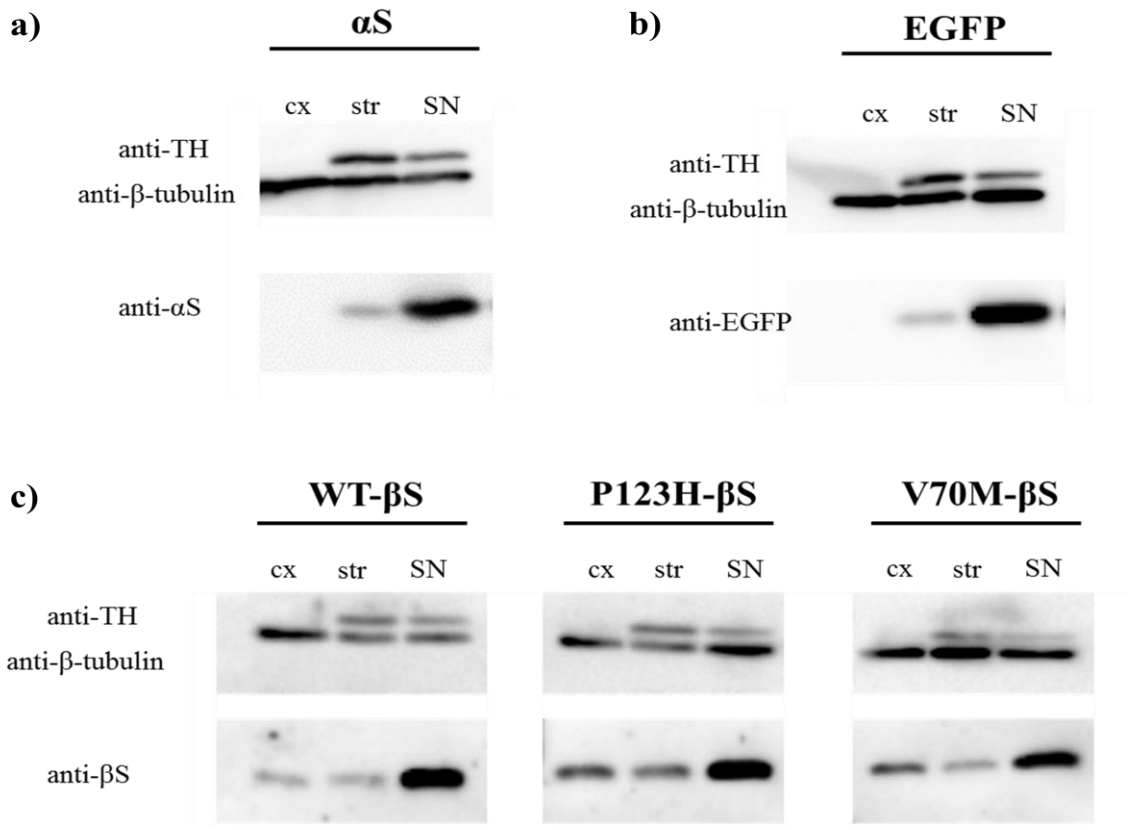

Figure 3.21. Immunodetection of the overexpressed proteins in cortex, striatum, and SN.

Adult female rats were injected unilaterally into the left SN with 1.2 x 10^8 tu of AAV2 vectors expressing either αS, WT-βS, P123H-βS, V70M-βS or EGFP under control of the neuron-specific hSyn 1 promoter.

The samples of cortices (cx), striata (str), and Substantia nigra (SN) were collected 3 weeks after virus administration. Immunoblotting against β-tubulin (~55 kDa band), TH (~62 kDa band), and the transgene proteins were performed.

(a) Human αS (~18 kDa band) was detected in the injected SN and, to a lower extent, in the striatal projections.

(b) The same pattern was observed for EGFP (~27 kDa band) which was mostly expressed in SN, and nearly $1/10^{th}$ of the transgene protein was present in the striatum.

(c) The immunostaining against βS detected both human and rat βS (~20 kDa band). These two proteins have almost identical sequences with the difference in only 2 amino acid residues; therefore, no βS antibody was able to detect only the human protein. The overexpression of βS or its mutants was 5-7-fold in comparison to the endogenous βS.

The protein lysates of SN were subjected to proteinase K (PK) digestion in order to evaluate possible PK resistance of WT-βS and its mutants which would be an indication of their aggregation state in dopaminergic neurons of SNpc. PK is a serine protease which has an ability to hydrolyze a wide variety of the peptide bonds, with exception of some β-sheet-rich proteins, such as prions or αS fibrils which show resistance to PK digestion. Here though, only relative "resistance" to PK is meant, which applies only to the mentioned below temperature, time, and PK concentration during the digestion.

After 5 min of PK digestion (final PK dilution 2 µl/2 ml) at 37^0 C, I observed that some amount of protein remained in case of αS, WT-βS, P123H-βS, and V70M-βS. The dopaminergic marker TH and the neuronal marker β-tubulin were completely digested under the same digestion conditions. Similar to the results of the PK digestion experiments in cell culture (see section 3.1.3.), a portion of the full-length αS (~18 kDa) was resistant to PK digestion at given conditions, and the undigested WT-βS, P123H-βS, and V70M-βS revealed a pattern of ~12 – 18 kDa bands in addition to a small amount of the remaining full-length protein (~18 kDa). The sizes of these fragments were identical in WT-βS, P123H-βS, and V70M-βS, although the amount of the remaining protein was diminished in V70M-βS which might indicate lower aggregation propensities of this protein (Figure 3.22.).

The amount of the PK-resistant protein in the V70M-βS-expressing dopaminergic neurons (15 $\pm$ 4%) was significantly lower than in αS (53 $\pm$ 21%) (Unpaired t-test, p = 0.0103, power (1-β err prob) = 0.92), WT-βS (39 $\pm$ 13%) (Unpaired t-test, p = 0.0108, power (1-β err prob) = 0.92), and P123H-βS (36 $\pm$ 11%) (Unpaired t-test, p = 0.0091, power (1-β err prob) = 0.93). P123H-βS did

not differ in its aggregation propensities from the WT-βS. The diminished aggregation of V70M-βS might be connected to the increased toxicity of this protein in the nigrostriatal projections.

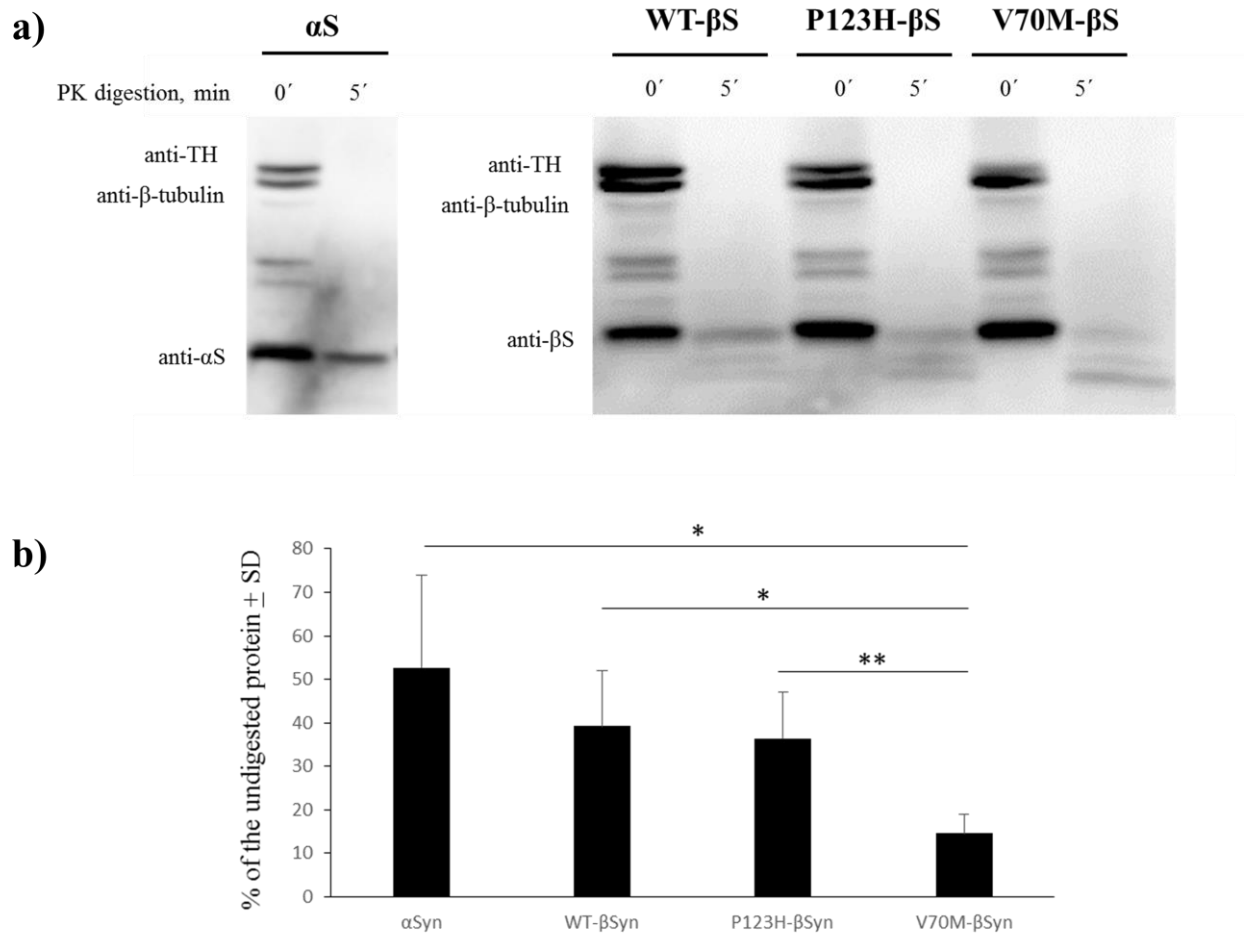

Figure 3.22. PK digestion of the injected SN.

Lysates of the SN, where αS, WT-βS, P123H-βS or V70M-βS were overexpressed, were digested for 0 min and 5 min with 2 µg/ml of proteinase K. 60 µg of protein is loaded per lane.

(a) Immunoblotting was performed with anti-αS (syn211 clone, Invitrogen 32-8100), anti-βS (Sigma, SAB1100305, detected amino acid residues 81-95), anti-β-tubulin (Sigma, T-4026) and anti-TH (Sigma, T1299) antibodies. In the case of αS, a portion of the full-length form of the protein remained after the PK digestion. For the WT-βS and P123H and V70M mutants, the fragments of 12 – 18 kDa were detected in addition to the low amount of the full-length protein remaining after the digestion. TH and β-tubulin were completely digested under the same conditions.

(b) Quantification of the bands intensity showed that αS had 53 ± 21% of the protein resistant to PK under applied conditions, WT-βS and P123H-βS had 39 ± 13% and 36 ± 11%, respectively (sum of the intensities of all remaining bands). V70M-βS with 15 ± 4% of the remaining material had significantly less remaining after digestion protein than αS (unpaired t-test, $p = 0.0103$), WT-βS (unpaired t-test, $p = 0.0108$), and P123H-βS (unpaired t-test, $p = 0.0091$). Data are represented as mean ± SD ($n = 4$ animals/group).

4. Discussion

The role of WT-βS in the development of synucleinopathies still remains under dispute. Both neuroprotective and neurotoxic properties of this protein were suggested in the literature, both fibrillation under certain conditions and counteraction with αS aggregation were shown in different models. Even less is known about the disease-associated mutants of WT-βS, P123H-βS and V70M-βS. Here, the abilities of WT-βS and both mutants to induce neurotoxicity and aggregate in primary cortical neuronal culture and dopaminergic neurons of SN were studied.

4.1. Aggregation and toxicity of WT-βS, P123H-βS, and V70M-βS in primary cortical neurons

4.1.1. The V70M mutation aggravates the neurotoxicity of WT-βS in cultured cortical neurons

A prominent neuronal loss is observed in several regions in the brains of DLB patients such as Substantia nigra, basal ganglia, and cerebral cortex including hippocampus etc. (Donaghy and McKeith, 2014). Therefore, it is of interest to study neurotoxicity of synuclein proteins in various cell culture models and specific regions of animal brains. For my *in vitro* experiments, a standardized model of primary cortical cultured neurons was employed. Although studying of synuclein toxicity in the culture of dopaminergic neurons would be also interesting, primary midbrain cultures include only 5 - 10% of dopaminergic neurons, which makes them inapplicable for viability and biochemistry assays (Falkenburger and Schulz, 2006). A future development of dopaminergic iPSCs models or other alternative models would be of advantage here.

Prior to the *in vivo* experiments in dopaminergic neurons of SN, I tested the neurotoxic potential of αS, WT-βS, P123H-βS, and V70M-βS in primary cortical cells where the transgene delivery was mediated by AAV6 viral vectors. All of these synuclein proteins induced significant neuronal loss starting from the day 12 after the virus administration in comparison with EGFP and γS controls. αS appeared to be the most toxic species at 12 dpt and 16 dpt. In the late culture at 20 dpt, I observed an increase in the V70M-βS-induced neuronal loss which reached the level of the αS toxicity (~60%) and was significantly higher than in WT-βS and P123H-βS-expressing

neurons (~40%). Surprisingly, the familial mutation of βS, P123H did not aggravate βS effects on the cell viability.

Such standardized cell culture model was already employed in Taschenberger *et al.,* 2013 for comparing neurotoxicity of αS, WT-βS, and γS proteins while the neurodegeneration in primary cortical neurons due to the disease-associated mutants P123H and V70M was described for the first time in this thesis. In comparison with my results, Taschenberger *et al.* showed somewhat higher neurotoxicity of both αS and WT-βS. Improved conditions for the cell culturing and prevention of the medium evaporation could have been the reason for a better viability of the current neuronal cultures. γS appeared to be non-toxic in both projects. Carefull examination of synuclein overexpression levels suggested that βS-induced neurodegeneration was aggravated by the presence of V70M mutation and not the difference in the protein expression levels.

Some previous publications indicated a neuroprotective role of WT-βS and even suggested its application as an anti-aggregating agent and a therapeutic factor in synucleinopathies (Hashimoto *et al.,* 2001). It was shown that WT-βS can inhibit apoptosis via downregulation of p53 and protection against caspase 3 activation in TSM1 neuronal cell line (da Costa *et al.,* 2003), and via regulation of Akt serine-threonine kinase in B103 neuroblastoma cells (Hashimoto *et al.,* 2004a). However, the toxicity of WT-βS may depend greatly on its concentration. Thus, Krassnig *et al.,* 2015 showed that modest WT-βS expression had some beneficial effects in the brain of tg AD mouse but locally highly elevated levels of WT-βS caused neurodegeneration. Taschenberger *et al.,* 2013 showed that when αS and WT-βS were co-expressed in primary cortical neurons, the ratio of both proteins was crucial: WT-βS had some neuroprotective effects when applied in ratio 1:30 or 1:10 to αS (although the cytotoxicity was not completely averted) but when more of WT-βS was present in the neurons no neuroprotection was observed.

To sum up, the V70M, but not the P123H mutation of βS aggravated neuronal loss in cultured cortical neurons.

4.1.2. Mitochondrial pathology precedes the neuronal cell death

Mitochondrial dysfunction has been intimately connected to interactions with αS in PD and DLB pathophysiology. Several familial PD and DLB mutations of SNCA gene - A53T, E46K, and

H50Q, as well as mutations of LRRK2, parkin, and PINK1, were associated with mitochondrial fragmentation and increase of ROS species production (Ryan *et al.*, 2015). Normal neuronal function depends on a plentiful and efficient supply of ATP to soma, axons, and dendrites by healthy mitochondria, which is especially challenged in dopaminergic neurons with their long and extensively arborized neurites. Therefore, mitochondria regularly undergo a "quality check" with help of dynamic processes of fusion/fission and mitophagy, a selective process through which damaged mitochondria are removed (Mullin and Schapira, 2013). Mitochondrial fusion is the process of merging of two or several mitochondria regulated by mitofusin (Mfn) proteins of the outer mitochondrial membrane (OMM) which results in elongation of mitochondria. Mitochondrial fission is a process of mitochondrial division into smaller structures directed by dynamin-related GTPase (Drp1) and Fis1 protein (Pozo Devoto and Falzone, 2017). WT-αS was shown to bind directly via its N-terminus to OMM and cause an increase in the membrane curvature leading to fragmentation (Kamp *et al.*, 2010; Dikiy and Eliezer, 2012). Mitochondrial fragmentation as a result of αS overexpression was described in several models before (Kamp *et al.*, 2010; Nakamura *et al.*, 2011). Both αS and WT-βS but not γS induced formation of rounded and swollen (condensed) mitochondria in primary cortical neurons without robust impairment of ATP production or changes in membrane potential (Taschenberger *et al.*, 2013). Recently, Tolö *et al.*, 2018 showed that deformation of mitochondria under the influence of αS was accompanied by permeabilization of OMM, thiol oxidation, and activation of apoptotic pathways, even though ATP production and ion handling were not disturbed in cortical neurons.

The results of this Ph.D. project on mitochondrial fragmentation under overexpression of αS, WT-βS, and γS were consistent with previous publications. The mutants of βS were for the first time characterized with respect to their influence on mitochondrial dysfunction. P123H-βS was not any more toxic than WT-βS while V70M-βS caused a decrease in the number of cells with elongated mitochondria and increase in the number of neurons with fully condensed mitochondria to an extent of αS-induced effects on mitochondrial morphology. These characteristics were dependent on the age of the culture and more prominent at the later stage (14 dpt). Whether V70M-βS might bind OMM with its highly conserved N-terminal region in a similar way to αS is not known. Increased mitochondrial condensation, which possibly led to the functional impairment of mitochondria, could have been one of the pathological mechanisms

explaining the increase in cytotoxicity of V70M-βS in comparison to WT-βS. The P123H mutant did not show such aggravation in abberant mitochondrial morphology when compared to WT-βS.

Analysis of mitochondrial morphology in the neurites revealed a decrease in mitochondrial length to width ratio under the expression of αS, WT-βS, P123H-βS, and V70M-βS in comparison to EGFP- and γS-expressing control cells, with the most prominent effects observed in αS and V70M-βS conditions. Still, such morphological changes in neurites were very moderate in comparison with mitochondrial deformation in the soma. Completely rounded and swollen mitochondria were observed only in somas but not in the neurites of cultured cortical neurons, which indicates that such deformations in morphology may lead to the inability of these mitochondria to move along the neurites. This speculation is supported by the absence of dramatic effects of synuclein on motility of mitochondria in these experiments. The mean speed of mitochondria in the neuronal processes amounted to ~45 μm/min, the maximal speed was approx. 85 μm/min in all the expression groups with exception of αS-expressing neurons, where the motility of mitochondria was slightly decreased. These results are consistent with previously published data on mitochondrial motility (Toloe J, Ph.D. thesis, 2013; MacAskill *et al.,* 2010; De Vos *et al.,* 2003).

In summary, in respect to influence on mitochondrial morphology in somas, V70M-βS but not P123H-βS aggravated mitochondrial condensation as compared to WT-βS, which may have been one of the pathophysiological mechanisms leading to the increased neurotoxicity of V70M-βS.

4.1.3. V70M-βS has lower resistance to PK-digestion than WT-βS

Aggregation properties of WT-βS are greatly dependent on the conditions of the reaction. Despite a suggested earlier non-amyloidogenic nature of WT-βS (Hashimoto *et al.,* 2001; Uversky *et al.,* 2002), it was shown that macromolecular crowding, the presence of pesticides or heavy metals can force fibrillation of this synuclein species (Yamin *et al.,* 2005). Formation of PK-resistant aggregates was observed under WT-βS-overexpression in rats SNpc (Taschenberger *et al.,* 2013). Changing in the pH to mildly acidic values can also trigger WT-βS fibrillation (Moriarty *et al.,* 2017).

The fact that WT-βS can aggregate despite missing 11 AA in the central region of the molecule corresponding to the αS NAC domain, shows that the structure of other domains may be also important for the fibrillation process. In this Ph.D. project, I tested the aggregation propensities of WT-βS, P123H-βS, and V70M-βS with the PK digestion assay. In all three proteins, a C-terminal region was cleaved off in the digestion reaction, in the contrast to αS where the full-length form of the protein was resistant to PK under given conditions. These findings are consistent with the synuclein chimera experiments of Moriarty *et al.,* 2017, where 8 versions of αS/WT-βS chimeric species with swapped domains were tested and showed higher stability and importance of the conserved N-terminal region for fibrillation of both proteins. At the same time, the C-terminal region, which has the least sequence homology between two synuclein species, had a specific influence on WT-βS and αS: the C-terminus of WT-βS, when introduced into αS, was able to prevent αS fibrillation, even at acidic pH, while WT-βS was fibrillating at pH 5.8. All three domains and interaction between them appeared to be important for the fibrillation properties specific to the synuclein species (Moriarty *et al.,* 2017; Landau M, 2017). The P123H mutation in the C-terminal region of βS renders its confirmation to be more similar to αS and was shown to increase the fibrillation under co-incubation with αS (Janowska and Baum, 2016). The C-terminal region of αS was earlier shown to stabilize long-range intramolecular electrostatic interaction with N-terminus, important for the stability of the molecule (Bertoncini *et al.,* 2005).

Although the sizes of PK-stable fragments were the same in WT-βS and mutants in my experiments, V70M-βS had a lower amount of protein remaining after the PK reaction. This might indicate a lower aggregation state of V70M-βS (for example, more monomers or/and short oligomers). How this lower aggregation state is connected to the increased cyto- and mitochondrial toxicity of the V70M mutant is not yet clear. In order to reveal further differences in mechanisms and kinetics of fibril formation in WT-βS and mutants, they can be studied in cell-free conditions with a variety of biophysical assays (e.g., thioflavin T assay, circular dichroism spectroscopy, NMR spectroscopy etc). The only previous publication addressing fibrillation of DLB-associated βS mutants, Wei *et al.,* 2007, showed that the recombinant V70M and P123H-βS were more prone to aggregation than WT-βS *in vitro*, however these recombinant proteins were 6xHis-tagged and aggregated under acidic conditions with a specific buffer which might not reproduce the physiological intracellular conditions.

Decreased PK resistance of the V70M mutant in my experiment may mean that less fibrils and more oligomers were present in the cultured cortical neurons, which subsequently resulted in the higher toxicity of V70M-βS, compared to P123H-βS and WT-βS.

4.2. Aggregation and toxicity of WT-βS, P123H-βS, and V70M-βS in rat's SN

4.2.1. Loss of SN dopaminergic neurons can be induced by P123H-βS and V70M-βS overexpression

In this thesis, P123H-βS and V70M-βS were for the first time studied in the AAV rat model with their respect to degeneration of dopaminergic neurons in SNpc and dopaminergic fiber loss in the striatum. Stereotaxic gene delivery with rAAV2 viruses allowed to introduce the unilateral lesion into SNpc and to use the contralateral side as a control for stereological cell counting. AAV vectors of serotype 2 produced a compact transduction in the injected SN, and hSyn1 gene promoter allowed for the neuron-specific expression of the transgenes. This animal model allows studying the effects on dopaminergic neurons of SN while their native properties and neuritic connections are retained. Besides, viral vector models are so far the only ones which demonstrate a progressive neuronal loss in SNpc, a major histopathological hallmark of PD and DLB which cannot be recapitulated in genetic mouse lines (Löw and Aebischer, 2012).

The results of neuronal loss in αS, WT-βS and EGFP control groups were consistent with the previously published data (Taschenberger *et al.,* 2012; Taschenberger *et al.,* 2013). Thus, in the experiments of this Ph.D. project αS caused loss of ~40% of dopaminergic neurons in the injected SNpc at 2 weeks after virus administration and ~58% after 8 weeks. The respective neuronal loss in Taschenberger *et al.,* 2012 amounted to 43% and 56% respectively, and in Taschenberger *et al.,* 2013 – to ~46% and 52%. WT-βS in my experiments also caused a progressive loss of dopaminergic neurons: ~20% and ~55% after 2 and 8 weeks of transgene expression. In Taschenberger *et al.,* 2013 dopaminergic neuronal loss due to WT-βS toxicity amounted to ~20 % and ~45 % at the same time points after transduction which is consistent with the data of this thesis. The data of other groups showed variable results in rAAV models of PD – from 15% (Davies *et al.,* 2014) to 90% neuronal loss (Gombash *et al.,* 2013) depending on the exact experimental layout, AAV serotype and concentration of the virus.

P123H-βS did not aggravate the βS neurotoxicity *in vivo*. V70M-βS was also not statistically different from WT-βS but the loss of dopaminergic neurons in V70M-βS has reached statistical significance earlier when compared to EGFP control (2 weeks after viral injection). At the same time there were no statistical differences between V70M-βS vs. WT-βS or V70M-βS vs. WT-βS even at the earlier time point. The level of βS overexpression (WT and mutants) estimated to 5-7-fold in the described experiments. Application of lower viral concentration and less dramatic impact on neuronal death in SN might reveal the difference between WT and mutant βS.

Loss of hippocampal neurons with regard to P123H mutation of βS was reported before in tg mouse line. The cross-breeding of P123H-βS and αS tg mice resulted in enhanced neuropathology and more pronounced loss of hippocampal neurons (Fujita *et al.,* 2010). At the same time, there was no comparable WT-βS control in the study of Fujita *et al.,* 2010. Thus, it is unclear if the P123H mutation or mere increase in the protein expression level was responsible for the cell loss.

In the experiments described in this Ph.D. thesis, TH-positive neurons were counted. Several previous publications showed that αS might not only kill dopaminergic neurons but also downregulate TH expression by inhibition of Nurr1 transcription factor (Baptista *et al.,* 2003; Yu *et al.,* 2004; Peng *et al.,* 2005; Chu *et al.,* 2006). Therefore, it was important to perform a control staining for the loss of dopaminergic neurons. Hence, using the VMAT2 marker of dopaminergic neurons would have been beneficial. However, the anti-VMAT2-antibody used in our lab was discontinued, and testing of approx. 15 new commercial antibodies for VMAT2 revealed that none of them can reliably stain the dopaminergic neurons of SN. No suitable anti-VMAT2 antibody was found at the time of my experiments. Therefore, IHC staining against TH was combined with the Nissl staining protocol and non-dopaminergic neurons were counted in the same regions as dopaminergic in order to exclude mere downregulation of TH. I revealed a true loss of dopaminergic neurons, numbers of non-dopaminergic neurons did not increase in any group or at any examined time point. Besides, a recent report of rAAV-αS models where TH- and VMAT2-positive cells were counted in parallel in the same animals, revealed the same cell numbers for both dopaminergic markers (Decressac *et al.,* 2012b).

In summary, V70M-βS caused significant neurodegeneration at earlier time point than WT-βS and P123H-βS in dopaminergic neurons of rat's SN.

4.2.2. V70M-βS induces greater axonal pathology than WT-βS

Axonal pathology in nigrostriatal projections accompanied the loss of SNpc neurons due to the expression of αS, WT-βS, P123H-βS, and V70M-βS. Two weeks after virus administration I have not observed any significant losses of dopaminergic fiber density but at 8 weeks post-transduction, ~40% of TH-positive fibers were lost in αS and V70M-βS animal groups, and ~23% in WT-βS and P123H-βS conditions. Although the loss of striatal projection was less dramatic than the loss of SNpc neurons, the remaining axons with transgene expression had pronounced axonal pathology at 8-weeks-time point: the neurites were swollen and axonal-bulb like structures highly immunopositive for synuclein and TH were detected. P123H-βS tg mice were characterized by pronounced axonal pathology in form of axonal swellings or retraction-like axonal bulbs (Sekigawa *et al.,* 2015). Similar pathological structures in the striatum were earlier described in αS-overexpressing rat brains (Taschenberger *et al.,* 2012; Decressac *et al.,* 2012a) but for the first time axonal bulbs are reported in rAAV model of WT-βS, P123H-βS and V70M-βS overexpression. Stronger striatal pathology in the αS-overexpressing brain in comparison to the WT-βS-overexpressing brain was reported before in Taschenberger *et al.,* 2013. Interestingly, P123H-βS effects were almost identical to WT-βS, while V70M-βS induced much more pronounced axonal pathology in both striatal fiber loss and axonal bulb formation in the striatum almost reaching the level of αS toxicity. A lesser extent of striatal vs. nigral pathology indicates that all four proteins may trigger very rapid detrimental effects in somas of SNpc dopaminergic neurons and axonal pathology follows. A possible reason for that could be higher synuclein concentration in cell bodies in comparison to anatomically remote striatal projections.

The pathological picture in the DLB patients' brains, where neuronal impairments develop over years, might be different. Sekigawa *et al.,* 2015 suggested that in DLB patients' axonal pathology may precede and trigger the cell death. Human histopathological data confirms that WT-βS (and possibly its mutants) could induce axonal pathology. Thus, βS was found in axonal lesions in hippocampi of DLB and PD patients (Galvin *et al.,* 1999). In brains of NBIA type 1 synucleinopathy, βS accumulated in form of axonal spheroids (Galvin *et al.,* 2000). Again, the rare V70M mutation drastically increased axonal pathology in comparison with WT-βS, which indicates that V70M-βS might significantly contribute to the DLB pathology but P123H does not.

4.2.3. Aggregation profiles of WT-βS and its mutants are similar *in vitro* and *in vivo*

The pattern of fragments produced in the PK digestion reaction was similar between WT-βS and its P123H and V70M mutants, as well as between cultured cortical neurons and dopaminergic neurons of SNpc of the rat. The C-terminal region of the molecule was less stable than the N-terminus and central domain. V70M-βS was less resistant to PK digestion. One could speculate that lower aggregation state of V70M-βS might have provided this synuclein species with more efficient motility and transport to the axonal terminals which might have led to the elevated accumulation of V70M in striatal fibers and increased axonal pathology.

Lower stability of V70M-βS against PK digestion may indicate a decrease in amount of β-sheet rich fibrils and a subsequent increase of oligomeric fraction of this synuclein species. By analogy with αS, toxic oligomers could actually be a molecular conformation of V70M-βS, responsible for the neurotoxicity. In αS research, growing evidence from a variety of experimental models links oligomeric species with neuronal impairment and propagation of PD and DLB. At the same time, Lewy bodies and Lewy neurites are suggested to be a protective form for sequestration of toxic αS (Bengoa-Vergniory *et al.*, 2017). Several facts support a "bystander" role of Lewy bodies. Firstly, nearly 10% of healthy individuals brains contain Lewy bodies without indication of increased neurodegeneration (Parkkinen *et al.*, 2005). Secondly, Lewy body pathology often does not correlate with the severity or the modality of PD or DLB symptoms (Parkkinen *et al.*, 2008). Finally, a familial form of PD was described where a G2019S mutation of LRRK2 led to neurodegeneration without formation of Lewy bodies (Gaig *et al.*, 2007).

"Toxic oligomers hypothesis" in case of αS is supported by numerous studies, where oligomers of αS, produced in cell-free conditions, were applied to cell cultures and brains and caused neurodegeneration, seeding and propagation of pathology (Danzer *et al.*, 2007; Karpinar *et al.*, 2009). At the same time, αS form with accelerated fibrillation and decrease in amount of oligomers (αS 30-110) did not cause dopaminergic neuronal loss in Substantia nigra of rats, unlike the oligomers-rich mutants (E57K-αS and E35K-αS) (Winner *et al.*, 2011).

Although oligomeric species of αS are highly heterogenous, recently some structural characteristics, which render αS oligomers toxicity, were described. Fusco *et al.* showed that an exposed lipophilic part of toxic oligomers caused reinforced interactions with cellular membranes and the rigid oligomeric core was essencial for the αS-induced membrane disruption and

subsequent cellular dysfunction. The N-terminus of αS, the membrane-bounding region, was especially important for the induction of oligomers toxicity (Fusco *et al.*, 2017). Close proximity of the V70M mutation to the N-terminus of βS and high homology between the N-terminal regions of αS and βS (Figure 4.1) may indicate a possible mechanism of "toxic gain of function" in V70M-βS. Valine to methionine substitution close to the border of the N-terminus and NAC-domain may cause conformational changes in these both regions of βS, rendering more stable oligomeric form and increased toxicity of V70M-βS.

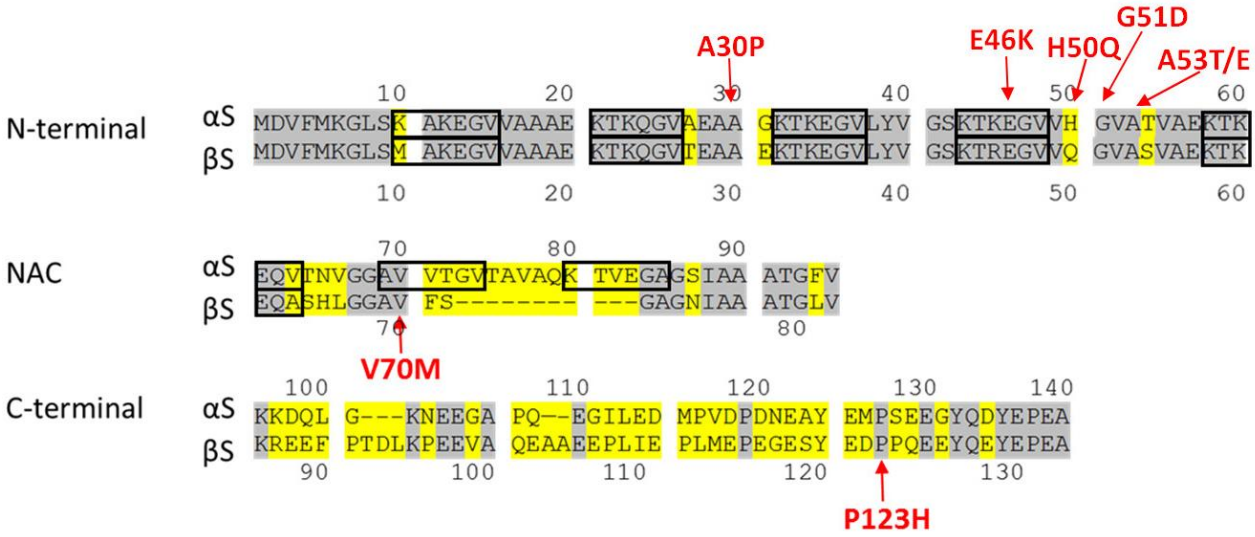

Figure 4.1. Amino acid sequences of αS and βS.

Amino acid sequences of αS and βS are aligned according to their 3 domains: N-terminus, NAC-domain and C-terminus. Identical aa residues are highlighted in gray, non-identical aa residues are highlighted in yellow, and deletions are shown as dashes. Red writing shows the known mutations of αS and βS.

4.3. Conclusion and perspectives

Taken together, the results of this Ph.D. thesis show that the V70M mutation of βS is pathogenic and may contribute to the neurodegeneration in dementia with Lewy bodies. P123H-βS did not aggravate the effects of WT-βS in any of the neurotoxicity or aggregation experiments of this project which might indicate that this mutation is coincidental and might not be relevant to the DLB pathogenesis. V70M-βS induced more pronounced neuronal loss in cortical culture, dopaminergic fiber loss and axonal pathologies in rats' striata. Some pathological mechanisms of

the V70M mutant may be related to its less stable aggregates (possibly toxic oligomers) in comparison to WT-βS and its ability to cause mitochondrial deformations – putative early events in cytopathology of synucleinopathies.

It would be interesting to study further V70M-βS aggregation properties in the cell-free conditions which could characterize features of its aggregation and kinetics of fibril formation in details. One could speculate that the location of the mutation at the position 70 may be a key to forming less fibrils and more stable oligomeric form of V70M-βS. Most of the αS familial mutations are also adjacent to this region. Since valine at the position 70 is conserved between αS and βS, one could also generate a V70M mutation in αS and test it for the possible increase in amount of oligomeric species and neurotoxicity. Besides, creating a chimeric αS/V70M-βS species, where, for example, the NAC-domain of V70M-βS is introduced into αS, could further reveal the role of the V70M mutation in the aggregation process.

Since V70M-βS caused more dramatic condensation of mitochondria than WT-βS, the mutant may be able to have stronger interactions with membranes. This process could be analogous to αS, where it was shown that αS could directly bind to OMM (Nakamura *et al.,* 2011) and αS oligomers but not monomers led to OMM permeabilization (Ludtmann *et al.,* 2018). Therefore, one could consider studying interactions of V70M-βS oligomeres with artificial and natural lipid bilayers, including OMM and IMM. Besides, further molecular mechanisms of V70M-βS induction of mitochondrial deformation and dysfuction could be elucidated *in vitro* and *in vivo,* e.g. with respect towards ROS species production and caspase activation.

A recent publication implicates pathological reduction of autophagy in brains of DLB patients due to elevated level of WT-βS expression (Evans *et al.,* 2018). Further studies of WT-βS and V70M-βS effects on autophagy pathways may be of the relevance for the development of therapeutics for DLB patients. Moreover, it is still not known how WT-βS and V70M-βS influence ER stress, glial and inflammatory responses, proteasomal and synaptic functions in the patients' brains, and could be addressed in the upcoming experiments.

In this Ph.D. project, a stronger difference between WT-βS and V70M-βS-induced neurotoxicity was observed in cortical cells in contrast to the dopaminergic neurons of Substantia nigra pars compacta. Although these results are compatible with DLB pathophysiology, where cognitive (cortical) symptoms often preceed motor (nigro-striatal) symptoms, it is not yet clear why cortical

neurons were more sensitive to V70M-βS then to WT-βS. One could try to validate these results in other *in vitro* and *in vivo* models, e.g. in cell cultures of dopaminergic and glutamatergic neurons produced from the same iPSCs. Interactions of overexpressed with endogenous synuclein could also play a role in animal and cell culture models, since endogenous αS and βS are abundant in various brain regions. The experiments including αS- and/or βS-KO models could show whether the neurotoxicity is dependent on the endogenous proteins.

5. Summary

Dementia with Lewy bodies is a progressive degenerative brain disorder which accounts for 7 to 25% of all dementia cases. Two rare missense mutations of β-synuclein, P123H and V70M were identified in familial and sporadic cases of DLB, respectively. Some previous publications showed that P123H and V70M mutations may contribute to the DLB pathology by aggregation (Janowska *et al.*, 2016), inducing neurodegeneration (Fujita *et al.*, 2010) or causing lysosomal pathology (Wei *et al.*, 2007). Still, their pathological roles were not clearly understood at the beginning of this project. Here, neurotoxicity and aggregation of WT-βS and its mutants, P123H-βS and V70M-βS, were studied *in vitro* in primary cultured cortical neurons and *in vivo* in dopaminergic neurons of SNpc of rat. V70M-βS was described for the first time in an *in vivo* model.

It was found that the V70M mutation in several conditions aggravated pathologic effects of WT-βS, namely, V70M-βS:

- increased cell loss in primary cortical neurons;
- induced more condensation of mitochondria in cultured neurons;
- caused more pronounced loss of nigrostriatal projections, and formation of axonal bulbs in rats striata;
- showed less fibril formation in cultured neurons and *in vivo* in Substantia nigra.

Increase in mitochondrial deformations under influence of V70M may have been an early cellular mechanism leading to the cell death. Moreover, increased neurotoxicity in primary cortical neurons correlated with lower resistance of V70M to PK digestion; this may indicate lower extent of V70M-βS fibril formation and increase in amount of “toxic oligomeric species”.

Altogether, these data indicate pathologic role of V70M mutation of βS and its putative relevance to DLB pathogenesis.

The P123H mutation did not contribute to the pathological features of WT-βS in any of the experiments of this Ph.D. project, which may indicate that it is coincidential to DLB pathology. However, further investigation of P123H-βS with respect to its long-term effects in different experimental models may be necessary to exclude its possible pathological role in DLB.

6. References

Abeliovich A, Schmitz Y, Farinas I *et al.* (2000) Mice lacking alpha-synuclein display functional deficits in the nigrostriatal dopamine system. *Neuron,* 25 (1): 239-252.

Ahn M, Kim S, Kang M *et al.* (2006) Chaperone-like activities of alpha-synuclein: alpha-synuclein assists enzyme activities of esterases. *Biochem Biophys Res Commun,* 346 (4): 1142-1149.

Alderson TR and Markley JL (2013) Biophysical characterization of α-synuclein and its controversial structure. *Intrinsically Disord Proteins,* 1 (1):18-39.

Allison JR, Rivers RC, Christodoulou JC *et al.* (2014) A relationship between the transient structure in the monomeric state and the aggregation propensities of α-synuclein and β-synuclein. *Biochemistry,* 53 (46): 7170-7183.

Baptista MJ, O'Farrell C, Daya S *et al.* (2003) Co-ordinate transcriptional regulation of dopamine synthesis genes by α-synuclein in human neuroblastoma cell lines. *J Neurochem,* 85: 957-968.

Barker RA and Williams-Gray CH (2016) The spectrum of clinical features seen with alpha-synuclein pathology. *Neuropathology and applied neurobiology,* 42 (1): 6-19.

Bartels T, Choi JG, and Selkoe DJ (2011) α-Synuclein occurs physiologically as a helically folded tetramer that resists aggregation. *Nature,* 477 (7362): 107-110.

Bédard C, Wallman MJ, Pourcher E (2011) Serotonin and dopamine striatal innervation in Parkinson's disease and Huntington's chorea. *Parkinsonism Relat Disord,* 17 (8): 593-598.

Bengoa-Vergniory N, Roberts RF, Wade-Martins R, and Alegre-Abarrategui J (2017) Alpha-synuclein oligomers: a new hope. *Acta Neuropathol*, 134: 819-838.

Bertoncini CW, Jung YS, Fernandez CO *et al.* (2005) Release of long-range tertiary interactions potentiates aggregation of natively unstructured alpha-synuclein. *Proc Natl Acad Sci U S A,* 102 (5): 1430-1435.

Biere AL, Wood SJ, Wypych J*et al.* (2000) Parkinson's disease-associated α-synuclein is morefibrillogenic than β-and γ-synuclein and cannot cross-seed its homologs. *Journal of Biological Chemistry*, 275 (44): 34574-34579.

Bonifati V, Rizzu P, van Baren MJ *et al.* (2003) Mutations in the DJ-1 gene associated with autosomal recessiveearly-onset parkinsonism. *Science*, 299: 256–259.

Bonner LT, Tsuang DW, Cherrier MM, *et al*. (2003) Familial dementia with Lewy bodies with an atypical clinical presentation. *J Geriatr Psychiatry Neurol*, 16: 59–64.

Bourdenx M, Koulakiotis NS, Sanoudou D *et al.* (2017) Protein aggregation and neurodegeneration in prototypical neurodegenerative diseases: examples of amyloidopathies, tauopathies and synucleopathies. *Progress in Neurobiology*, 155: 171-193.

Braak H, Del Tredici K, Rub U *et al.* (2003) Staging of brain pathology related to sporadic Parkinson's disease. *Neurobiol Aging*, 24: 197–211.

Braak H, Rüb U, Jansen Steur ENH *et al.* (2005) Cognitive status correlates with neuropathologic stage in Parkinson disease. *Neurology*, 64 (8): 1404-1410.

Buchman VL, Hunter HJA, Pinõn LGP *et al.* (1998) Persyn, a member of the synuclein family, has a distinct pattern of expression in the developing nervous system. *J Neurosci*,18 (22): 9335-9341.

Burger C, Gorbatyuk OS, Velardo MJ *et al.* (2004) Recombinant AAV viral vectors pseudotyped with viral capsids from serotypes 1, 2, and 5 display differential efficiency and cell tropism after delivery to different regions of the central nervous system. *Mol Therapy*, 10 (2): 302-317.

Burré J, Sharma M, Tsetsenis T *et al.* (2010) Alpha-synuclein promotes SNARE-complex assembly *in vivo* and *in vitro*. *Science*, 329 (5999): 1663-1667.

Campion D, Martin C, Heilig R *et al.* (1995) The NACP/synuclein gene: chromosomal assignment and screening for alterations in Alzheimer disease. *Genomics*, 26 (2): 254-257.

Cetin A, Komai S, Eliavara M *et al.* (2007) Stereotaxic gene delivery in the rodent brain. *Nature Protocols*, 1: 3166–3173.

Chandra S, Fornai F, Kwon HB *et al.* (2004) Double-knockout mice for alpha- and beta-synucleins: effect on synaptic functions. *Proc Natl Acad Sci U S A*, 101 (41): 14966-71.

Chen L, Cagniard B, Mathews T*et al.* (2005) Age-dependent motor deficits and dopaminergic dysfunction in DJ-1 null mice. *J Biol Chem*, 280: 21418–21426.

Chu Y, Le W, Kompoliti K *et al.* (2006) Nurr1 in Parkinsons disease and related disorders. *J Comp Neurol*, 494 (3): 495-514.

Cleveland DW, Fischer SG, Kirschner MW and Laemmli UK (1977) Peptide mapping by limited proteolysis in sodium dodecyl sulfate and analysis by gel electrophoresis. *Journal of Biological Chemistry*, 252 (3): 1102-6.

Colla E, Coune P, Liu Y *et al.* (2012) Endoplasmic reticulum stress is important for the manifestation of α-synucleinopathy *in vivo*. *J Neurosci*, 32: 3306-3320.

Coons AH (1958) Fluorescent antibody methods. *General Cytochemical Methods.* Academic Press Inc., New York. 399.

Crabtree DM, Zhang J (2012) Genetically engineered mouse models of Parkinson's disease. *Brain Res Bull,* 88 (1): 13-32.

da Costa CA, Masliah E, and Checler F (2003) Beta-synuclein displays an antiapoptotic p53-dependent phenotype and protects neurons from 6-Hydroxydopamine-induced caspase 3 activation. *J Biol Chem,* 278 (39): 37330-37335.

Danzer KM, Haasen D, Karow AR *et al.* (2007) Different species of alpha-synuclein oligomers induce calcium influx and seeding. *J Neurosci,* 27: 9220-9232.

Davies SE, Hallett PJ, Moens T *et al.* (2014) Enhanced ubiquitin-dependent degradation by Nedd4 protects against alpha-synuclein accumulation and toxicity in animal models of Parkinson's disease. *Neurobiol Dis,* 64: 79-87.

Decressac M, Mattsson B and Björklund A (2012 a) Comparison of the behavioral and histological characteristics of the 6-OHDA and α-synuclein rat models of Parkinson's disease. *Exp Neurol,* 235 (1): 306-15.

Decressac M, Mattsson B, Lundblad M *et al.* (2012 b) Progressive neurodegenerative and behavioural changes induced by AAV-mediated overexpression of α-synuclein in midbrain dopamine neurons. *Neurobiol Dis,* 45 (3): 939-953.

Decressac M, Mattsson B, Weikop P *et al.* (2013) TFEB-mediated autophagy rescues midbrain dopamine neurons from alpha-synuclein toxicity. *Proc Natl Acad Sci USA,* 110: E1817-E1826.

Deleersnijder A, Gerard M, Debyser Z and Baekelandt V (2013) The remarkable conformational plasticity of alpha-synuclein: blessing or curse? *Trends Mol Med,* 19 (6): 368-377.

Devi K, Raghavendran V, Prabhu BM *et al.* (2008) Mitochondrial import and accumulation of αS impair complex I in human dopaminergic neuronal cultures and Parkinson disease brain. *J Biol Chem,* 283 (14): 9089-9100.

de Pedro-Cuesta J, Rábano A, Martínez-Martín P*et al.* (2015) Correction: Comparative Incidence of Conformational, Neurodegenerative Disorders. *PLOS ONE,* 10 (10): e0140304.

De Vos KJ, Sable J, Miller KE, and Sheetz MP (2003) Expression of phosphatidylinositol (4,5) bisphosphate-specific pleckstrin homology domains alters direction but not the level of axonal transport of titochondria. *Mol Biol Cell,* 14 (9): 3636–3649.

Dikiy I and Eliezer D (2012) Folding and misfolding of alpha-synuclein on membranes. *Biochimica et Biophysica Acta,* 1818: 1013-1018.

Donaghy PC and McKeith IG (2014) The clinical characteristics of dementia with Lewy bodies and a consideration of prodromal diagnosis. *Alzheimer's research & therapy, 6* (4): 1.

Donaghy P, Thomas AJ, O'Brien JT (2015) Amyloid PET Imaging in Lewy body disorders. *Am J*

Geriatr Psychiatry, 23 (1): 23-37.

Drew L (2016) Two hundred steps. *Nature,* 538: 2–3.

Ebeling W *et al.* (1974) Proteinase K from *Tritirachium album* Limber. *European Journal of Biochemistry,* 47 (1): 91-7.

Erkkinen MG, Kim MO, and Geschwind MD (2018) Clinical Neurology and Epidemiology of the Major Neurodegenerative Diseases. *Cold Spring Harb Perspect Biol*, 10: a033118.

Evans T, Kok WL, Cowan K *et al.* (2018) Accumulation of beta-synuclein in cortical neurons is associated with autophagy attenuation in the brains of dementia with Lewy body patients. *Brain research,* 1681: 1-13.

Exner N, Treske B, Paquet D *et al.* (2007) Loss-of-function of human PINK1 results in mitochondrial pathology and can be rescued by parkin. *The Journal of Neuroscience,* 27 (45): 12413–12418.

Falkenburger BH and Schulz JB (2006) Limitations of cellular models in Parkinson's disease models. *Journal of neural transmission,* 70: 261-268.

Farrer M, Kachergus J, Forno L *et al.* (2004) Comparison of kindreds with parkinsonism and α-synuclein genomic multiplications. *Annals of neurology*, *55* (2): 174-179.

Fauvet B, Mbefo MK, Fares MB *et al.* (2012) alpha-Synuclein in central nervous system and from erythrocytes, mammalian cells, and Escherichia coli exists predominantly as disordered monomer. *J Biol Chem,* 287: 15345–15364.

Francis PT, Perry EK (2007) Cholinergic and other neurotransmitter mechanismsin Parkinson's disease, Parkinson's disease dementia, and dementia with Lewy bodies. *Mov Disord,* 22 (17): 351–357.

Fujita M, Sugama S, Sekiyama K *et al.* (2010) A [beta]-synuclein mutation linked to dementia produces neurodegeneration when expressed in mouse brain. *Nature communications*, 1: 110.

Fujiwara H, Hasegawa M, Dohmae N *et al.* (2002) alpha-Synuclein is phosphorylated in synucleinopathy lesions. *Nat Cell Biol,* 4: 160–164.

Funayama M, Hasegawa K, Kowa H *et al.* (2002) A new locus for Parkinson's disease (PARK8) maps to chromosome 12p11.2-q13.1. *Ann Neurol*, 51: 296–301.

Funayama M, Hasegawa K, Ohta E *et al.* (2005) An LRRK2 mutation as a cause for the parkinsonism in the original PARK8 family. *Ann Neurol*, 57 (6): 918-921.

Fusco G, Chen SW, Williamson PTF *et al.* (2017) Structural basis of membrane disruption and cellular toxicity by α-synuclein oligomers. *Science*, 358 (6369): 1440-1443.

Gaig C, Martí MJ, Ezquerra M, Cardozo A, Rey MJ, Tolosa E (2007) G2019S LRRK2 mutation causing Parkinson's disease without Lewy bodies. *J Neurol Neurosurg Psychiatry*, 78: 626-628.

Gallegos S, Pacheco C, Peters C*et al.* (2015) Features of alpha-synuclein that could explain the progression and irreversibility of Parkinson's disease. *Frontiers in Neuroscience*, 9: 59. http://doi.org/10.3389/fnins.2015.00059

Galvin JE, Uryu K, Lee VMY, and Trojanowski JK (1999) Axon pathology in Parkinson's disease and Lewy body dementia hippocampus contains α-, β-, and γ-synuclein. *Proc Natl Acad Sci USA*, 96 (23): 13450–13455.

Galvin JE, Giasson B, Hurtig HI *et al*. (2000) Neurodegeneration with brain iron accumulation, type 1 is characterized by alpha-, beta-, and gamma-synuclein neuropathology. *Am J Pathol*, 157 (2): 361-368.

Galvin JE, Lee VM, Trojanowski JQ (2001) Synucleinopathies: clinical and pathological implications. *Arch Neurol*, 58: 186 –190.

Giasson BI, Duda JE, Quinn SM *et al*. (2002) Neuronal alpha-synucleinopathy with severe movement disorder in mice expressing A53T human alpha-synuclein. *Neuron*, 34: 521–533.

Goedert M, Jakes R, Spillantini MG (2017) The Synucleinopathies: Twenty Years On. *Journal of Parkinson's Disease*, 7 (1): 51-69. doi: 10.3233/JPD-179005.

Gombash SE, Manfredsson FP, Kamp CG *et al.* (2013) Morphological and behavioral impact of AAV2/5-mediated overexpression of human wildtype alpha synuclein in the rat nigrostriatal system. *PLoS ONE*, 8: e81426.

Graham RC and Karnovsky MJ (1966) The early stages of absorption of injected horseradish peroxidase in the proximal tubules of mouse kidney: Ultrastructural cytochemistry by a new technique. *J. Histochem. Cytoehem*, 14: 291.

Gray SJ (2012) Gene therapy and neurodevelopmental disorders. *Neuropharmacology*, 68: 136-142.

Green MR and Sambrook J (2012) Molecular Cloning: A Laboratory Manual. -4th ed. *Cold Spring Harbor Laboratory Press*, Cold Spring Harbor, New York. 1881 p.

Greten-Harrison B, Polydoro M, Morimoto-Tomita M *et al.* (2010) αβγ-Synuclein triple knockout mice reveal age-dependent neuronal dysfunction. *Proc Natl Acad Sci U S A*, 107 (45): 19573-8.

Grieger JC and Samulski RJ (2012) Adeno-associated virus vectorology, manufacturing, and clinical applications. *Methods in Enzymology*, 507: 229-254.

Halliday GM, Song YJ, Harding AJ (2011) Striatal beta-amyloid in dementia with Lewy bodies but not Parkinson's disease. *J Neural Transm*, 118: 713–719.

Hara S, Arawaka S, Sato H*et al.* (2013) Serine 129 phosphorylation of membrane-associated α-synuclein modulates dopamine transporter function in a G protein-coupled receptor kinase-dependent manner. *Mol. Biol. Cell*, 24 (11): 1649-1660, S1-3.

Harding AJ, Broe GA, Halliday GM (2002) Visual hallucinations in Lewy body disease relate to Lewy bodies in the temporal lobe. *Brain*, 125 (2): 391-403.

Hashimoto M, Rockenstein E, Mante M *et al.* (2001) Beta-synuclein inhibits alpha-synuclein aggregation: a possible role as an anti-parkinsonian factor. *Neuron*, 32: 213–223.

Hashimoto M, Bar-on P, Ho G*et al.* (2004a) Beta-synuclein regulates Akt activity in neuronal cells. *J Biol Chem*, 279 (22): 23622-23629.

Hashimoto M, Rockenstein E, Crews L, and Masliah E (2004b) Role of protein aggregation in mitochondrial dysfunction and neurodegeneration in Alzheimer's and Parkinson's disease. *Neuromol Med*, 4: 21-36.

Hoffman-Zacharska D, Koziorowski D, Ross OA (2013) Novel A18T and pA29S substitutions in α-synuclein may be associated with sporadic Parkinson's disease. *Parkinsonism Relat Disord*, 19 (11): 1057-1060.

Hogan DB, Fiest KM, Roberts JI *et al.* (2016) The prevalence and incidence of dementia with Lewy bodies: a systematic review. *Can J Neurol Sci*, 43: S83-S95.

Hoyer W, Cherny D, Subramaniam V, and Jovin TM (2004) Impact of the acidic C-terminal region comprising amino acids 109-140 on alpha-synuclein aggregation in vitro. Biochemistry, 43 (51): 16233-16242.

Ibanez P, Bonnet AM, Debarges B *et al.* (2004) Causal relation between alpha-synuclein gene duplication and familial Parkinson's disease. Lancet 364: 1169–1171.

Iwai A, Masliah E, Yoshimoto M *et al.* (1995) The precursor protein of non-A beta component of Alzheimer's disease amyloid is a presynaptic protein of the central nervous system. *Neuron,* 14 (2): 467-475.

Janowska MK and Baum J (2016) The loss of inhibitory C-terminal conformations in disease associated P123H β-synuclein. *Protein Science,* 25: 286-294.

Jellinger KA (2012) Neuropathology of sporadic Parkinson's disease: evaluation and changes of concepts. *Mov Disord*, 27: 8–30.

Jellinger KA and Korczyn AD (2018) Are dementia with Lewy bodies and Parkinson's disease dementia the same disease? *BMC Med*, 16 (1): 34.

Ji H, Liu YE, Jia T *et al.* (1997) Identification of a breast cancer-specific gene, BCSG1, by direct differential cDNA sequencing. *Cancer Res*, 57 (4): 759-764.

Jin H and Clayton DF (1997) Localized changes in immediate-early gene regulation during sensory and motor learning in zebra finches. *Neuron*, 19 (5): 1049-1059.

Kahle PJ, Neumann M, Ozmen L *et al.* (2000) Subcellular localization of wild-type and Parkinson's disease-associated mutant alpha-synuclein in human and transgenic mouse brain. *J Neurosci*, 20: 6365–6373.

Kamp F, Exner N, Lutz AK *et al.* (2010) Inhibition of mitochondrial fusion by α-synuclein is rescued by PINK1, Parkin and DJ-1. *The EMBO Journal*, 29 (20): 3571–3589.

Karpinar DP, Balija MB, Kugler S *et al.* (2009) Pre-fibrillar alpha-synuclein variants with impaired beta-structure increase neurotoxicity in Parkinson's disease models. *EMBO J*, 28: 3256–3268.

Kawamoto Y, Akiguchi I, Nakamura S *et al.* (2002) 14-3-3 proteins in Lewy bodies in Parkinson disease and diffuse Lewy body disease brains. *J Neuropathol Exp Neurol*, 61 (3): 245-253.

Kiely AP, Asi YT, Kara E *et al.* (2013) Alpha-synucleinopathy associated with G51D SNCA mutation: a link between Parkinson's diseaseand multiple system atrophy? *Acta Neuropathol*, 125: 753-769.

Kitada T, Asakawa S, Hattori N *et al.* (1998) Mutations in the parkin gene cause autosomal recessive juvenile parkinsonism. *Nature*, 392: 605–608.

Krassnig S, Schweinzer C, Taub N *et al.* (2015) Influence of lentiviral β-synuclein overexpression in the hippocampus of a transgenic mouse model of Alzheimer's disease on amyloid precursor protein metabolism and pathology. *Neurodegener Dis*, 15: 243-257.

Kraytsberg Y, Kudryavtseva E, McKee AC *et al.* (2006) Mitochondrial DNA deletions are abundant and cause functional impairment in aged human substantia nigra neurons. *Nat Genet*, 38 (5): 518-520.

Kruger R, Kuhn W, Muller T *et al.* (1998) Ala30Pro mutation in the gene encoding alpha-synuclein in Parkinson's disease. *Nat Genet*, 18: 106-108.

Kügler S, Hahnewald R, Garrido M, and Reiss J (2007) Long-term rescue of a lethal inherited disease by adeno-associated virus-mediated gene transfer in a mouse model of molybdenum-cofactor deficiency. *American Journal of Human Genetics*, 80: 291-297.

Kügler S, Kilic E and Bähr M (2003) Human synapsin 1 gene promoter confers highly neuron-specific long-term transgene expression from an adenoviral vector in the adult rat brain depending on the transduced area. *Gene Therapy*, 10 (4): 337–347.

Kuusisto E, Parkkinen L and Alafuzoff I (2003) Morphogenesis of Lewy bodies: dissimilar

incorporation of alpha-synuclein, ubiquitin, and p62. *J Neuropathol Exp Neurol*, 62 (12): 1241-1253.

Laemmli UK (1970) Cleavage of structural proteins during the assembly of the head of bacteriophage T4. *Nature*, 227: 680–685.

Landau M (2017) Getting in charge of β-synuclein fibrillation. *J Biol Chem*, 292 (39): 16380-16381.

Larsen KE, Schmitz Y, Troyer MD *et al.* (2006) Alpha-synuclein overexpression in PC12 and chromaffin cells impairs catecholamine release by interfering with a late step in exocytosis. *J Neurosci*, 26 (46): 11915-11922.

Lashuel HA, Overk CR, Oueslati A and Masliah E (2013) The many faces of α-synuclein: from structure and toxicity to therapeutic target. *Nat Rev Neurosci*, 14 (1): 38-48.

Lavedan C, Leroy E, Dehejia A *et al.* (1998) Identification, localization and characterization of the human gamma-synuclein gene. *Hum Genet*, 103 (1): 106-112.

Leitao A, Bhumkar A, Hunter DJB *et al.* (2018) Unveiling a selective mechanism for the inhibition of α-Synuclein aggregation by β-Synuclein. *Int J Mol Sci*, 19 (2).

Li WW, Yang R, Guo JC *et al.* (2007) Localization of alpha-synuclein to mitochondria within midbrain of mice. *Neuroreport*, 18 (15): 1543-1546.

Lowe J, Blanchard A, Morrell K *et al.* (1988) Ubiquitin is a common factor in intermediate filament inclusion bodies of diverse type in man, including those of Parkinson's disease, Pick's disease, and Alzheimer's disease, as well as Rosenthal fibres in cerebellar astrocytomas, cytoplasmic bodies in muscle, and mallory bodies in alcoholic liver disease. *J Pathol*, 155 (1): 9-15.

Löw K, Aebischer P (2012) Use of viral vectors to create animal models for Parkinson's disease. *Neurobiology of Disease*, 48: 189-201.

Lu XH, Fleming SM, Meurers B *et al.* (2009) Bacterial artificial chromosometransgenic mice expressing a truncated mutant parkin exhibit age-dependent hypokinetic motordeficits, dopaminergic neuron degeneration, and accumulation of proteinase K-resistant alpha-synuclein. *J Neurosci*, 29: 1962-1976.

Ludtmann MHR, Angelova PR, Horrocks MH *et al.* (2018) α-synuclein oligomers interact with ATP synthase and open the permeability transition pore in Parkinson's disease. *Nature Communications*, 9: 2293.

MacAskill AF and Kittler JT (2010) Control of mitochondrial transport and localization in neurons. *Trends in Cell Biol*, 20 (2): 102–112.

Maroteaux L, Campanelli JT and Scheller RH (1988) Synuclein: a neuron-specific protein

localized to the nucleus and presynaptic nerve terminal. *J Neurosci*, 8 (8): 2840-2815.

Martin LJ, Pan Y, Price AC *et al.* (2006) Parkinson's disease α-synuclein transgenic mice develop neuronal mitochondrial degeneration and cell death. *J Neurosci,* 26 (1): 41-50.

McKeith IG, Dickson DW, Lowe J *et al.* (2005) Diagnosis and management of dementia with Lewy bodies third report of the DLB consortium. *Neurology,* 65 (12): 1863-1872.

Miotto MC, Pavese MD, Quintanar L *et al.* (2017) Bioinorganic chemistry of Parkinson's disease: affinity and structural features of Cu(I) binding to the full-length β-Synuclein protein. *Inorg Chem,* 56 (17): 10387-10395.

Mishizen-Eberz AJ, Guttmann RP, Giasson BI *et al.* (2003) Distinct cleavage patterns of normal and pathologic forms of alpha-synuclein by calpain I in vitro. *J Neurochem*, 86 (4): 836-47.

Mor F, Quintana F, Mimran A, and Cohen IR (2003) Autoimmune encephalomyelitis and uveitis induced by T cell immunity to self beta-synuclein. *J Immunol,* 170 (1): 628-634.

Mori F, Nishie M, Yoshimoto M *et al.* (2003) Reciprocal accumulation of beta-synuclein in alpha-synuclein lesions in multiple system atrophy. *Neuroreport*, 14: 1783–1786.

Mori F, Tanji K, Yoshimoto M *et al.* (2002) Immunohistochemical comparison of α- and β-synuclein in adult rat central nervous system. *Brain research,* 941 (1): 118-126.

Moriarty GM, Olson MP, Atieh TB *et al.* (2017) A pH-dependent switch promotes β-synuclein fibril formation via glutamate residues. *J Biol Chem,* 292 (39): 16368-16379.

Mullin S and Schapira A (2013) α-Synuclein and mitochondrial dysfunction in Parkinson's disease. *Mol Neurobiol,* 47 (2): 587–597.

Nakajo S, Omata K, Aiuchi T *et al.* (1990) Purification and characterization of a novel brain-specific 14-kDa protein. *J Neurochem,* 55 (6): 2031-2038.

Nakajo S, Tsukada K, Omata K *et al.* (1993) A new brain-specific 14-kDa protein is a phosphoprotein. Its complete amino acid sequence and evidence for phosphorylation. *Eur J Biochem,* 217 (3): 1057-1063.

Nakamura K, Nemani VM, Azarbal F *et al.* (2011) Direct membrane association drives mitochondrial fission by the Parkinson disease-associated protein α-synuclein. *J Biol Chem,* 286 (23): 20710–20726.

Nakane PK and Pierce GB (1967) Enzyme-labeled antibodies for the light and electron microscopic localization of tissue antigens. *J Cell Biol,* 33 (2): 307–318.

Neumann M *et al.* (2002) Misfolded proteinase K–resistant hyperphosphorylated α-synuclein in aged transgenic mice with locomotor deterioration and in human α-synucleinopathies. *Journal of Clinical Investigations,* 110: 1429–1439.

Ninkina NN, Alimova-Kost MV, Paterson JW *et al.* (1998) Organization, expression and polymorphism of the human presyn. *Hum Mol Genet,* 7: 1417-1424.

Nussbaum RL (2017) Genetics of Synucleinopathies.*Cold Spring Harb Perspect Med,* pii: a024109. doi: 10.1101/cshperspect.a024109. [Epub ahead of print]

Obi T, Nishioka K, Ross OA (2008) Clinicopathologic study of a SNCA gene duplication patient with Parkinson disease and dementia. *Neurology,* 70: 238–241.

Ohtake H, Limprasert P, Fan Y *et al.* (2004) β-synuclein gene alterations in dementia with Lewy bodies. *Neurology*, 63 (5): 805-811.

Ortolano S, Spuch C, Navarro C (2012) Present and future of adeno associated virus based gene therapy approaches. *Recent Patents on Endocrine, Metabolic & Immune Drug Discovery*, 6: 47-66.

Pacifici M and Peruzzi F (2012) Isolation and culture of rat embryonic neural cells: a quick protocol. *J Vis Exp* 63: e3965.

Paleologou KE, Kragh CL, Mann DM *et al.* (2009) Detection of elevated levels of soluble alpha-synuclein oligomers in post-mortem brain extracts from patients with dementia with Lewy bodies. *Brain,* 132: 1093–1101.

Parihar MS, Parihar A, Fujita M *et al.* (2008) Mitochondrial association of alpha-synuclein causes oxidative stress. *Cellular and Molecular Life Sciences,* 65 (7): 1272-1284.

Parkkinen L, Pirttila T, and Alafuzoff I (2008) Applicability of current staging/categorization of α-synuclein pathology and their clinical relevance. *Acta Neuropathol*, 115: 399-407.

Parkkinen L, Pirttila T, Tervahauta M, and Alafuzoff I (2005) Widespread and abundant α-synuclein pathology in a neurologically unimpaired subject. *Neuropathology*, 25: 304-314.

Parkinson J. (2002) An essay on the shaking palsy. 1817. *J Neuropsychiatry Clin Neurosci*. 14 (2): 223-36.

Pasanen P, Myllykangas L, Siitonen M *et al.* (2014) Novel α-synuclein mutation A53E associated with atypical multiple system atrophy and Parkinson's disease-type pathology. *Neurobiol Aging*, 35 (9): 2180.e1-5.

Payton JE, Perrin RJ, Woods WS and George JM (2004) Structural determinants of PLD2 inhibition by alpha-synuclein. *J Mol Biol,* 337 (4): 1001-1009.

Paxinos G (2014) The rat nervous system: edition 4. *Academic Press*. 1052 p.

Paxinos G and Watson C (1986) The rat brain in stereotactic coordinates, *Academic Press,* San Diego, USA.

Peelaerts W, Bousset L, Van der Perren A *et al.* (2015) α-Synuclein strains cause distinct synucleinopathies after local and systemic administration. *Nature*, 522 (7556): 340-4. doi: 10.1038/nature14547.

Peeraully T, Tan EK (2012) Genetic variants in sporadic Parkinson's disease: East vs West. *Parkinsonism Relat Disord*, 18 (1): 63-65.

Peng XM, Tehranian R, Dietrich P *et al.* (2005) α-Synuclein activation of protein phosphatase 2A reduces tyrosine hydroxylase phosphorylation in dopaminergic cells. *J Cell Science,* 118: 3523-3530.

Piggott MA, Marshall EF, Thomas N *et al.* (1999) Striatal dopaminergic markers in dementia with Lewy bodies, Alzheimer's and Parkinson's diseases: rostrocaudal distribution. *Brain*, 122 (8): 1449–1468.

Polymeropoulos MH, Higgins JJ, Gorbe LI *et al.* (1996) Mapping of a gene for Parkison's disease to chromosome 4q21-q23. *Science,* 274: 1197-1199.

Polymeropoulos MH, Lavedan C, Leroy E *et al.* (1997) Mutation in the alpha-synuclein gene identified in families with Parkinson's disease. *Science*, 276: 2045-2047.

Pozo Devoto VM and Falzone TL (2017) Mitochondrial dynamics in Parkinson's disease: a role for α-synuclein? *Dis Model Mech,* 10 (9): 1075–1087.

Proukakis C, Dudzik CG, Brier T *et al.* (2013) A novel alpha-synuclein missense mutation in Parkinson disease. *Neurology*, 80: 1062-1064.

Puspita L, Chung SY, and Shim JW (2017) Oxidative stress and cellular pathologies in Parkinson's disease. *Mol Brain,* 10 (1): 53.

Ramirez A, Heimbach A, Grundemann J *et al.* (2006) Hereditary parkinsonism with dementia is caused by mutations in ATP13A2, encoding a lysosomal type 5 P-type ATPase. *Nat Genet*, 38 (10): 1184-1191.

Rockenstein E, Mallory M, Hashimoto M *et al.* (2002) Differential neuropathological alterations in transgenic mice expressing alpha-synuclein from the platelet-derived growth factor and Thy-1 promoters. *J Neurosci Res*, 68: 568–578.

Rogaeva E, Johnson J, Lang AE *et al.* (2004) Analysis of the PINK1gene in a large cohort of cases with Parkinson disease. *Arch Neurol* 61: 1898–1904.

Ryan BJ, Hoek S, Fon EA, and Wade-Martins R (2015) Mitochondrial dysfunction and mitophagy in Parkinson's: from familial to sporadic disease. *Trends Biochem Sci,* 40 (4): 200-210.

Sajnani G and Requena JR (2012) Prions, proteinase K and infectivity. *Prion* 6 (5): 430–432.

Savica R, Grossardt BR, Bower JH *et al.* (2013) Incidence of dementia with Lewy bodies and Parkinson disease dementia. *JAMA Neurol*, doi:10.1001/jamaneurol.2013.3579.

Schapira AH, Cooper JM, Dexter D *et al.* (1989) Mitochondrial complex ideficiency in Parkinson's disease. *Lancet*, 1 (8649): 126.

Schapira AH (2012) Mitochondrial diseases. *Lancet*, 379: 1825–1834.

Sekigawa A, Fujita M, Sekiyama K *et al.* (2012) Distinct mechanisms of axonal globule formation in mice expressing human wild type α-synuclein or dementia with Lewy bodies-linked P123H β-synuclein. *Molecular Brain*, 5: 34.

Sekigawa A, Takamatsu Y, Sekiyama K *et al.* (2013) Diversity of mitochondrial pathology in a mouse model of axonal degeneration in synucleinopathies. *Oxid Med Cell Longev*, 2013: 817807.

Sekigawa A, Takamatsu Y, Sekiyama K and Hashimoto M (2015) Role of α-and β-synucleins in theaxonal pathology of Parkinson's disease and related synucleinopathies. *Biomolecules*, 5 (2): 1000-1011.

Sekiyama K, Takamatsu Y, Waragai M, and Hashimoto M (2014) Role of genomics in translational research for Parkinson's disease. *Biochemical and biophysical research communications*, 452 (2): 226-235.

Shibayama-Imazu T, Okahashi I, Omata K *et al.* (1993) Cell and tissue distribution and developmental change of neuron specific 14 kDa protein (phosphoneuroprotein 14). *Brain Res*, 622 (1-2): 17-25.

Singleton AB, Farrer M, Johnson J *et al.* (2003) Alpha-synuclein locus triplication causes Parkinson's disease. *Science*, 302 (5646): 841.

Smith PK, Krohn RI, Hermanson GT *et al.* (1987) Measurement of protein using bicinchoninic acid. *Analytical Biochemistry*, 150: 76-85.

Snyder H, Mensah K, Hsu C *et al.* (2005) α-Synuclein reduces proteasomal inhibition by alpha-synuclein but not gamma-synuclein. *J Biol Chem*, 280 (9): 7562-7569.

Snyder L *et al.* (2015) Lewy body dementia. Information for patients, families and professionals. National Institute of Health. Publication No. 15-7907.

Spillantini MG, Divane A, and Goedert M (1995) Assignment of human alpha-synuclein (SNCA) and beta-synuclein (SNCB) genes to chromosomes 4q21 and 5q35. *Genomics*, 27 (2): 379-381.

Spillantini MG, Crowther RA, Jakes R*et al.* (1998) α-Synuclein in filamentous inclusions of Lewy bodies from Parkinson's disease and dementia with Lewy bodies. *Proceedings of the National Academy of Sciences*, 95 (11): 6469-6473.

Stereo Investigator users guide version 9 (2009) MicroBrightField, Inc.

Surguchov A (2008) Molecular and Cellular Biology of Synucleins. *International Review of Cell and Molecular Biology*, 270: 225-317.

Surguchov A (2013) Synucleins: are they two-edged swords? *Journal of Neuroscience Research*, 91: 161-166.

Surmeier JD and Sulzer D (2013) The pathology roadmap in Parkinson disease. *Prion*, 7 (1): 85-91.

Taschenberger G, Garrido M, Tereshchenko Y *et al.* (2012) Aggregation of αSynuclein promotes progressive in vivo neurotoxicity in adult rat dopaminergic neurons. *Acta Neuropathol*, 123: 671-683.

Taschenberger G, Toloe J, Tereshchenko J *et al.* (2013) β-synuclein aggregates andinduces neurodegeneration in dopaminergic neurons. *Annals of neurology*, 74 (1): 109-118.

Tenreiro S, Rosado-Ramos R, Gerhardt E *et al.* (2016) Yeast reveals similar molecular mechanisms underlying alpha- and beta-synuclein toxicity. *Hum Mol Genet*, 25 (2): 275-290.

Thavarajah R, Mudimbaimannar VK, Elizabeth J *et al.* (2012) Chemical and physical basics of routine formaldehyde fixation. *J Oral Maxillofac Pathol*, 16 (3): 400–405.

Tolö J (2013) Effects of α/β/γ-Synuclein overexpression on the mitochondria and viability of neurons, examinedusing genetically encoded fluorescent sensors. *Ph.D. thesis.*

Tolö J, Taschenberger G, Leite K *et al.* (2018) Pathophysiological consequences of neuronal α-synuclein overexpression: impacts on ion homeostasis, stress signaling, mitochondrial integrity, and electrical activity. *Front Mol Neurosci*, 11: 49. doi: 10.3389/fnmol.2018.00049

Tong Y, Pisani A, Martella G *et al.* (2009) R1441C mutationin LRRK2 impairs dopaminergic neurotransmission in mice. *Proc Natl Acad Sci U S A*, 106: 14622–14627.

Trojanowski JQ, Lee VM (1998) Aggregation of neurofilament and alpha-synuclein proteins in Lewy bodies: implications for the pathogenesis of Parkinson disease and Lewy body dementia. *Arch Neurol*, 55 (2): 151-152.

Tsigelny IF, Bar-On P, Sharikov Y *et al.* (2007) Dynamics of α-synuclein aggregation and inhibition of pore-like oligomer development by α-synuclein. *FEBS J*, 274: 1862-1877.

Tsuang DW, DiGiacomo L and Bird TD (2004) Familial occurrence of dementia with Lewy bodies. *The American journal of geriatric psychiatry*, 12 (2): 179-188.

UniProt: the universal protein knowledge base (2017) Nucleic Acids Res. 45: D158-D169.

Uryu K, Richter-Landsberg C, Welch W *et al.* (2006) Convergence of heat shock protein 90 with ubiquitin in filamentous alpha-synuclein inclusions of alpha-synucleinopathies. *Am J Pathol,* 168 (3): 947-961.

Uversky VN, Li J, Souillac P *et al.* (2002) Biophysical properties of the synucleins and their propensities to fibrillate: inhibition of alpha-synuclein assembly by beta- and gamma-synucleins. *J Biol Chem,* 277: 11970–11978.

Valente EM, Abou-Sleiman PM, Caputo V *et al.* (2004) Hereditary early-onset Parkinson's disease caused by mutations in PINK1. *Science,* 304: 1158–1160.

van der Putten H, Wiederhold KH, Probst A *et al.* (2000) Neuropathology in mice expressing human alpha-synuclein. *J Neurosci,* 20: 6021–6029.

Vann Jones SA and O'Brien JT (2014) The prevalence and incidence of dementia with Lewy bodies: A systematic review of population and clinical studies. *Psychol Med,* 44: 673– 683.

Van Pelt LF (1977) Ketamine and xylazine for surgical anesthesia in rats. *J Am Vet Med Assoc,* 171 (9): 842-4.

Volpicelli-Daley L, Kirik D, Stoyka LE *et al.* (2016) How can rAAV-α-synuclein and the fibril α-synuclein models advance our understanding of Parkinson's disease? *J Neurochem,* 139 (1): 131-155.

Von Bohlen und Halbach O (2004) Synucleins and their relationship to Parkinson's disease. *Cell and tissue research,* 318 (1): 163-174.

Wakabayashi K, Engelender S, Yoshimoto M *et al.* (2000) Synphilin-1 is present in Lewy bodies in Parkinson's disease. *Ann Neurol,* 47 (4): 521-523.

Wei J, Fujita M, Nakai M *et al.* (2007) Enhanced lysosomal pathology caused by beta-synuclein mutants linked to dementia with Lewy bodies. *J Biol Chem,* 282 (39): 28904-14.

Wei J, Fujita M, Nakai M *et al.* (2009) Protective role of endogenous gangliosides for lysosomal pathology in a cellular model of synucleinopathies. *Am J Pathol,* 174 (5): 1891-1909.

Weinberg MS, Samulski RJ, McCown TJ (2013) Adeno-associated virus (AAV) gene therapy for neurological disease. *Neuropathology,* 69: 82-88.

Winner B, Jappelli R, Maji SK *et al.* (2011) In vivo demonstration that alpha-synuclein oligomers are toxic. *Proc Natl Acad Sci U S A,* 108: 4194–4199.

Yamin G, Uversky VN and Fink AL (2003) Nitration inhibits fibrillation of human alpha-synuclein *in vitro* by formation of soluble oligomers. *FEBS Lett,* 542: 147–152.

Yamin G, Munishkina LA, Karymov MA *et al.* (2005) Forcing nonamyloidogenic beta-synuclein to fibrillate. *Biochemistry,* 44 (25): 9096-107.

Yavin E and Menkes JH (1973) The culture of dissociated cells from rat cerebral cortex. *The Journal of Cell Biology*, 57 (1): 232–237.

Yu S, Zuo X, Li Y *et al.* (2004) Inhibition of tyrosine hydrolase expression in α-synuclein-transfected dopaminergic neuronal cells. *Neuroscience letters*, 367: 34-39.

Zaccai J, McCracken C, and Brayne C (2005) A systematic review of prevalence and incidence studies of dementia with Lewy bodies. *Age Ageing*, 34: 561–566.

Zarranz J, Alegre J, Gomez-Esteban J *et al.* (2004) The new mutation, E46K, of alpha-synuclein causes Parkinson and Lewy body dementia. *Ann Neurol*, 55: 164–173.

Zufferey R, Donello JE, Trono D, Hope TJ (1999) Woodchuck hepatitis virus posttranscriptional regulatory element enhances expression of transgenes delivered by retroviral vectors. *Journal of Virology*, 73 (4): 2886-2892.

7. Abbreviations

αS – alpha synuclein

βS – beta synuclein

γS – gamma synuclein

µg – microgram

µl– microliter

µm– micrometer or micron

µM– micromolar

AA – amino acid residue

AAV – adeno-associated virus

Aβ – amyloid beta

aCSF – artificial cerebrospinal fluid

AD – Alzheimer's disease

ALS – amyotrophic lateral sclerosis

Amp – ampicillin

ANOVA – analysis of variance

AP– anterior-posterior

APS– ammonium peroxide sulfate

ATP– adenosine triphosphate

BCA – bicinchoninic acid

Bcl-xL – B-cell lymphoma-extra large

bp– base pairs

BPB– bromophenol blue sodium salt

BSA– bovine serum albumin

CA 2/3 – Cornu Ammonis area 2/3 of hippocampus

cDNA – complementary DNA

CJD – Creutzfeldt-Jakob disease

CMF – Ca^{2+}/Mg^{2+}-free medium

CNS – central nervous system

COX IV – cytochrome c oxidase subunit 4

Cy2 – cyanine fluorophore

Cy3 – indocarbocyanine fluorophore

DAB– 3,3'-diaminobenzidin

DAPI– 4',6-diamidino-2-phenylindole

DJ1 – protein and nucleotide deglycase

ddH_2O – sterile ultra-pure water

DLB – dementia with Lewy bodies

DMEM – Dulbecco's modified Eagle's medium

DMSO–dimethyl sulfoxide

DNA – desoxyribonucleic acid

dNTP – deoxynucleotide triphosphate

DPX – distyrene, plasticizer, and xylene

DTT– dithiothreitol

DV– dorsoventral

E – embryonic day

ECL–enhanced chemoluminescence solution

ECM – extracellular matrix

EDTA– ethylenediaminetetraacetic acid

EGFP– enhanced green fluorescent protein

ER – endoplasmic reticulum

ESI-MS – electrospray ioinization mass spectroscopy

EtBr– ethidium bromide

FCS – fetal calf serum

FPLC– fast protein liquid chromatography

FTLD – fronto-temporal lobar degeneration

g – gravitational constant

GWAS – genome-wide association studies

h –hour

HBSS – Hank's balanced salt solution

HCl – hydrogen chloride

HCN – hippocampal and cortical neuron medium

HEPES– (4-(2-hydroxyethyl)-1-piperazineethanesulfonic acid)

HF – high fidelity

H_2O_2 – hydrogen peroxide

HRP – horse reddish peroxidase

hSyn1 – human synapsin 1 gene promoter

IF– immunofluorescence

IHC– immunohisochemistry

IMM – inner mitochondrial membrane

IPTG – isopropyl-beta-D-thiogalactopyranoside

kb – kilobase

KCl – potassium chloride

kDa– kilodalton

KO – knock-out

kV–kilovolt

L-DOPA – levodopa or L-3,4-dihydroxyphenylalanine

LB – Lewy body

LB-medium – Luria broth

LN – Lewy neurite

LRRK – leucine-rich repeat kinase

M–Mole

$MgCl_2$–magnesium chloride

$MgSO_4$ – magnesium sulphate

min or ´– minute

ML – mediolateral

mm – millimeter

MPTP – 1-methyl-4-phenyl-1,2,3,6-tetrahydropyridine

mRNA – messenger RNA

MSA – multiple system atrophy

NAC – non-Aß component of Alzheimer's disease amyloid

NaCl – sodium chloride

$NaHCO_3$ – sodium bicarbonate

NaH_2PO_4 – sodium phosphate monobasic monohydrate

NaN_3 – sodium azide

NaOH – sodium hydroxide

NBIA – neurodegeneration with brain iron accumulation

NDD – neurodegenerative disorder

ng– nanogramm

NGS – normal goat serum

nl – nanoliter

NLS – nuclear localization sequence

nm – nanometer

NSAID – non-steroidal anti-inflammatory drug

nuc – nuclear

OD – optical density

OMM – outer mitochondrial membrane

PAGE – polyacrylamide gel electrophoresis

PBS– phosphate buffered saline

PCR – polymerase chain reaction

PD – Parkinson's disease

PDD – Parkinson's disease dementia

PET – positron-emission tomography

PFA – paraformaldehyde

PINK1 – PTEN-induced putative kinase 1

PK – proteinase K

PLD2 – phospholipase D2

PLO – Poly-L-Ornithine

PSN – penicillin, streptomycin, and neomycin antibiotic mixture

PTEN – phosphatidylinositol-3,4,5-trisphosphate 3-phosphatase

qPCR – quantitative or real time PCR

REM – rapid eye movement

RNA – ribonucleic acid

ROS – reactive oxygen species

rpm – revolutions per minute

RT – room temperature

SD – standard deviation

SDS – sodium dodecylsulfate

SDS-PAGE– polyacrylamide gel electrophoresis

SN – Substantia nigra

SNARE – soluble N-ethylmaleimide-sensitive factor attachment protein receptor

SNCA – α-synuclein gene

SNCB – β-synuclein gene

SNpc – Substantia nigra pars compacta

SNpr – Substantia nigra pars reticulata

TBE – Tris/Borate/EDTA buffer

TBS – Tris-buffered saline

TBS-T – Tris-buffered saline with Tween20

TE – Tris/EDTA buffer

TEM – transmission electron microscopy

TEMED– tetraeminethylendiamine

tg – transgenic

ThioT – thioflavin T

TRor ITR– inverted terminal repeats

Tris – 2-amino-2-hydroxymethyl-propane-1,3-diol

tu – transducing units

UTR – untranslated region

V– Volt

VAMP2 – vesicle-associated membrane protein 2

VDAC1 – voltage-dependent anion-selective channel 1

vg – vector genome copies

VMAT – vesicular monoamine transporter

VTA – ventral tegmental area

WB – Western blot

WPRE - Woodchuck hepatitis virus posttranscriptional regulatory element

WT – wild type

8 Attachments

8.1 Curriculum Vitae

Content removed from the electronic version

Content removed from the electronic version

8.2 Publications and posters on doctoral project

“V70M-β-synuclein induces neurotoxicity in cultured cortical neurons and dopaminergic neurons of Substantia nigra in a similar way with α-synuclein but P123H-β-synculein does not” (manuscript in preparation).

CMPB Ph.D. retreat 2014, with oral presentation: *"Aggregation of alpha-Synuclein: what turns a friend into an enemy"*, Leipzig, Germany, 03/12/14 - 05/12/14

U4 Graduate School "The Aging Brain", with poster presentation: *"Neurotoxic and aggregation properties of beta-synuclein and beta-synuclein-P123H mutant"*, Uppsala, Sweden, 23/08/15 - 29/08/15

6th biennial neuroscience conference Neurizons 2015: notes of an orchestrated brain, with poster presentation: *"Characterization of toxicity and aggregation properties of synucleins in primary cortical cells"*, Göttingen, Germany, 26/05/15 - 29/05/15

4th GGNB Science Day, with poster presentation: *"Parkinson's disease and dementia with Lewy bodies: from cell culture-based model to gene therapy"*, Göttingen, Germany, 5/12/16

Encephalon-2017, with poster presentation: *"Neurotoxicity and aggregation of β-synuclein and its P123H and V70M mutants associated with dementia with Lewy bodies"*, Göttingen, Germany, 1/12/17

Acknowledgements

A Ph.D. research project is always an achievement of not only a doctoral student but many other people: those who lead us, those who inspire us, those who take part of our work on their shoulders. Here is my turn to commemorate all who helped me with my Ph.D. work in the last 4 years.

First of all, my gratefulness and appreciation go to my supervisor Dr. Sebastian Kügler. He has been a great support throughout these 4 years. I am grateful to Prof. Dr. Mathias Bähr for accepting me to his department and helpful advice at the department seminars.

I would also like to thank all the members of Waldweg lab, former and current, for creating great working environment and helping me on every stage of the project. Dr. Grit Taschenberger shared with me protocols for proteinase K digestion and stereological cell counting. Dr. Yulia Tereshchenko taught me all animal procedures, including stereotaxic brain injections and perfusion. Dr. Johan Toloe showed me Ca^{2+}-imaging. Sabine Ceramella helped me with DAB stainings of rat's striata and SN.

Many thanks to Claudia Fokkman, Monika Zebski and Sonja Heyroth for their excellent technical help, cell culture training and leading me in everyday tasks in the lab.

Thanks to Anupam and our mutual lab rotation students Pauline, Dodo and Sofia, for having a lot of fun with protein purification project.

Thanks to my thesis committee members, Prof. Dr. Tiago Outeiro and Prof. Dr. Markus Zweckstetter, for their thoughtful advices on the projects and for giving a chance to use the equipment and protocols from their labs.

Thanks to Prof. Dr. Michael Hörner and all CNMPB students for inspiring and captivating seminars, „Encephalon" conference, and our great retreats.

I also have to thank the whole GGNB Office team, especially to Kirsten Pöhlker for coordinating the doctorate program, organization of numerous valuable courses, and for inspiring the creation of "GGNB: Times".

I learned throughout my Ph.D. studies also how important a family base is. This is why I especially want to thank my family members. First of all, my parents who always believed in me and taught me to become an independent woman. And, of course, my fiancé Alex who has always been there for me and made sure that I would never forget that there is a life next to the Ph.D. project and that the impossible is always possible if there is a strong will and a high motivation. He encouraged me to press on against seemingly impossible odds and inspired to succeed. Then, I also have to thank Nini and Biba, Alex´s parents who took me in their family as if I am their daughter. And finally, thanks to Timmy, our little sweet white dog that uses every opportunity to make me smile.